INFLUENCE OF COMPOSITION ON THE STRUCTURE AND PROPERTIES OF Fe-Pd-P AND Ni-Pd-P AMORPHOUS ALLOYS

Thesis by

Philippe Louis Maitrepierre

In Partial Fulfillment of the Requirements

For the Degree of
Doctor of Philosophy

California Institute of Technology

Pasadena, California

1969

(Submitted March 17, 1969)

A MA FEMME ET

MES PARENTS

ACKNOWLEDGMENTS

It has been a privilege to work under the direction of Professor Pol Duwez, and I want to express here my deepest gratitude for the guidance and encouragement with which he provided me. I also thank R. Hasegawa and Dr. Tsuei for stimulating discussions, and P. Bourgain, L. Cyrot and R. Binst for assisting in some of the experiments.

I am grateful to the technicians of this laboratory for their help and to Mrs. Sue Williams for her care and diligence in the typing of my thesis.

The financial support of the Atomic Energy Commission during this doctoral work is gratefully acknowledged.

ABSTRACT

Ternary alloys of nickel-palladium-phosphorus and iron-palladium-phosphorus containing 20 atomic % phosphorus were rapidly quenched from the liquid state. The structure of the quenched alloys was investigated by X-ray diffraction. Broad maxima in the diffraction patterns, indicative of a glass-like structure, were obtained for 13 to 73 atomic % nickel and 13 to 44 atomic % iron, with palladium adding up to 80%.

Radial distribution functions were computed from the diffraction data and yielded average interatomic distances and coordination numbers. The structure of the amorphous alloys could be explained in terms of structural units analogous to those existing in the crystalline Pd_3P, Ni_3P and Fe_3P phases, with iron or nickel substituting for palladium. A linear relationship between interatomic distances and composition, similar to Vegard's law, was shown for these metallic glasses.

Electrical resistivity measurements showed that the quenched alloys were metallic. Measurements were performed from liquid helium temperatures (4.2°K) up to the vicinity of the melting points (900°K-1000°K). The temperature coefficient in the glassy state was very low, of the order of $10^{-4}/^{\circ}K$. A resistivity minimum was found at low temperature, varying between 9°K and 14°K for Ni_x-Pd_{80-x}-P_{20} and between 17°K and 96°K for Fe_x-Pd_{80-x}-P_{20}, indicating the presence of a Kondo effect. Resistivity measurements, with a constant heating

rate of about 1.5°C/min, showed progressive crystallization above approximately 600°K.

The magnetic moments of the amorphous Fe-Pd-P alloys were measured as a function of magnetic field and temperature. True ferromagnetism was found for the alloys Fe_{32}-Pd_{48}-P_{20} and Fe_{44}-Pd_{36}-P_{20} with Curie points at 165°K and 380°K respectively. Extrapolated values of the saturation magnetic moments to 0°K were 1.70 μ_B and 2.10 μ_B respectively. The amorphous alloy Fe_{23}-Pd_{57}-P_{20} was assumed to be superparamagnetic. The experimental data indicate that phosphorus contributes to the decrease of moments by electron transfer, whereas palladium atoms probably have a small magnetic moment. A preliminary investigation of the Ni-Pd-P amorphous alloys showed that these alloys are weakly paramagnetic.

TABLE OF CONTENTS

I. INTRODUCTION

During recent years a growing interest has been shown in the study of non-crystalline solids, which have been alternately qualified as "glassy" or "amorphous". The main difference between amorphous and crystalline solids resides in the absence of long range order in the amorphous structure[1], although some type and degree of short range order can generally be recognized[2,3,4]. In this respect, glasses may be characterized as supercooled liquids[5]. Differences between glasses and supercooled liquids arise when other properties such as thermal and electrical conductivities, density, etc. are considered. Hence, glasses constitute a type of solids with specific characters differentiating them from both crystalline solids and undercooled liquids.

Whereas silicate glasses have been known and investigated for a long time, new developments have extended the field of amorphous inorganic materials. Experimental techniques such as high vacuum vapor deposition[6,7,8,9] electrodeposition[10] and chemical deposition[11] have been successful in yielding amorphous phases of normally crystalline materials. Direct attempts to obtain glasses by drastic cooling from the liquid state[12,13,14] at rates of about 10^{6}°C/sec, have been successful in yielding glassy structures in Au-Si[15], Pd-Si[16] Fe-P-C[17] alloys as well as in several tellurium base alloys (with Ge, Ga, In)[18]. Glass forming in these rapidly quenched alloys seems to be closely related to the existence of deep eutectics as well as rather high viscosity in the liquid state. However, only rather

narrow ranges of composition have yielded amorphous structures in these systems. This turned out to be a serious restriction in studying the changes in the amorphous structure with composition as well as the effect of composition on electrical and magnetic properties.

Alloys which would contain at least one strongly ferromagnetic element (Fe, Co or Ni) and would give reasonable chances of structural continuity with changing composition were considered for this investigation. The existence of rather low eutectics in the binary systems Fe-P, Ni-P and Pd-P at about 20% atomic phosphorus (cf. Appendix I), as well as the complete solid solubility of iron and nickel in palladium, was an important criterion for starting the investigation of Fe-Pd-P and Ni-Pd-P ternary alloys. Amorphous structures were successfully obtained by rapid quenching from the liquid state for Fe_{13}-Pd_{67}-P_{20} to Fe_{44}-Pd_{36}-P_{20} alloys and Ni_{13}-Pd_{67}-P_{20} to Ni_{73}-Pd_{7}-P_{20} alloys. Strong ferromagnetism was shown in Fe_{32}-Pd_{48}-P_{20} and Fe_{44}-Pd_{36}-P_{20} amorphous alloys. A study of the influence of composition on the structure and properties of these amorphous Fe-Pd-P and Ni-Pd-P alloys is the object of the present investigation.

II. ALLOYS PREPARATION

A. Composition ranges and sintering

Ternary alloys of Ni-Pd-P and Fe-Pd-P were prepared from 99.99% palladium powder from Engelhard Industries Inc., 99.9% nickel and iron from Charles Harvey Inc., and red amorphous phosphorus from Allied Chemical. The phosphorus was kept in a dessicator to prevent it from being hydrated. After different trials, the composition in phosphorus was set at 20 atomic % (except in one case were it turned out to be only 15%), whereas the ranges of Ni-Pd and Fe-Pd were explored. The extent of the range of compositions was from 13 to 73 atomic % nickel and from 13 to 44 atomic % iron, for reasons which will be explained below. Samples of 2 to 8 g in total mass were prepared from carefully weighed powders. A thorough mixing of the powders was performed before agglomeration under a pressure of 60,000 psi. Phosphorus improved greatly the coherency of the pressed briquets. These briquets were sintered in two stages, in order to insure an optimum degree of bonding between phosphorus and the metallic elements. The following procedure was found to be successful in reaching this objective. The samples, placed in evacuated pyrex tubes, were slowly heated up to 350^{o}C and kept for two days at temperature. The pyrex tubes were subsequently opened to release whatever gas pressure might be present, and the samples were placed in evacuated quartz tubes. They were heated up to about 550^{o}C for two more days, to complete the sintering process. The sintered briquets were then melted in a quartz crucible under argon gas (induction furnace) and

the melted alloys were cast into rods by sucking the liquid alloy into capillary quartz tubes 2 mm in diameter. The absence of reaction between the melted alloy and the quartz tubes attested to the high degree of bonding between phosphorus and metallic elements.

B. Quenching technique

The "piston and anvil" technique used to quench the alloys from the melt is described in references 12 and 13 and a schematic drawing of this apparatus is given in Fig. 1. The alloy is contained in a fused silica tube 3 mm in diameter having a small opening at its bottom end. The alloy is melted by induction through the susceptor E. The liquid globule is ejected by application of a small helium pressure and quenching is achieved by squeezing the liquid drop between the fixed anvil A and the moving piston B. Both A and B are lined with copper-beryllium discs C. When the globule is released, it cuts a light beam between a source G and a photocell H and an appropriate delay circuit triggers the release of the finger F which retains the piston B, which is actuated by a gas pressure of 200 psi. The rate of cooling is of the order of 10^{6o}C/sec [19]. The resulting samples are thin foils of about 2 cm in diameter, and 30 to 40 μ in thickness. Typical sample appearance is shown in Fig. 2. These foils are suitable for X-ray diffraction investigations as well as for magnetic and electrical measurements. The "lace like" edges of the foils can be directly used for transmission electron-microscopy, though for such investigations it is preferable to thin down the center of the foil, which is more representative of the bulk of the

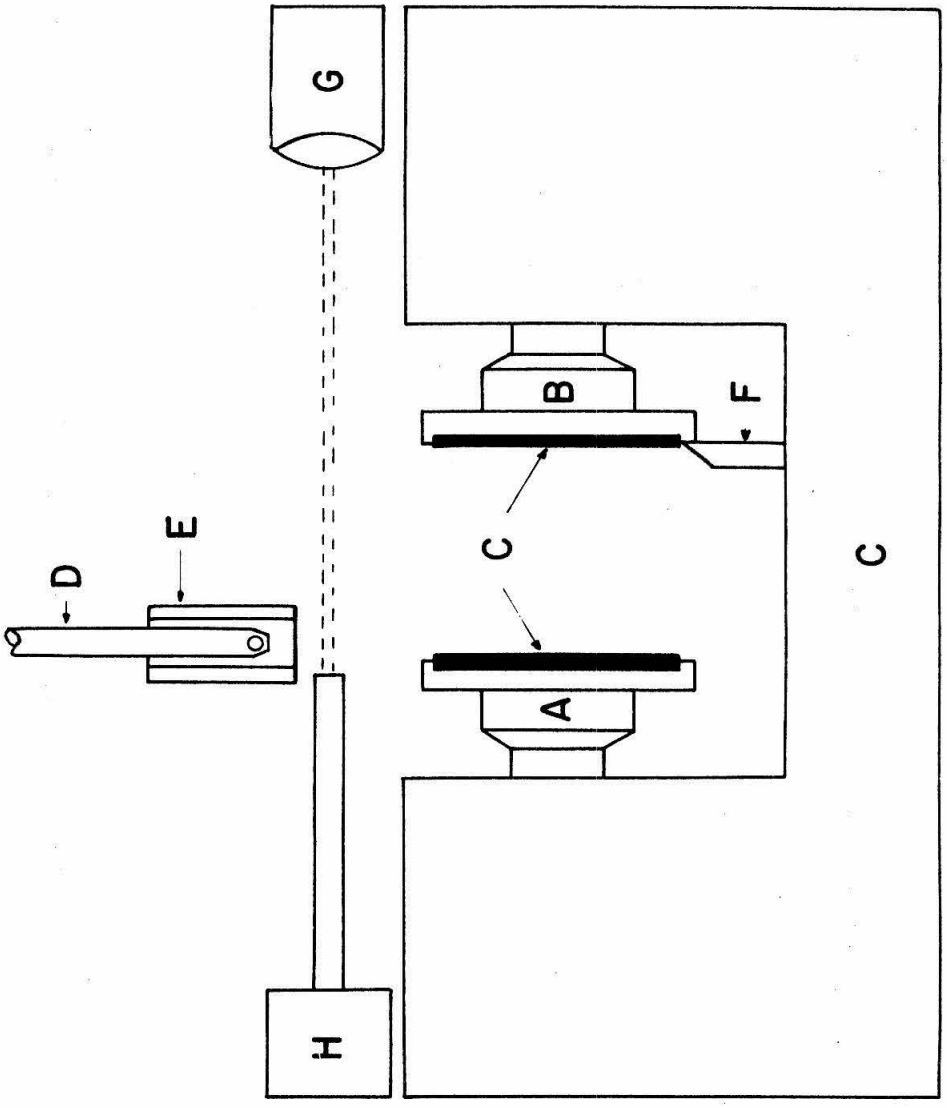

Fig. 1. "Piston and anvil" quenching device

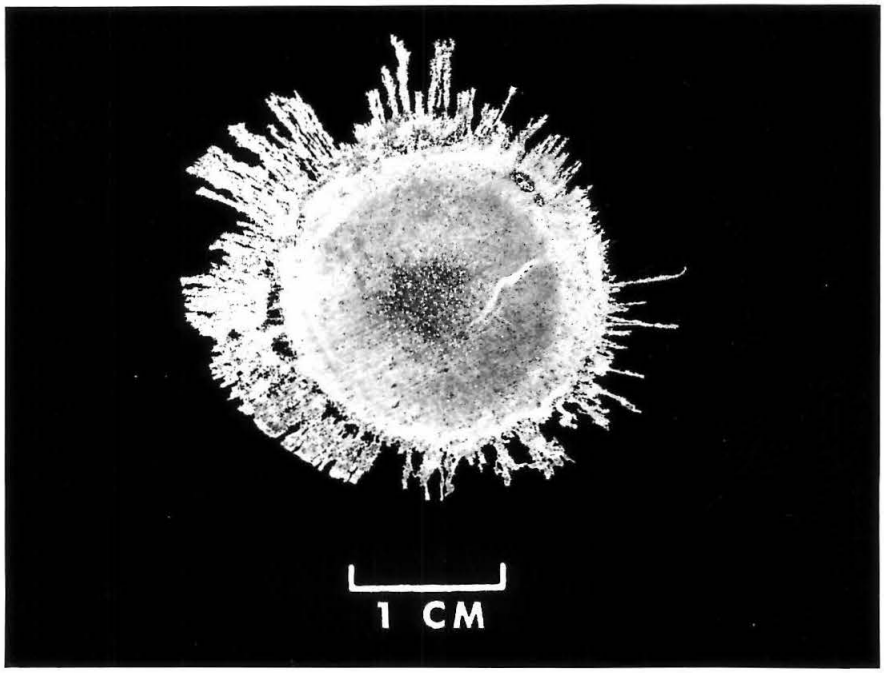

Fig. 2. Typical quenched foil appearance

quenched sample.

C. Verification of the structure of quenched specimens

The main drawback of the piston and anvil technique resides in the difficulty to duplicate exactly the rate of cooling from one sample to the other, though the order of magnitude is usually maintained. Consequently, each quenched foil was checked by X-ray diffraction with CuK_α radiation and step scanning (one point every $2\theta = 0.05^o$). The foils were then classified as "good", "doubtful" and "rejected". By "good" it was implied that the diffraction spectrum exhibited no definite crystalline peaks (Bragg reflections) but instead large amorphous bands. "Doubtful" were the samples with some evidence of small crystalline peaks superimposed on the amorphous bands. "Rejected" were samples exhibiting well-defined crystalline peaks. In some cases, it appeared possible to suppress the crystalline peaks by removing a small layer from the top of the foil (about 1 to 5 μ). This result seemed to indicate that some small crystals might have been nucleated on the surface of the quenched globule, during the early stages of the quenching. The lack of penetrating power of CuK_α radiation makes it particularly sensitive to surface effects on the quenched specimen. As expected, MoK_α radiation was less sensitive to the presence of such surface crystallites. Consequently, these two radiations were used concurrently to assert the truly amorphous character of the quenched specimens. Only some ranges of composition yielded amorphous diffraction bands. For Ni_x-$Pd_{80-x}P_{20}$ alloys

the range of x allowed varied from 13 to 73 (Pd consequently going from 67 to 7 atomic %) whereas for $Fe_xPd_{80-x}P_{20}$ the range appeared smaller with x varying from 13 to 44 (Pd consequently ranging from 67% to 36 atomic %).

The chemical composition of some of the samples was checked after quenching from the melt, and found very close to the initial composition before sintering. Table I gives the result of the chemical analysis performed on about 0.5 g to 1 g of quenched samples in each case, as well as the complete range of amorphous structure in both Fe-Pd-P and Ni-Pd-P systems.

TABLE I

AMORPHOUS ALLOYS IN THE IRON-PALLADIUM-PHOSPHORUS AND NICKEL-PALLADIUM-PHOSPHORUS SYSTEMS

Alloy designation	Initial composition before sintering (at.%)			Actual composition after quenching (at.%)		
	Ni	Pd	P	Ni	Pd	P
Ni_{13}-Pd_{67}-P_{20}	13	67	20	-	-	-
Ni_{32}-Pd_{53}-P_{15}	33	47	20	32.2	52.8	15.0
Ni_{43}-Pd_{37}-P_{20}	43	37	20	42.8	36.9	20.3
Ni_{53}-Pd_{27}-P_{20}	53	27	20	53.0	27.5	19.5
Ni_{63}-Pd_{17}-P_{20}	63	17	20	62.2	16.5	21.3
Ni_{73}-P_{7}- P_{20}	73	7	20	72.6	7.4	20.0
	Fe	Pd	P	Fe	Pd	P
Fe_{13}-Pd_{67}-P_{20}	13	67	20	-	-	-
Fe_{23}-Pd_{57}-P_{20}	23	57	20	-	-	-
Fe_{32}-Pd_{48}-P_{20}	33	47	20	32.4	47.6	20.0
Fe_{44}-Pd_{36}-P_{20}	43	37	20	43.9	35.7	20.4

III. STRUCTURE INVESTIGATION BY X-RAY DIFFRACTION

The amorphous Fe-Pd-P and Ni-Pd-P alloys under consideration allow rather large variations of composition. Interatomic distances, in these alloys, may be expected also to vary substantially with composition, yielding valuable comparisons with possible models. Diffraction studies with X-rays are particularly suitable for investigating disordered structures because of the informations they provide on interatomic distances as well as on the average ligancy of the atoms. The diffraction spectrum of amorphous alloys leads, after the appropriate corrections, to an interference function. This function can then be used, through a Fourier transformation, to yield an atomic or electronic radial distribution function. This is a rather straightforward procedure in a monoatomic system, but requires some approximations in binary and ternary systems. In any case, the numerical Fourier inversion of the diffraction data requires the use of a computer. The program used for the computation of the radial distribution functions (RDF) of Fe-Pd-P and Ni-Pd-P amorphous alloys is described in appendix II.

A. Scattering of X-rays by an amorphous solid

The total scattered intensity I_t (in arbitrary units), at a given angle, consists of the coherently scattered intensity I_c plus the modified intensity I_{in} (Compton scattering) and a background intensity I_b. All of these are also affected by a polarization factor $P(2\theta)$ and an absorption factor $A(2\theta)$. I_t is given by the following equation:

$$I_t(2\theta) = [I_c(2\theta) + I_{in}(2\theta) + I_b\ (2\theta)]P(2\theta)\ A(2\theta)$$

The most important term is the coherently scattered intensity I_c, which leads to the radial distribution function after the derivations described in the following paragraphs.

1. Scattering of X-rays by a polyatomic system

The formula for coherent scattering was given by Debye[20] under the assumption of equal probability for all orientations of any given interatomic vector. The scattered intensity, in electron units, is:

$$I_{ch}(s) = \sum_n \sum_m f_n f_m (\sin sr_{nm}/sr_{nm}) \qquad (1)$$

where $s = 4\pi \sin\theta/\lambda$ and r_{nm} is the interatomic distance between atom n and atom m, the summation being extended to the entire solid. Equation (1) can be rewritten as:

$$I_{ch}(s) = N\left[\sum_i x_i f_i^2 + \sum_i x_i \sum_{j\neq i} f_i f_j\ (\sin sr_{ij}/sr_{ij})\right] \qquad (2)$$

where N is the total number of atoms in the sample and x_i is the atomic concentration of element i. In the present case i goes from 1 to 3 (that is P, Ni, Pd) and j means all the atoms in the system except the chosen atom i. The atomic density functions $\rho_{ij}(r)$, which give the number of atoms of type j at a distance between r_1 and r_2 from an atom i, can be introduced through the integral $\int_{r_1}^{r_2} 4\pi r^2 \rho_{ij}(r)$ dr. The $\rho_{ij}(r)$ are obviously spherically symmetrical by definition,

which is consistent with the assumptions of the Debye's formula. Equation (2) becomes:

$$I_{ch}(s) = N\left[\sum_i x_i f_i^2 + \sum_i x_i f_i \sum_k \int_o^\infty 4\pi r^2 f_k \rho_{ik}(r)(\sin sr/sr)dr\right] \qquad (3)$$

where i = 1,2,3 and k = 1,2,3 also, with 1=P, 2=Ni and 3=Pd. Introducing ρ_o, which is the average density of atoms, it is possible to correct equation (3) in the following way:

$$I_{coh}(s)=N\left[\sum_i x_i f_i^2 + \sum_i \sum_k x_i f_i f_k \int_o^\infty 4\pi r\rho_{ik}(r)(\sin sr/sr)dr \right. \qquad (4)$$

$$\left. -(\sum_i x_i f_i)^2 \int_o^\infty 4\pi r\rho_o(\sin sr/sr)dr\right]$$

where the last term is the small angle scattering of the uniformly dense material and is not experimentally observed: hence, it must be subtracted from I_{ch} to give I_{coh}, which can then be related to the experimentally observed coherent intensity. Finally, the structure sensitive intensity is (per atom, in electron unit):

$$I_{coh}(s) = \sum_i x_i f_i^2 + \sum_i \sum_k x_i f_i f_k/s \int_o^\infty 4\pi r\rho_{ik}(r) \sin sr\, dr \qquad (5)$$

$$-(\sum_i x_i f_i)^2 \int_o^\infty 4\pi r\rho_o \sin sr\, dr$$

All the f_i and f_k are functions of s, so that all the integrals in the double sum depend on s in a different way. It is therefore impossible to get the distribution function as a result of a direct Fourier

inversion, as in the case of a monoatomic system. An approximate solution was provided by Warren[21] and has since been commonly used[22,23]. It consists of assuming that a reduced scattering factor $f_e(s)$ can be defined and used for different elements such that:

$$f_e(s) = f_i(s)/K_i$$

where K_i is approximately equal to Z_i, number of electrons of the scatterer i. A typical selection is:

$$f_e(s) = \sum_i x_i f_i(s) / \sum_i x_i Z_i$$

This is usually a rather good approximation, as it was found in the present investigation. Equation (5) becomes:

$$s(I_{coh}(s) - \sum_i x_i f_i^2)/f_e^2 = \sum_i x_i \sum_k K_i K_k \int_o^\infty 4\pi r \rho_{ik}(r) \sin sr \, dr$$

$$- (\sum_i x_i K_i)^2 \int_o^\infty 4\pi r \rho_o \sin sr \, dr \qquad (6)$$

This equation shows that $s(I_{coh}(s) - \sum_i x_i f_i^2)/f_e^2 = sI(s)$ is the Fourier transform of:

$$4\pi r(\sum_i x_i \sum_k K_i K_k \rho_{ik}(r) - (\sum_i x_i K_i)^2 \rho_o)$$

Performing the Fourier transformation leads to:

$$4\pi r \sum_i x_i \sum_k K_i K_k \rho_{ik}(r) = 4\pi r (\sum_i x_i K_i)^2 \rho_o + 2/\pi \int_o^\infty sI(s) \sin sr \, ds \qquad (7)$$

Let:

$$W(r) = 4\pi r(\sum_i x_i \sum_k K_i K_k \rho_{ik}(r) - (\sum_i x_i K_i)^2 \rho_o) \qquad (8)$$

The maxima of the function W(r) will correspond to the average interatomic distances. However, the interpretation of these interatomic distances will require a more careful look at the distribution function, since it is a weighed sum of partial distribution functions.[24].

2. Radial distribution function, interatomic distances and coordination numbers

Equation (8) can be rewritten as:

$$W(r) = 4\pi r(\rho(r) - \rho_o)\ (\sum_i x_i K_i)^2 \text{ with } \begin{cases} \rho(r) = \sum_i \sum_k \omega_{ik}\rho_{ik}(r) \\ \omega_{ik} = x_i K_i K_k / (\sum_i x_i K_i)^2 \end{cases} \quad (9)$$

Hence $\rho(r)$ appears as an atomic density function which is simply the weighed sum of all the partial density functions $\rho_{ik}(r)$. The actual radial distribution function is obtained by multiplying equation (7) by r so as to yield:

$$4\pi r^2 (\sum_i x_i K_i)^2\ \rho(r) = 2r/\pi \int_o^\infty s\, I(s) \sin sr\, ds + 4\pi r^2 (\sum_i x_i K_i)^2 \rho_o \quad (10)$$

The interatomic distances can be obtained by considering the maxima of W(r), which is the Fourier transform of s I(s)[6,23]. It is W(r), and not the final radial distribution function rW(r), which yields the actual interatomic distances, as its peaks are left symmetrical and unshifted by the use of modification factors such as $1/f_e^2(s)$ or a damping factor $\exp(-as^2)$ in the function s I(s). This also is a consequence of the definition of $\rho(r)-\rho_o$[25]. However, some authors

have sometimes considered the maxima of $r^2W(r)$ as meaningful[26], especially when the peaks of the RDF appear rather symmetrical. These can be related to the center of the shell represented by the peak and the mean interatomic distances given by this procedure will also be considered. If there is a discrete peak in the RDF between r_1 and r_2, from the definition of $\rho_o, \rho_{ik}(r)$ and $\rho(r)$, the integral $\int_{r_1}^{r_2} 4\pi r^2 \rho(r)\, dr$ can be related to the number of atoms at distances between r_1 and r_2 from an atom taken as origin. Actually, the meaning of this number appears more clearly by writing ρ (r) explicitly:

$$A = \int_{r_1}^{r_2} 4\pi r^2 \rho(r) dr = \sum_i \sum_k \omega_{ik} \int_{r_1}^{r_2} 4\pi r^2 \rho_{ik}(r)\, dr$$

Let $\int_{r_1}^{r_2} 4\pi r^2\, \rho_{ik}(r)\, dr = n_{ik}$, that is the number of atoms k at a distance between r_1 and r_2 from an atom i. Then

$$A = \sum_i \sum_k \omega_{ik}\, n_{ik} \qquad (11)$$

In this expression, the n_{ik} are the coordination numbers, A is an experimental quantity equal to the area under the peak divided by $(\sum_i x_i K_i)^2$, and the ω_{ik} can be computed from equation (9). From here on, the n_{ik} can be obtained through certain assumptions or approximations. A rather frequent case is the one for which the peak in the RDF is believed to be only due to ij pairs. Equation (11) then reduces to:

$$A = (n_{ij}\, x_i + n_{ji}\, x_j)\, K_i K_j / (\sum_i x_i K_i)^2$$

which, if there is no short range order ($n_{ij}/x_j = n_{ji}/x_i$), reduces further to:

$$A = 2\, x_i\, n_{ij}\, K_i\, K_j / (\sum_i x_i\, K_i)^2$$

Another assumption (which will be used later) is that of equal atomic densities of j and k around atoms j and atoms k. Namely:

$$\rho_{jk} + \rho_{jj} = \rho_{kj} + \rho_{kk}$$

$$n_{jj} + n_{jk} = n_{kj} + n_{kk} = n$$

Then the following relationships are verified:

$$n/(x_j + x_k) = n_{jk}/x_k = n_{kj}/x_j = n_{jj}/x_j = n_{kk}/x_k$$

It can be noticed that $n_{kj} = n_{jj}$ and $n_{jk} = n_{kk}$, which is consistent with the hypothesis of no short range order for atoms j and k. Equation (11) becomes then (assuming that only j and k atoms are involved):

$$A = \frac{n(x_j\, K_j + x_k\, K_k)^2}{(x_j + x_k)(\sum_i x_i\, K_i)^2} \qquad (12)$$

One can therefore obtain from the area under the RDF curve, an average coordination number n for the pairs (j or k) - (j or k)[25]. This reduced formula (12) will be used later for Ni-Pd or Fe-Pd type pairs. In the cases of overlapping distributions, assumptions are made on the relative importance of, for instance ρ_{ij} and ρ_{jk}, as it will appear later

in the case of phosphorus as i, and j and k as Ni and Pd (or Fe and Pd).

3. Direct interpretation of the diffraction spectrum

The direct interpretation of the broad diffraction peaks has sometimes been attempted, but it has often been a deceiving, if not completely erroneous[27,28], procedure. This can be readily seen from the Debye's formula giving the coherently scattered intensity (equation 1):

$$I_{ch}(s) = \sum_m \sum_n f_m(s)\, f_n(s)\, (\sin sr_{mn}/s\, r_{mn}) \qquad (1)$$

where the summation is extended to all the atoms of the sample, and r_{mn} is the interatomic distance between atom m and atom n. To obtain the maxima of $I_{ch}(s)$, equation (1) must be differentiated, which yields a complicated function depending on all the r_{mn}. Some simplifications can be made, like neglecting the variation of the scattering factor with s and considering only one interatomic distance r_1[22,29]. Then : $4\pi \sin\theta_1 r_1/\lambda = A_1$ where $A_1 = 4\pi/E$, E = 1.627 is the Ehrenfest's constant and $4\pi \sin\theta_1/\lambda = s_1$ is the value of s for which $I_{ch}(s)$ has its first maximum. This relation is very approximate and a different approach seems preferable. The interference function I(s), defined in III-A.1, is a function of the product sr only. Suppose that the first maximum of I(s) occurs for $s = s_1$ for a given alloy. Then s_1 verifies $s_1\, r_{mn} = A_{mn}$, with a different A_{mn} for each r_{mn}. Suppose also that all the r_{mn} vary with composition according to the same law, for instance all the ratios r_{mn}/r_{pq} stay constant. For another alloy, let $r'_{mn} = r_{mn}\,(1+a)$, and a be a small percentage. Then I(s) will have

its first maximum for $s_1' = s_1/(1+a)$ and s_1' will satisfy $s_1' r'_{mn} = A_{mn}$ for all m and n. If such an hypothesis stands, it will then be sufficient to obtain only one r_{mn} and the corresponding s_1; this will give A_{mn}, and any r'_{mn}, provided s_1' is known. Another immediate consequence of such a situation will be the invariance of the ratios s_1/s_2, s_1/s_3, etc. from one composition to the other. Reciprocally, if these ratios are constant, it will be a strong indication of the invariance of the ratios r_{mn}/r_{pq} from one composition to the other. The direct interpretation may consequently yield valuable information on the ratios of the interatomic distances, and on the interatomic distances provided some of the interatomic distances are already known through other channels such as the Fourier inversion of the interference function, leading to the radial distribution function.

B. Experimental procedure

The thickness of the foils obtained by the piston and anvil quenching method varied between 30 and 45 μ. In order to avoid any angular dependent absorption correction, several foils were stuck together with duco-cement on a bakelite substrate. Table II gives the mass absorption coefficients for the compositions investigated, for both CuK_α and MoK_α radiation. It can be seen from the values of μ/ρ, and the knowledge of the density of the alloys (around 9 g/cm^3), that only three or four foils were necessary in the case of MoK_α radiation, and more than necessary for CuK_α radiation, to eliminate the necessity of including an absorption factor in the present analysis.

TABLE II

MASS ABSORPTION COEFFICIENTS OF THE Fe-Pd-P AND Ni-Pd-P ALLOYS FOR CuK_α AND MoK_α RADIATIONS

Composition (at.%)			CuK_α $\mu/\rho(cm^2/g)$	MoK_α $\mu/\rho(cm^2/g)$
Ni	Pd	P		
13	67	20	183.0	27.2
32	53	15	159.7	30.1
43	37	20	138.9	32.4
53	27	20	120.8	34.6
63	17	20	97.6	37.1
73	7	20	72.7	40.1
Fe	Pd	P		
13	67	20	207.2	26.3
23	57	20	215.4	27.1
32	48	20	224.0	27.9
44	36	20	236.4	29.1

The specimens so prepared were mounted on the sample holder of a G.E. diffractometer with vertical axis. Two similar units were used, one for MoK_α radiation and the other for CuK_α radiation. The units were run under 45 kV and 38 mA, to provide a sufficient intensity. The incident beam was collimated by a system of slits which allowed different beam divergences. A LiF monochromator with double curvature was placed in the diffracted beam to eliminate K_β, the white spectrum, the fluorescent scattering[30] and most of the incoherent scattering, though not completely[31,32]. A combination scintillation counter and pulse height analyzer was used as a detector. For the experiments performed with MoK_α leading to the determination of radial distribution functions, the pulse height analyzer was adjusted to eliminate $\lambda/2$, which is let through the monochromator. The contribution of intensity due to $\lambda/2$ was checked to be of the order of 15 counts/sec to 10,000 counts/sec for K_α, which is indeed negligible (in the absence of pulse height analyzer, the $\lambda/2$ contribution was still small, though about 10 times the above value).

Since a complete scanning of the diffraction pattern of an amorphous alloy required as long as ten days, the reliability of the data depended on the stability of the intensity of the incident X-rays, as well as that of the counter. First, the stability of the counter was checked by using a radioactive source. Different levels, in the range of intensity used for the diffraction experiments, were checked. These tests showed stability within 1% for periods of time up to 120 hours. The same experiments were repeated with the MoK_α radiation

and an amorphous Ni-Pd-P specimen. The same levels of intensity were again checked and no appreciable fluctuations recorded for periods of time up to 120 hours. For MoK_α diffraction experiments, the experimental data were obtained with a rate of scanning of $0.02^\circ/100$ sec in 2θ. A printer gave a reading of the accumulated counts every 200 seconds, which yielded 25 prints/degree (2θ). The beam divergences used were: For 2θ going from 2° to 20°: 0.1° divergence. Restart at $2\theta = 10^\circ$ with 1° divergence and match curves on common range of 2θ (10° to 20°) until $2\theta = 62^\circ$. Restart from 48° with 3° divergence, with one data point every 1000 sec up to 160° and matching of the curves on the range 58° to 62°.

C. Treatment of data

In order to determine the coherent intensity in electron units, the experimentally obtained intensity $I_t(2\theta)$ must be corrected for absorption, polarization, fluorescent scattering, Compton scattering and background. These corrected data must then be scaled to the units of $\sum_i x_i f_i^2$ for the computation of the interference function. Since the specimens used for recording the diffraction patterns could be considered as infinitely thick, the absorption correction is independent of angle and can be included in the scaling factor. The polarization correction is angle dependent and results in dividing the experimental intensity by a factor P (2θ) such that:

$$P(2\theta) = (1 + \cos^2 2\beta \cos^2 2\theta)/(1 + \cos^2 2\beta),$$

where β is the Bragg angle for the radiation considered, incident on a (200) plane of LiF. Actually, one need only take into account the angular dependence of $P(2\theta)$ and the factor $1/(1 + \cos^2 2\beta)$ can be included in the scaling constant.

In the present investigation, the fluorescent radiation is practically negligible, as a consequence of the presence of the monochromator in the diffracted beam, as well as the use of a pulse-height analyzer with the counter. The use of a monochromator in the diffracted beam introduces, however, some difficulties as far as the evaluation of the Compton (or incoherent) scattering is concerned[31]. This problem has been rather thoroughly studied by Ruland[32]. Ruland showed that the elimination of the incoherent scattering requires the evaluation of an attenuation function $Q(2\theta)$ (or $Q(s)$, where $s = 4\pi \sin\theta/\lambda$). The determination of $Q(s)$ requires a knowledge of the "pass-band" of the monochromator. The value of $Q(s)$ decreases with increasing s to become essentially negligible above a value of s which depends on the integral width of the pass-band. However, $Q(s)$ depends on several unknown parameters, and we will only be able to evaluate $Q(s)\, I_{in}(s)$, where $I_{in}(s)$ is the Compton scattering, by approximations which will be justified by the good fitting of $\alpha\, I_c(s)$ to $\sum_i x_i f_i^2$, as well as by the behavior of the Fourier transform of $s\, I(s)$ in the region in which $r < 2\text{Å}$. Experiments were performed with the same apparatus on a monocrystal of silicon, and a qualitative shape of the variation of $Q(s)\, I_{in}(s)$ was deduced from these experiments. A similar variation was assumed to hold for the

Fe-Pd-P and Ni-Pd-P alloys, and a trial and error process was used to adjust the contribution of the incoherent scattering (cr. III-D). The background electronic noise was substracted from the measured intensities. For 2θ angles less than about 10^{o}, the background increased with decreasing angle because of the divergence of the incident beam. Measurements below 10^{o} were considered unreliable and the experimental intensity curve was extrapolated to zero at $2\theta = 0^{o}$.

The scaling of the experimental data to electron units was performed on the coherent fraction of the experimental scattered intensity. The atomic scattering factors were corrected for anomalous dispersion. That is:

$$f = f_o + \Delta f' + i\,\Delta f''$$

and

$$|f|^2 = (f_o + \Delta f')^2 + (\Delta f'')^2$$

The values of f_o, $\Delta f'$ and $\Delta f''$ were taken from reference 33 and checked with the values given in the International Tables for X-ray Crystallography[34]. The experimental corrected intensity $I_c(s)$ was scaled by making use of the fact that $I_{coh}(s) - \sum_i x_i f_i^2$ converges toward 0 for large enough s (that is, interatomic interferences become negligible at high angles). This procedure has been most commonly used by earlier investigators of liquid and amorphous structures[25,35] and is quite appropriate when experimental data can be obtained up to $s = 10\ \text{Å}^{-1}$ and above. This is the situation with MoK_α radiation, for which s goes up to $17.4\ \text{Å}^{-1}$ for $2\theta = 160^{o}$. A fitting factor α can be

found such that: α (s) $I_c(s) = \sum_i x_i f_i^2(s)$ for s = 13 $\mathring{A}^{-1}$ to s = 17.4 $\mathring{A}^{-1}$. Provided all the corrections have been done properly, the fitting is quite good. One must especially look for drifts in α (s) as indications of errors in $I_c(s)$. An average value is taken for α at the conclusion of the scaling process. The function s I(s) which is then going to be Fourier transformed is finally: $sI(s) = s(\alpha I_c(s) - \sum_i x_i f_i^2(s))/f_e^2(s)$.

The Fourier inversion of s I(s) was done on a 7094 IBM computer through a program written in Fortran-IV language (see Appendix II). The intervals in s values were taken small enough so that $\Delta s \leq \pi/r_{max}$, r_{max} being the distance beyond which the RDF has no significant variations[36]. In the present case, taking $r_{max} \approx 20$ $\mathring{A}$, led to $\Delta s \leq 0.16$ $\mathring{A}^{-1}$ which was well satisfied over the whole range of s values. Plots of the fitting of $I_c(s)$ to $\sum_i x_i f_i^2$, of I(s), of the Fourier transform $4\pi r(\rho(r)-\rho_o)(\sum_i x_i K_i)^2 = W(r)$ and of the final RDF were provided together with the printed output of the program.

D. Error treatment

Several causes of errors can greatly diminish the amount of information yielded by the radial distribution function, especially with respect to the determination of coordination numbers. These errors are mainly normalization (or scaling) errors, errors on the scattering factors and termination errors. Several authors have discussed the errors involved in the determination of radial distribution functions, but reference is mainly being made here to the extensive review of Kaplow et al.[30]. The causes of errors in the RDF (or in

W(r), the Fourier transform of s I(s)) are numerous and are always present. However, each type of error usually has some specific features which make it recognizable. Also, the relationship of Fourier transformation which relates s I(s) and W(r) is of great use, as the back Fourier transformation of corrected W(r) can be used to check s I(s) and eventually trace down the range of erroneous data. In the following argument, $F(s) = s\ I(s)$ and $W(r) = 2/\pi \int_o^\infty F(s) \sin sr\ ds$, as previously defined.

Considering first the normalization error, let the error on α be $\Delta\alpha$. The resulting error $\Delta F(s)$ on F(s) is then:

$$\Delta F(s) = s\ \Delta\alpha\ I_c(s)/f_e^2$$

or

$$\Delta F(s) = (\Delta\alpha/\alpha)F(s) + s\ (\sum_i x_i\ f_i^2/f_e^2)\Delta\alpha/\alpha$$

The resultant $\Delta W(r)$ is then the true W(r) multiplied by $\Delta\alpha/\alpha$, plus the transform of a ramp of slope $(\sum_i x_i\ K_i^2)\ \Delta\alpha/\alpha$. The transform of such a ramp has the form:

$$\Delta W(r) = \Delta\alpha/\alpha\ (\sum_i x_i K_i^2) \left[\sin s_m\ r/r^2 - s_m \cos s_m r/r \right]$$

where s_m is the upper boundary of integration in the Fourier integral. The analytical behavior of $\Delta W(r)$ with r is shown in Fig. 3, for Ni_{32}-Pd_{53}-P_{15} as an example ($\Delta\alpha/\alpha = 0.01$).

The effects of errors on the scattering factors were specifically studied in reference 30. The present case, however, is more complicated due to the use of the reduced scattering factor $f_e(s)$. This is

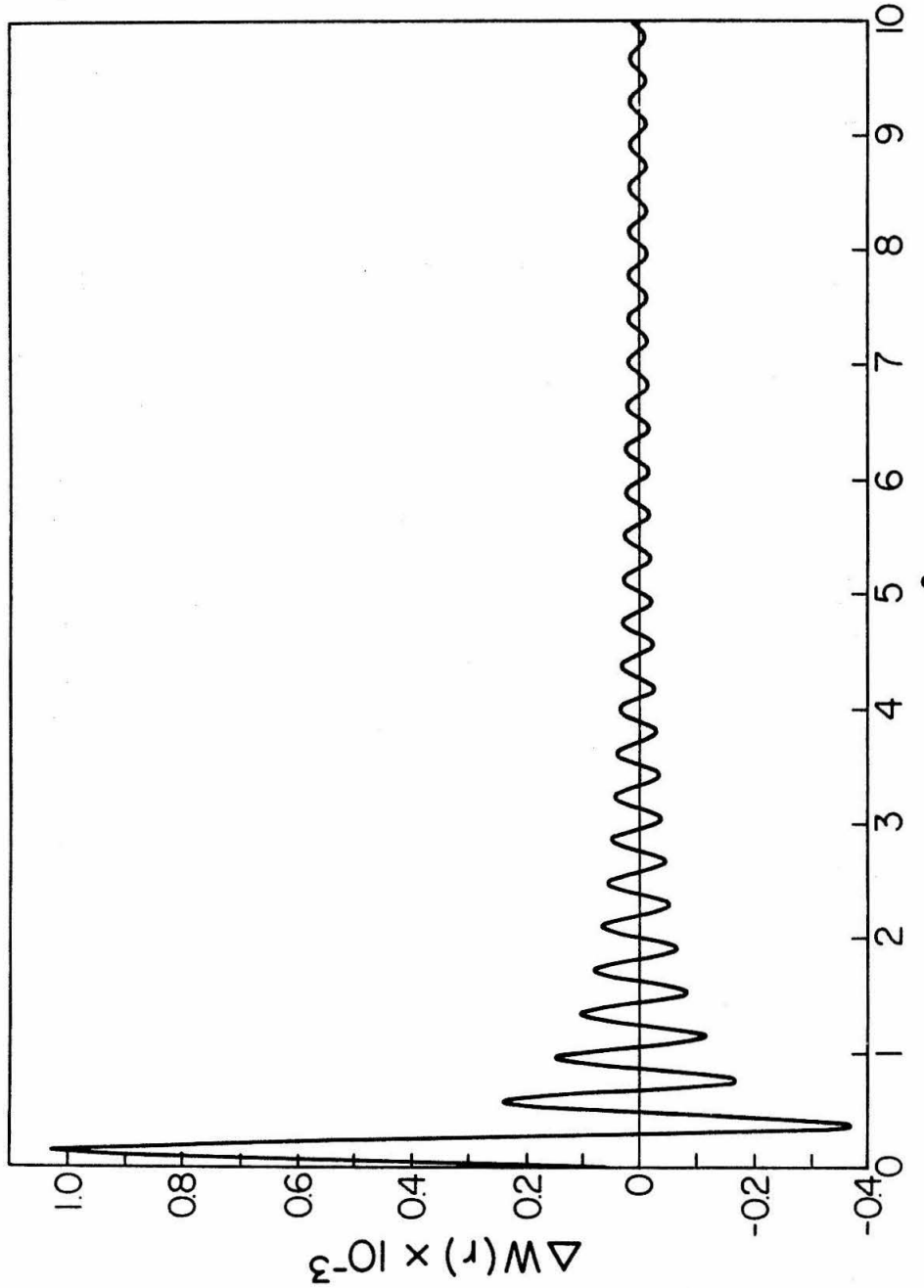

Fig. 3. Error on W(r) due to 1% scaling error for a Ni_{32}-Pd_{53}-P_{15} alloy.

only an approximation and, consequently, will necessarily generate some error. An error of the form $\Delta F(s) = \epsilon(s)\, s\, \alpha\, I_c(s)/f_e^2(s)$ is rather likely, with $\epsilon(s)$ being a slowly varying function of s. The error $\Delta F(s)$ can also be expressed as $\Delta F(s) = \epsilon(s)\, F(s) + (\sum_i x_i K_i^2)s\, \epsilon(s)$. The first term of the transform of $\Delta F(s)$ will consist of the convolution of the cosine transform of $\epsilon(s)$ with the true W(r), which, if $\epsilon(s)$ varies slowly, will only be comparable to a change of scale. The second term will, as in the case of normalization error, give a transform with its most significant features obtained for small value or r, and dying off rather rapidly.

Termination errors arise from termination of experimental data at $s = s_m$ instead of $s = \infty$. They are maximum around the main peak portion of the RDF[23,37] and usually quite small if s_m is large enough (which is our case, with $s_m = 17.4$ Å^{-1} for MoK_α radiation). But the use of $f_e^2(s)$ in the interference function I(s) amplifies the oscillations of s I(s) at large values of s and consequently increases the termination errors.

The procedure of error corrections made use of the fact that, physically, no interatomic distances smaller than approximately 2 Å can exist. Consequently, for $r < 2$ Å, the function W(r) should be equal to $-4\pi r\rho_o(\sum_i x_i K_i)^2$. Such a function is a straight line in a plot of W(r) versus r. Any deviation from such a straight line is an indication of error and it is possible to recognize the type of error involved. In the present investigation, the errors were found to consist mainly of scaling errors and errors at large values of s, due

to the sharpening effect of $f_e^2(s)$. A commonly used procedure to reduce the influence of errors at large s is the use of an artificial "temperature" factor $\exp(-as^2)$, so that the function which is Fourier transformed is $s\,I(s)\exp(-as^2)$. The value of a is usually chosen of the order of 0.01, so that the exponential factor does not affect too much the main peaks of $s\,I(s)$. The use of a temperature or damping factor whereas it compensated spurious details due to errors at high s, also decreased the resolution of the final W(r) and rW(r) though it did not affect the location of the maxima of W(r) and the area under the peaks,[6,23] but simply modified the peaks width and height. The scaling errors, which could sometimes be large due to an unprecise knowledge of the incoherent scattering going through the monochromator, were corrected in the following way: a trial and error method was used to adjust the contribution of the incoherent scattering such that $\alpha\, I_c(s)$ would give a good fitting along $\sum_i x_i f_i^2$ and the final transform W(r) would show only reduced oscillations along the straight line $-4\pi r\rho_o(\sum_i x_i K_i)^2$. When the spurious details at small r became small enough to indicate no important error on α, the procedure was stopped. In some cases, an additional verification was performed: the small r part of W(r) was approximated to a straight line and a Fourier inversion performed giving $F'(s) = \int_o^{r_m} W(r) \sin sr\, dr$ If F'(s) was reasonably close to F(s) (apart from an inevitable termination effect)W(r) and subsequent r W(r) were the accepted distribution functions for the composition investigated. An additional error was

always present, due to the uncertainty on ρ_o, the atomic density. From experimental measurements, the value of ρ_o was known with an uncertainty of $\pm$ 5%.

E. Results

1. Nickel-palladium-phosphorus alloys

Six different compositions were investigated (cf. Table I). For two of them, MoK_α radiation was used and the diffraction patterns were analyzed to yield electronic radial distribution functions. For the other compositions, CuK_α radiation was used for the diffraction experiments and the pattern was restricted to the first amorphous band.

Diffraction experiments with MoK_α radiation were performed on $Ni_{32}Pd_{53}P_{15}$ and $Ni_{53}Pd_{27}P_{20}$ alloys. The uncorrected diffraction pattern for $Ni_{32}Pd_{53}P_{15}$ is shown in Fig. 4, as an example. Several amorphous bands (or peaks) are easily recognizable. A comparison of the diffraction patterns of these two Ni-Pd-P amorphous alloys reveals that the amorphous peaks are displaced towards larger values of 2θ with increasing percentage of nickel. The fitting to $\sum_i x_i f_i^2$ of the corrected coherent intensity is shown in Fig. 5 and the resulting interference function I(s) is plotted in Fig. 6 (in both cases for Ni_{32}-Pd_{53}-P_{15}, as an example). All the numerical results for both Ni_{32}-Pd_{53}-P_{15} and Ni_{53}-Pd_{27}-P_{20} are gathered in Table III, concerning both the actual diffraction spectrum and the interference function. The Fourier inversion of $F(s) = s\,I(s)$ was performed according to the

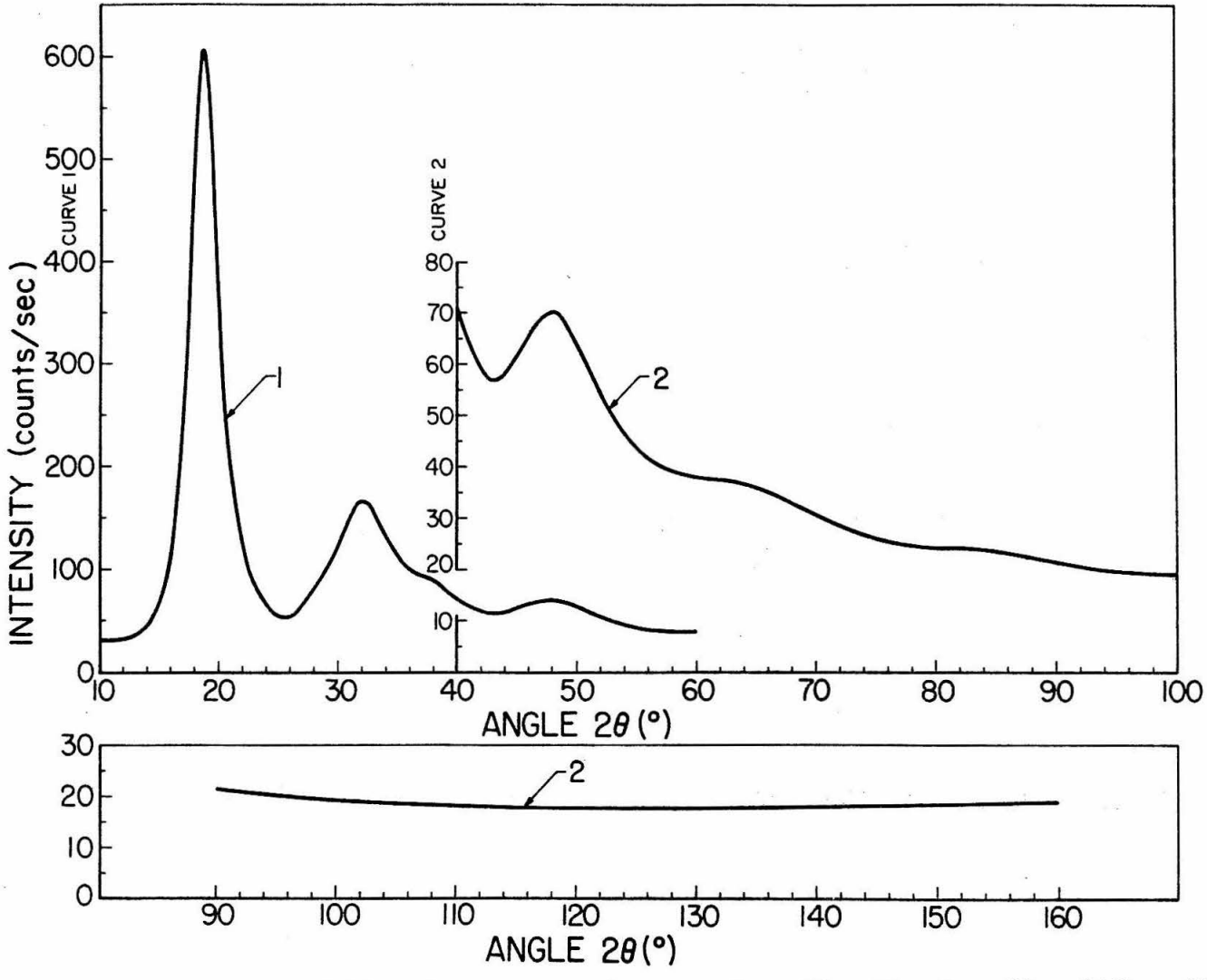

Fig. 4. Experimental diffraction pattern of an amorphous Ni_{32}-Pd_{53}-P_{15} alloy (MoK_{α} radiation)

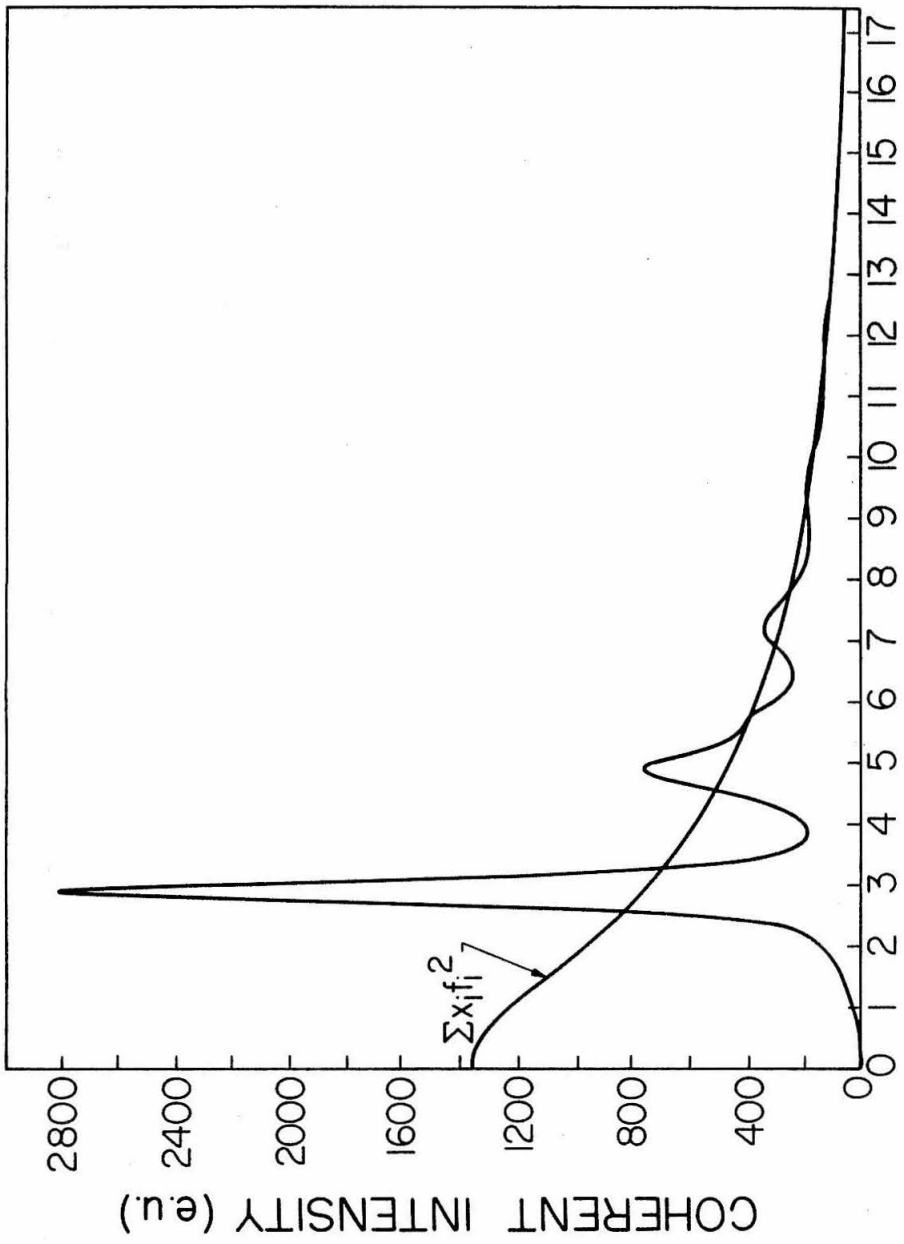

Fig. 5. Coherently scattered intensity from an amorphous Ni_{32}-Pd_{53}-P_{15} alloy (MoK_α radiation).

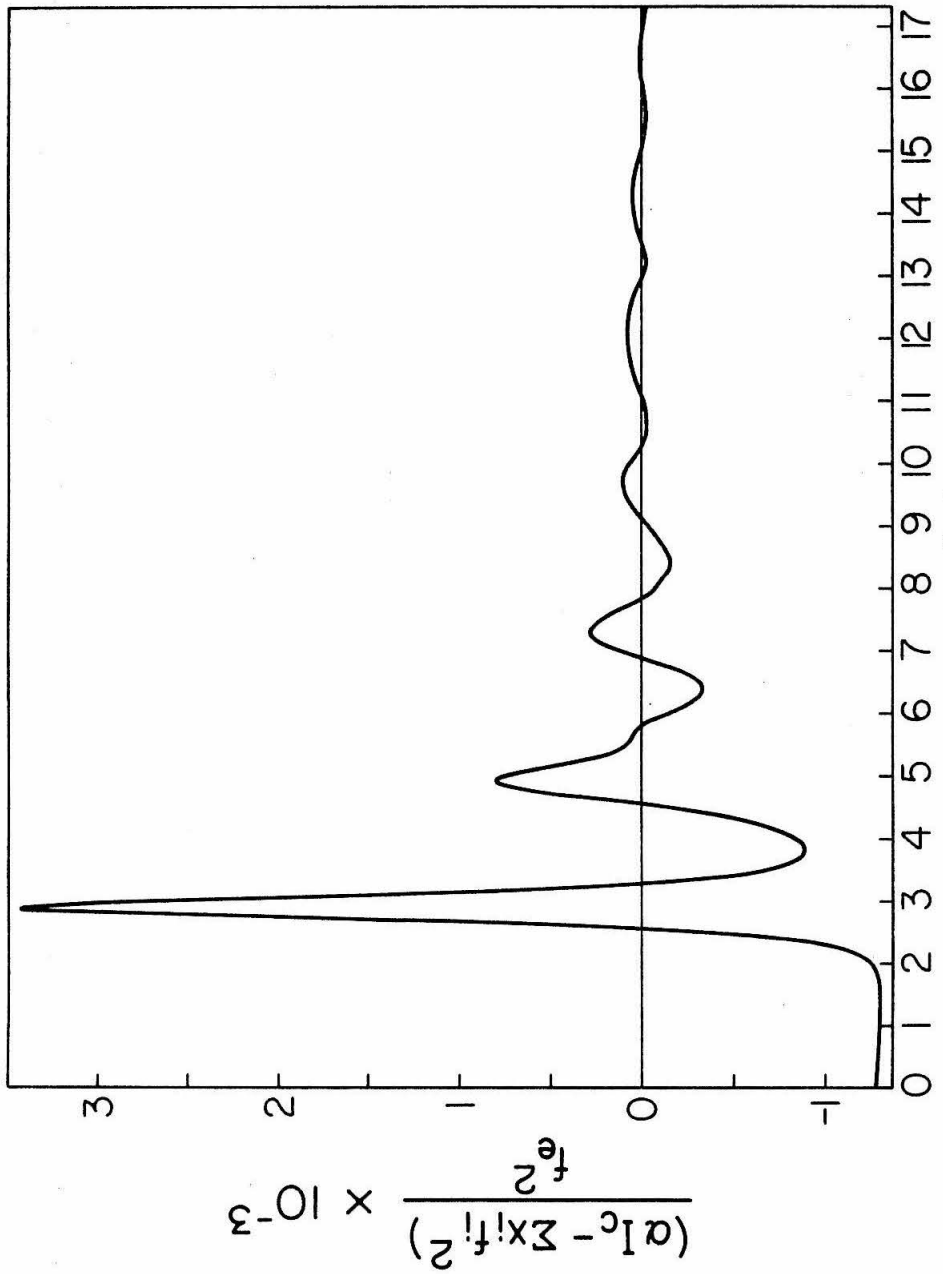

Fig. 6. Interference function I(s) for an amorphous Ni_{32}-Pd_{53}-P_{15} alloy (MoK_α radiation).

TABLE III

VALUES OF 2θ AND s CORRESPONDING TO THE TWO FIRST PEAKS OF THE DIFFRACTION PATTERNS AND TO THE MAXIMA OF THE INTEREFERENCE FUNCTIONS (MoK_α RADIATION)

Composition		Ni_{32}-Pd_{53}-P_{15}	Ni_{57}-Pd_{23}-P_{20}
First peak	2θ (deg.)	18.70	19.35
	s ($Å^{-1}$)	2.888	2.961
Half width of first peak (2θ)		2.95	3.25
Second peak	2θ (deg.)	32.15	33.18
	s ($Å^{-1}$)	4.90	5.07
Successive maxima of I(s)			
1st		2.890	2.980
2nd		4.92	5.11
3rd		7.32	7.50
4th		9.66	9.87

description given in III-C. The resulting functions W(r) and r W(r) are shown in Fig. 7 and 8 for the Ni_{32}-Pd_{53}-P_{15} alloy, and in Fig. 9 for Ni_{53}-Pd_{27}-P_{20}. The interference function of Ni_{53}-Pd_{27}-P_{20} was multiplied by a temperature factor $\exp(-0.01\ s^2)$ (cf. III-D) to correct the oversharpening effect of $1/f_e^2$. The radial distribution function of Ni_{53}-Pd_{27}-P_{20} shows consequently less details than the RDF obtained for Ni_{32}-Pd_{53}-P_{15} which did not require the use of a temperature factor. The upper value in r was chosen to be 10 Å for practical purposes, since a sufficient number of interatomic distances are smaller than 10 Å. In both cases, the theoretical straight line $-4\pi r\rho_o \left(\sum_i x_i K_i\right)^2$ is shown on the graphs of W(r). Spurious oscillations can be observed for $r < 2$ Å, on all W(r) plots, corresponding to remaining small errors. Their amplitude is however small and, as it can be seen on the plot of W(r), these spurious oscillations seem to be damped rather fast with increasing r. As it was explained in III-A.2, the interatomic distances can be either related to the radius of symmetry r of the function W(r) or to the radius r' corresponding to the maximum of r W(r). Both r and r' are given in Table IV. The third peaks are rather ill defined and the values given are only approximate.

The area under the first peak of the RDF has been evaluated in each case by using a gaussian approximation. This procedure, as it appears in Fig. 10 for Ni_{32}-Pd_{53}-P_{15} as an example, gives a satisfactory fitting of the first peak of the RDF[6,26]. In addition, the width of the peak at half height gives an indication on the mean square

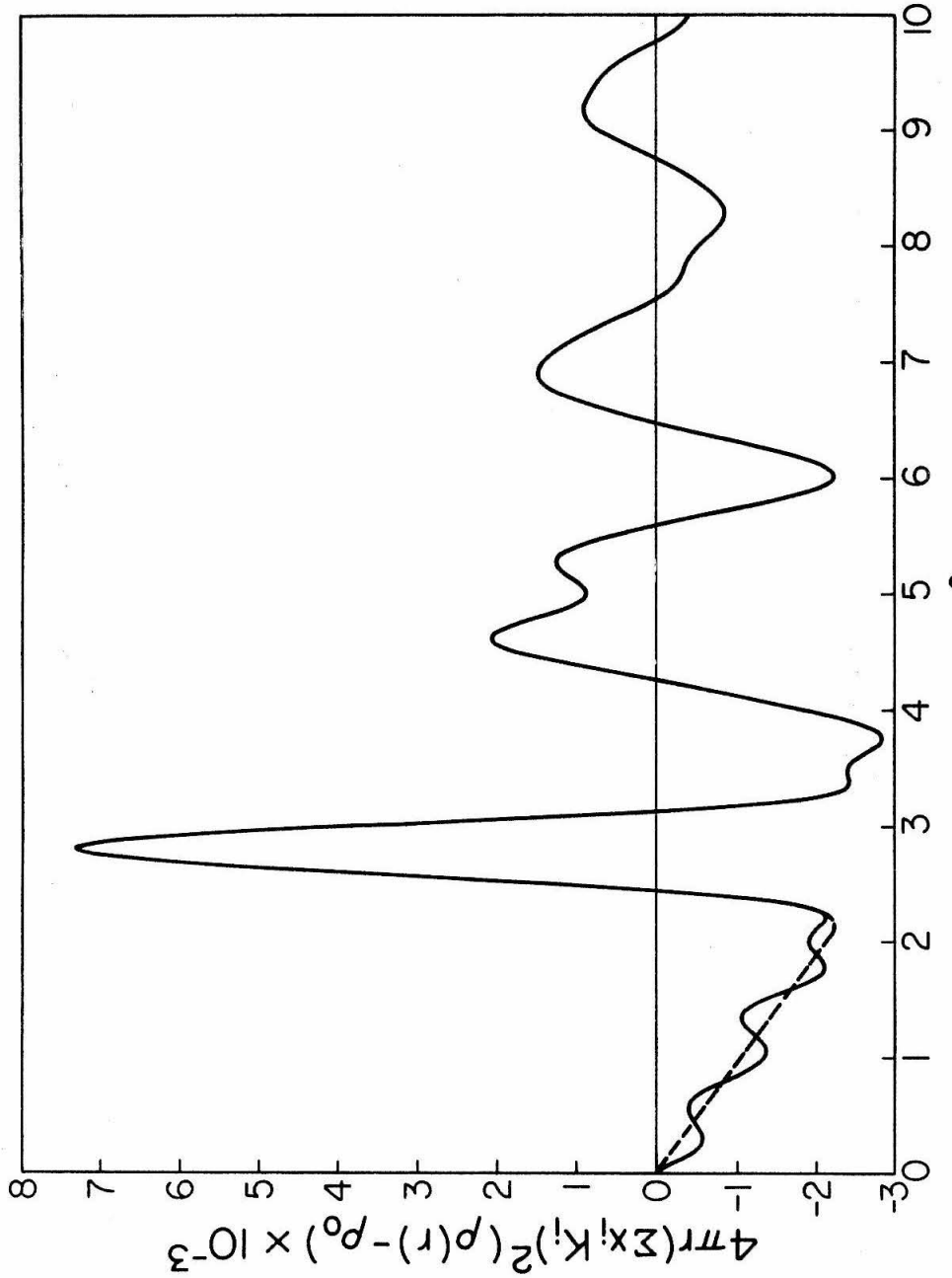

Fig. 7. Distribution function W(r) for an amorphous Ni_{32}-Pd_{53}-P_{15} alloy.

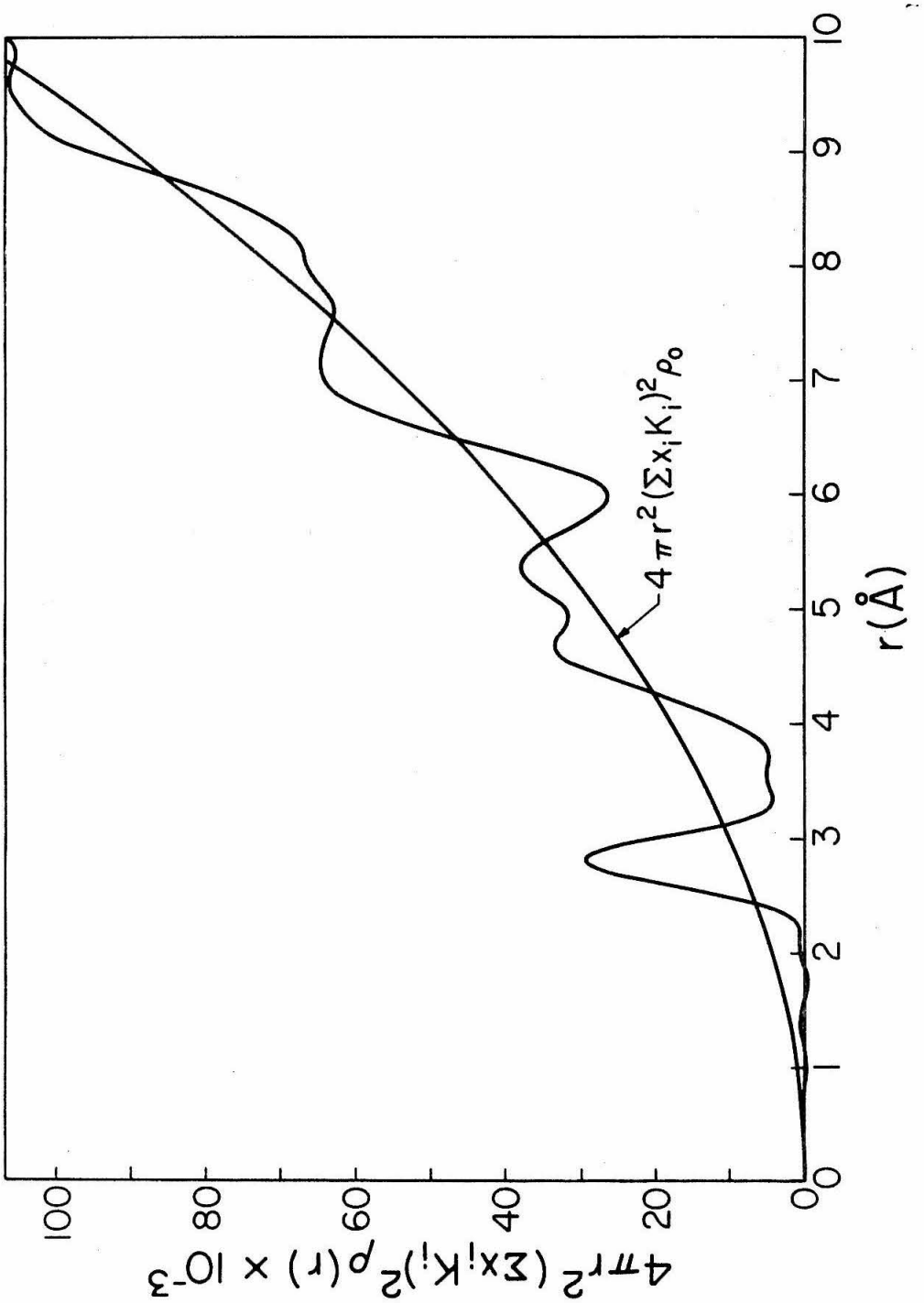

Fig. 8. Radial distribution function for an amorphous Ni_{32}-Pd_{57}-P_{15} alloy.

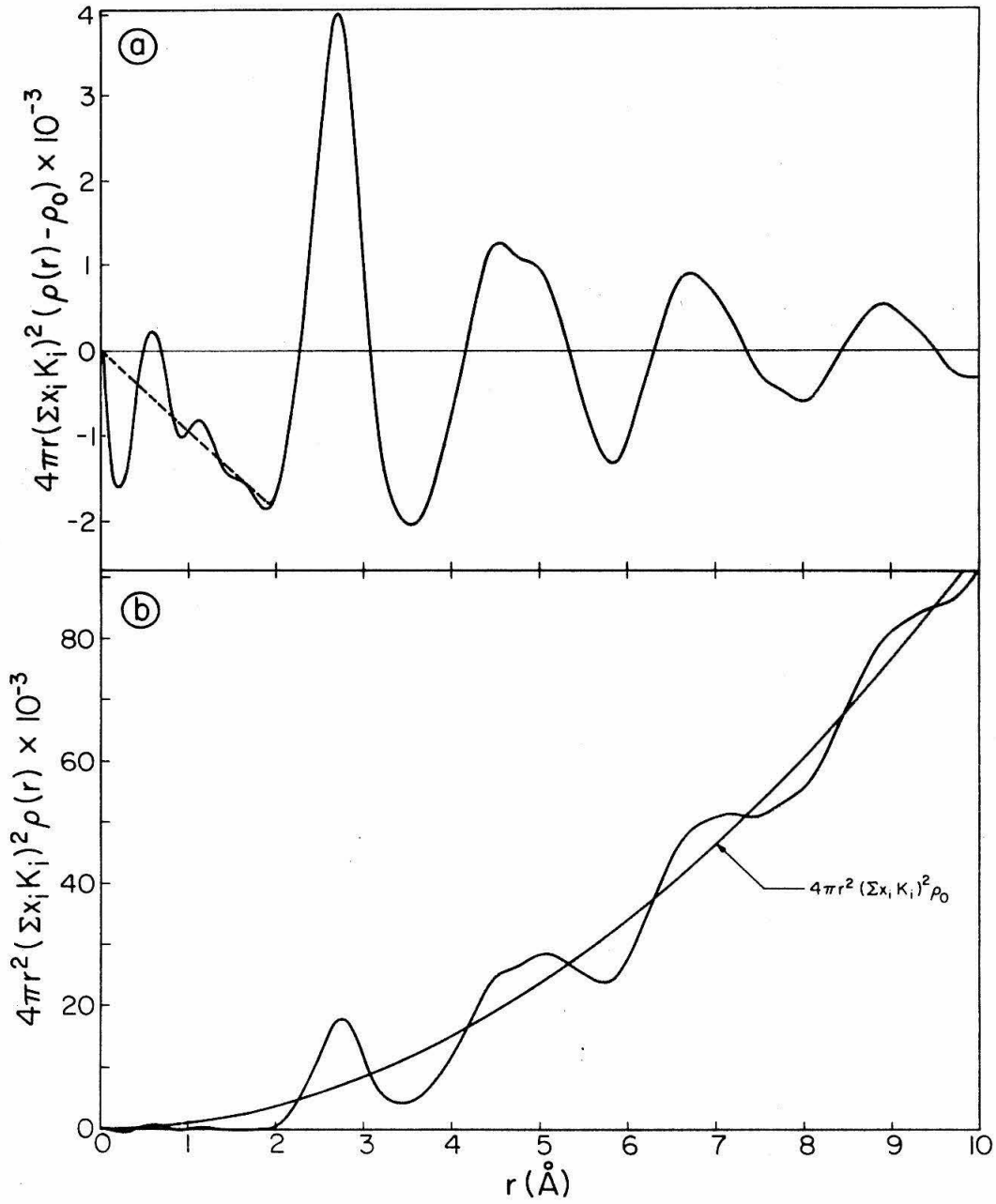

Fig. 9. Amorphous Ni_{53}-Pd_{27}-P_{20} alloy: a) function W(r); b) radial distribution function.

TABLE IV

INTERATOMIC DISTANCES IN Ni_{32}-Pd_{53}-P_{15} AND Ni_{53}-Pd_{27}-P_{20} AMORPHOUS ALLOYS

Composition	Ni_{32}-Pd_{53}-P_{15}		Ni_{53}-Pd_{37}-P_{26}	
Successive peaks in the RDF	r(Å)	r'(Å)	r(Å)	r'(Å)
1st	2.79	2.81	2.72	2.74
2nd	4.62	4.65	4.52	4.57
3rd	(5.40)	(5.36)	(5.17)	(5.13)
4th	6.90	6.94	6.75	6.83

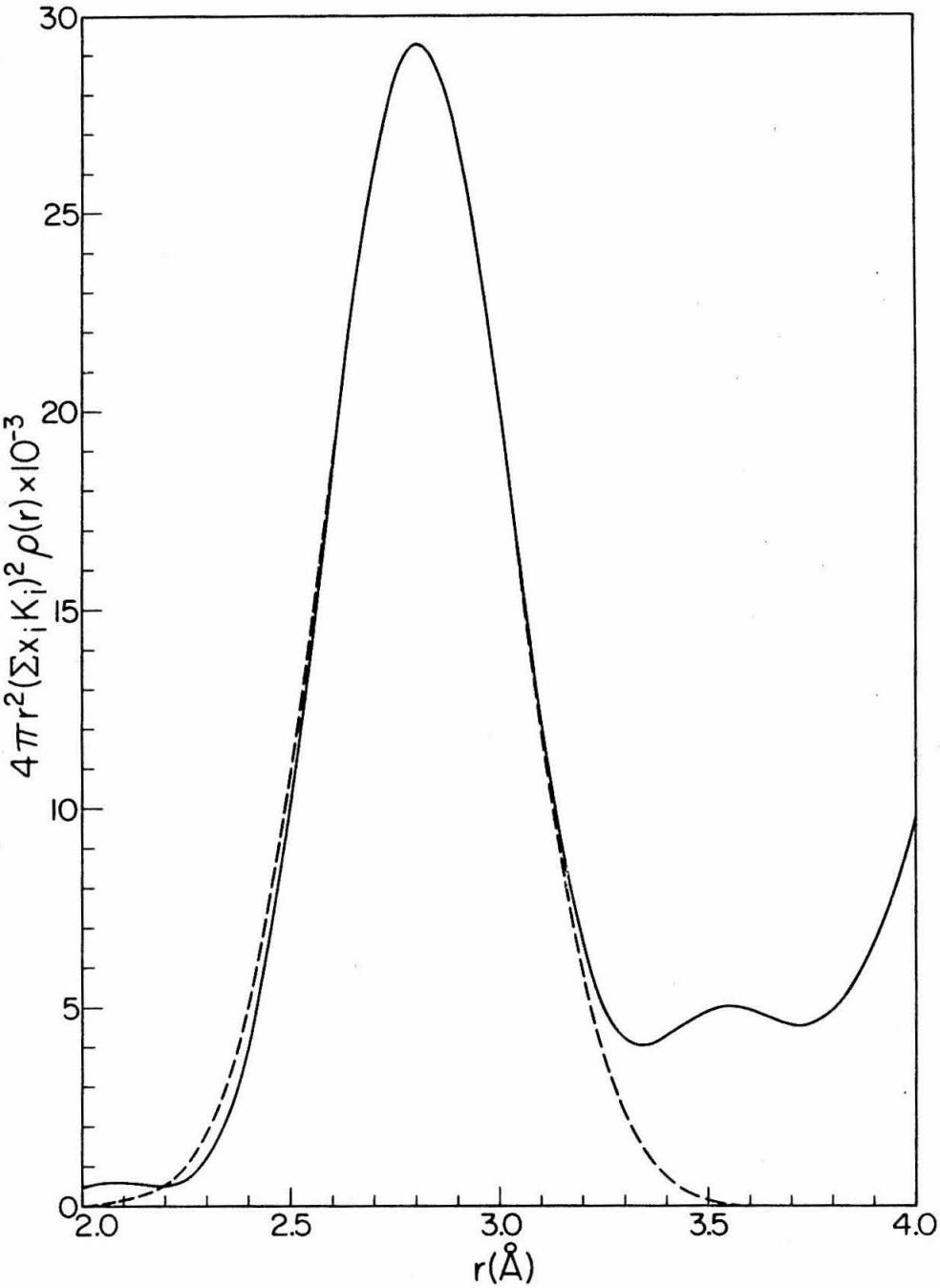

Fig. 10. First peak of the radial distribution function of the amorphous Ni_{32}-Pd_{53}-P_{15} alloy, with Gaussian approximation (dashed-line).

deviation of r (or r'), assuming always a gaussian approximation. Then the first peak can be analytically represented by:

$$r\,W(r) = \left[A_1 \exp(-(r-r_1)^2/4(\sigma_1+a)) \right] / \left[4\pi(\sigma_1+a) \right]^{\frac{1}{2}}$$

where $2\sigma_1$ is the mean square deviation of r_1 and a(= 0.01) is the constant in the temperature factor $\exp(-as^2)$, when such a factor is used to counterbalance the oversharpening due to $1/f_e^2(s)$. The area under the first peak, is then A_1. Hence, if B is the width at half height, the following relationship is verified:

$$2\sigma_1 = \overline{\Delta r_1^2} = (B^2/8 \text{ Log } 2)-2a$$

Average values for A_1 and $(\overline{\Delta r_1^2})^{\frac{1}{2}}$ are listed in Table V, together with the coordination numbers for the first atomic shell. The average coordination number, N_m, was computed under the assumptions that all types of pairs were contributing to the first peak and that there were equal atomic densities of Ni, Pd and P atoms around any atom (cf. III-A.2). Consequently, N_m was defined as:

$$N_m = A_1 / (\sum_i x_i K_i)^2$$

The metallic coordination number, N_{me}, was computed by subtracting the contributions due to phosphorus-metal and phosphorus-phosphorus pairs. This was performed by assuming that the ligancy of phosphorus was equal to 9, as in most transition metal phosphides rich in metal[38]. The value of N_{me} was then computed by direct application of equation (12) (cf. III-A.2). An error of about $\pm$ 0.5 atom on N_m and N_{me} was

TABLE V

COORDINATION NUMBERS, RATIOS OF s VALUES AND OF INTERATOMIC DISTANCES IN Ni_{32}-Pd_{53}-P_{15} AND Ni_{53}-Pd_{27}-P_{20} AMORPHOUS ALLOYS

Composition	Ni_{32}-Pd_{53}-P_{15}	Ni_{53}-Pd_{27}-P_{20}
A_1 (electrons^2)	16000	12300
$(\overline{\Delta r_1^2})^{\frac{1}{2}}$	0.22	0.23
N_m	12.7 $\pm$ 0.5	13.3 $\pm$ 0.5
N_{me}	10.5 $\pm$ 0.5	10.1 $\pm$ 0.5
Ratio s_i/s_1		
1	1.00	1.00
2	1.70	1.70
3	2.53	2.52
4	3.34	3.32
Ratio r_i/r_1		
1	1.00	1.00
2	1.655	1.660
3	1.90	1.89
4	2.47	2.48

considered likely, due to the remaining errors in the experimentally determined distribution functions W(r) and r W(r) and to the error on ρ_o

It appeared of interest, in the light of the remarks made in III-A.3, to compute the ratios of s values corresponding to the maxima of the interference function I(s), and the ratios of interatomic distances, which were determined by taking the average value of r and r'. The references were s_1 and r_1, corresponding to the first maxima in I(s) and in the distribution function respectively. These successive ratios are also given in Table V.

All Ni-Pd-P amorphous alloys (6 compositions) were used for diffraction experiments with CuK_α radiation, using the same diffractometer as for the experiments with MoK_α radiation. Only the first amorphous band was recorded, as this appeared to be sufficient to investigate the influence of large variations of composition on the diffraction pattern, and subsequently on the interatomic distances. For increasing values of the ratio Ni/Pd, the first amorphous peak decreased in intensity and was shifted towards higher angles. The results of the investigation with MoK_α radiation, showing rather constant ratios of r_i/r_1 together with an invariance of the ratios s_i/s_1 with varying compositions, led to make use of the argument developed in III-A.3. The product $s_1 r_1$ was calculated for Ni_{32}-Pd_{53}-P_{15} and Ni_{53}-Pd_{27}-P_{20} and was found quite constant and equal to 8.11 ± 0.02. The relation: $s_1 r_1 = 8.11$ was used to compute r_1 for all 6 compositions.

As previously defined, s_1 is the value of s at the first peak of the diffraction pattern and can be taken as a good approximation of s for the first maximum of the interference function.

The results are given in Table VI and the variation of r_1 with composition is shown in Fig. 11. The linear dependence of r with the ratio Ni/(Ni+Pd) where Ni and Pd are in atomic %, appears quite clearly, except for the Ni_{32}-Pd_{53}-P_{15} alloy which gives a value of r_1 smaller than expected. This is not surprising, considering that this alloy contains only 15 atomic % phosphorus compared with 20 atomic % for the other compositions. This result suggests that the Ni-Pd-P alloys present some strong structural similarities with the transition metal phosphides. In these phosphides, homogeneity ranges exist around the stoechiometric composition[38,39], and the average interatomic distances decrease with decreasing phosphorus content, probably because of a better packing of the metallic atoms. A point corresponding to $Ni_{83}P_{17}$ amorphous electrodeposited Kanigen nickel studied by Guinieret al.[11] is also shown in Fig. 11.

2. Iron-palladium-phosphorus alloys

Three different compositions were investigated. The alloys Fe_{32}-Pd_{48}-P_{20} and Fe_{44}-Pd_{36}-P_{20} were both studied with MoK_α and CuK_α radiations, whereas the alloy Fe_{23}-Pd_{57}-P_{20} was studied only with CuK_α radiation. The diffraction experiments performed with MoK_α radiation on Fe_{32}-Pd_{48}-P_{20} and Fe_{44}-Pd_{36}-P_{20} showed several amorphous peaks, as in the case of Ni-Pd-P alloys. The position of these peaks was also

TABLE VI

s VALUES FOR THE FIRST AMORPHOUS PEAK AND FIRST INTERATOMIC DISTANCE r_1 IN NICKEL-PALLADIUM-PHOSPHORUS AMORPHOUS ALLOYS

Composition	$S_1(\mathring{A}^{-1})$	$r_1(\mathring{A})$
Ni_{13}-Pd_{67}-P_{20}	2.79	2.90±0.01
Ni_{32}-Pd_{53}-P_{15}	2.89	2.80±0.01
Ni_{43}-Pd_{37}-P_{20}	2.92	2.78±0.01
Ni_{53}-Pd_{27}-P_{20}	2.98	2.73±0.01
Ni_{63}-Pd_{17}-P_{20}	3.02	2.68(5)±0.01
Ni_{73}-Pd_{7}- P_{20}	3.07	2.64±0.01

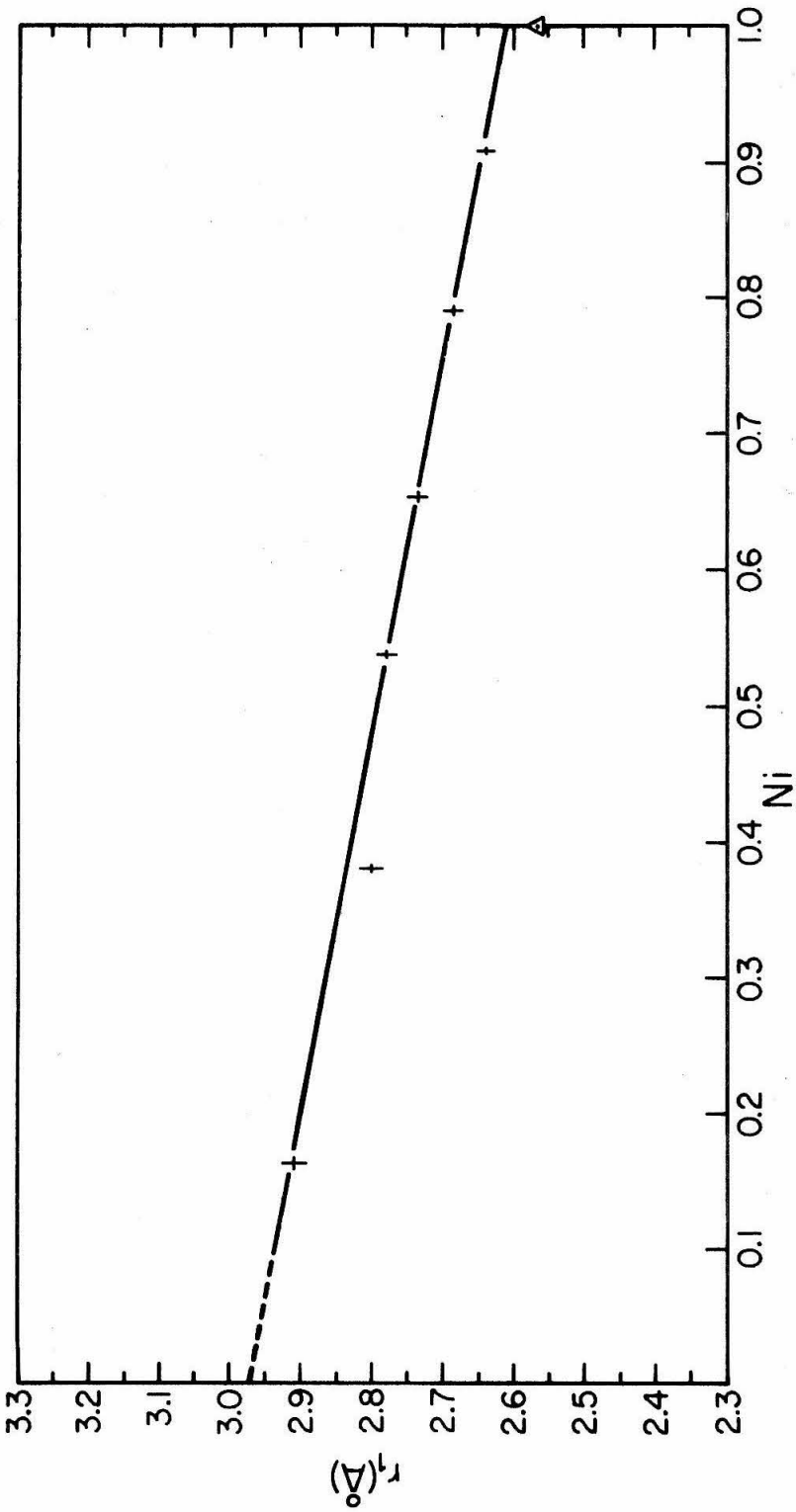

Fig. 11. Nearest neighbors interatomic distance in Ni-Pd-P amorphous alloys.

displaced toward larger values of 2θ (or s) with increasing percentage of iron. Table VII gathers the numerical results with respect to the diffraction patterns and to the maxima of the interference function I(s). The Fourier transformations leading to the radial distribution functions were performed in the same way as for the Ni-Pd-P alloys (cf. III-A). The resultant distribution functions W(r) and r W(r) are given in Fig. 12 and 13. In both cases a temperature factor equal to $\exp(-0.01\ s^2)$ was used in an effort to reduce the oversharpening effect of $1/f_e^2$. The values of r and r', referred to W(r) and r W(r) respectively, are given in Table VIII for the first four atomic shells. As in the case of Ni-Pd-P alloys, the fitting of the first peak of the RDF to a gaussian shape was quite satisfactory. The coordination numbers N_m and N_{me}, as well as the mean square deviation $\overline{\Delta r_1^2}$ are defined as in III-E.1. These numbers, as well as the ratios s_i/s_1 and r_i/r_1 are given in Table IX.

Only the first amorphous peak was recorded in the experiments performed with CuK_α radiation. This first peak is shown in Fig. 14 for the three compositions investigated. As expected, the amorphous band is displaced towards larger angles and decreases in intenstiy with increasing iron content. As in the case of Ni-Pd-P alloys, the good invariance of the ratios r_i/r_1 and s_i/s_1 led to establish a relation between s_1 and r_1 (cf. III-A.3). For the Fe-Pd-P alloys, this relation was: $s_1 r_1 = 8.08$. This relation was used to compute r_1 for the alloy Fe_{23}-Pd_{57}-P_{20}. The results for all three compositions

TABLE VII

VALUES OF 2θ AND s CORRESPONDING TO THE TWO FIRST PEAKS OF THE DIFFRACTION PATTERNS AND TO THE MAXIMA OF THE INTERFERENCE FUNCTIONS (MoK_α RADIATION)

Composition		Fe_{32}-Pd_{48}-P_{20}	Fe_{44}-Pd_{36}-P_{20}
First peak	2θ (deg.)	18.58	18.77
	s ($Å^{-1}$)	2.851	2.887
Half width of first peak (2θ)		2.84	3.02
Second peak	2θ (deg.)	31.81	32.04
	s ($Å^{-1}$)	4.85	4.88
Successive maxima of I(s)			
1st		2.85	2.88
2nd		4.89	4.92
3rd		7.22	7.28
4th		9.55	9.60

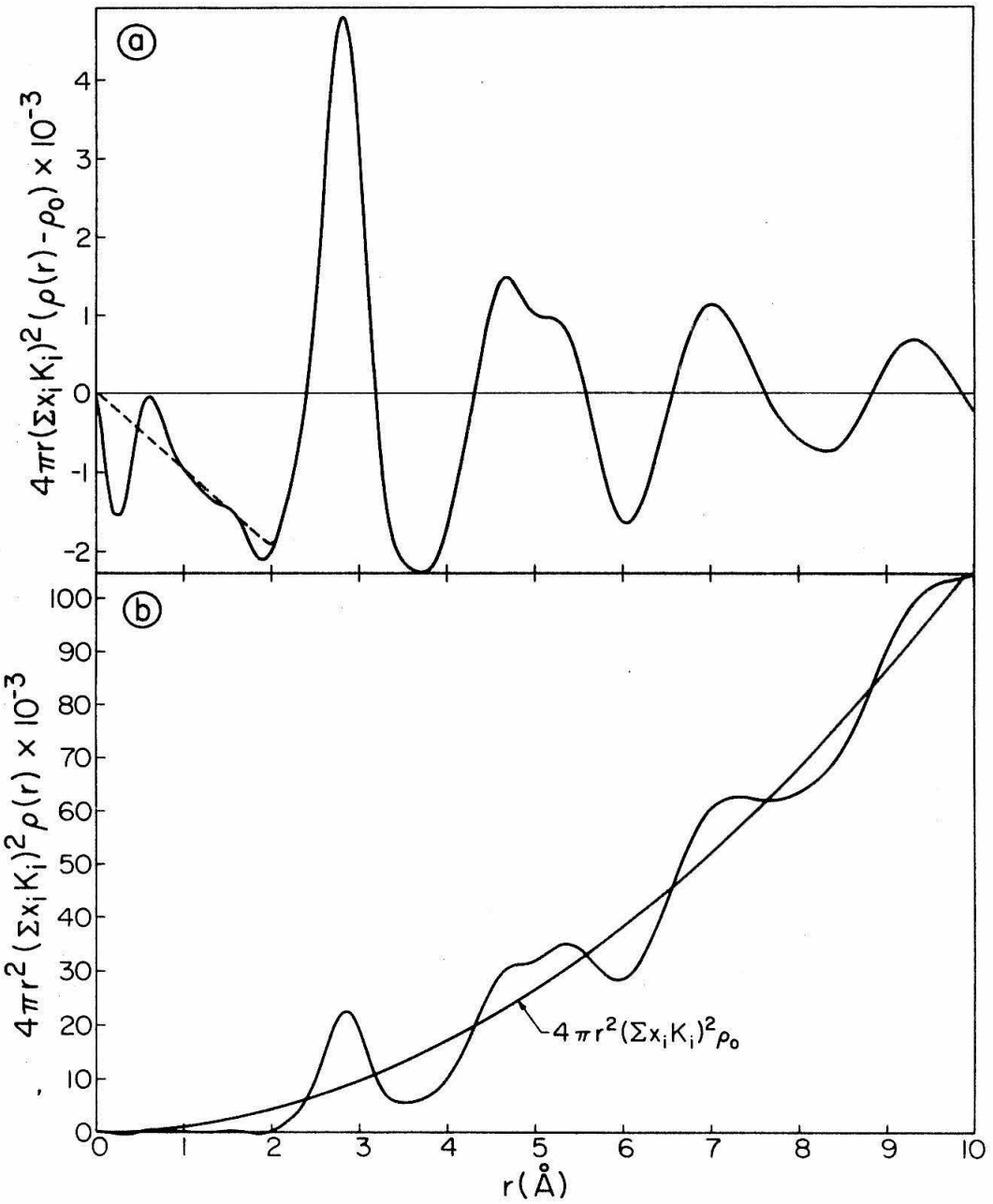

Fig. 12. Amorphous Fe_{32}-Pd_{48}-P_{20} alloy: a) function W(r); b) radial distribution function.

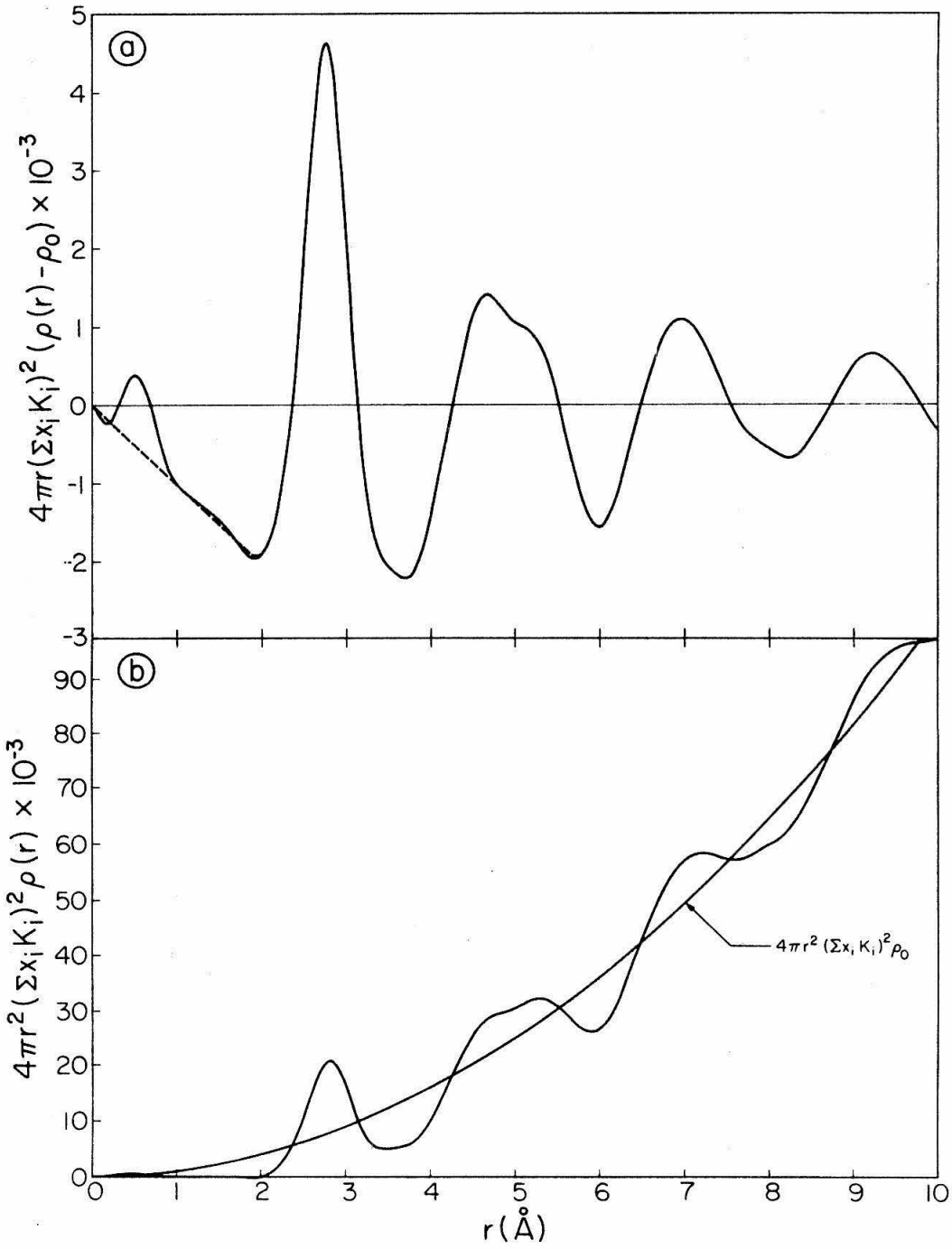

Fig. 13. Amorphous Fe_{44}-Pd_{36}-P_{20} alloy: a) function W(r); b) radial distribution function.

TABLE VIII

INTERATOMIC DISTANCES IN Fe_{32}-Pd_{48}-P_{20} AND Fe_{44}-Pd_{36}-P_{20} AMORPHOUS ALLOYS

Composition	Fe_{32}-Pd_{48}-P_{20}		Fe_{44}-Pd_{36}-P_{20}	
Successive peaks in the RDF	r(Å)	r'(Å)	r(Å)	r'(Å)
1st	2.82	2.855	2.775	2.825
2nd	4.66	4.70	4.675	4.685
3rd	(5.38)	(5.35)	(5.25)	(5.28)
4th	7.03	7.20	6.97	7.20

TABLE IX

COORDINATION NUMBERS, RATIOS OF s VALUES AND OF INTERATOMIC DISTANCES IN Fe_{32}-Pd_{48}-P_{20} AND Fe_{44}-Pd_{36}-P_{20} AMORPHOUS ALLOYS

Composition	Fe_{32}-Pd_{48}-P_{20}	Fe_{44}-Pd_{36}-P_{20}
A_1 (electrons^2)	14700	14000
$(\overline{\Delta r_1^2})^{\frac{1}{2}}$	0.24	0.23
N_m	13.2±0.5	14.6±1.0
N_{me}	10.2±0.5	11.6±1.0
Ratio s_i/s_1		
1	1.00	1.00
2	1.71	1.71
3	2.53	2.53
4	3.37	3.33
Ratio r_i/r_1		
1	1.00	1.00
2	1.66	1.67
3	1.90	1.87
4	2.52	2.53

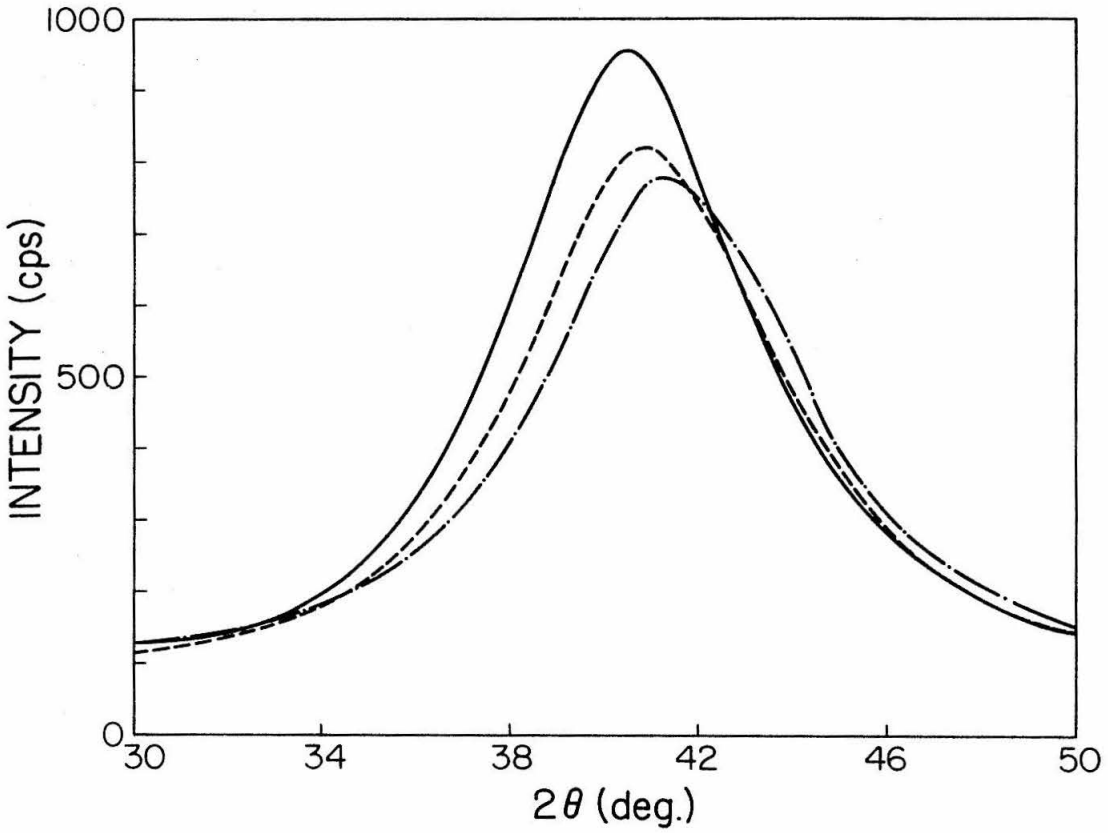

Fig. 14. First amorphous peak in Fe-Pd-P amorphous alloys: —— Fe_{23}-Pd_{57}-P_{20}; ---- Fe_{32}-Pd_{48}-P_{20}; —·—·— Fe_{44}-Pd_{36}-P_{20}.

are given in Table X and plotted in Fig. 15 versus the ratio Fe/(Fe+Pd). As in the case of Ni-Pd-P alloys, a linear relationship with composition can be recognized.

TABLE X

s VALUES FOR THE FIRST AMORPHOUS PEAK AND FIRST INTERATOMIC DISTANCE r_1 IN IRON-PALLADIUM-PHOSPHORUS AMORPHOUS ALLOYS

Composition	s_1 ($\AA^{-1}$)	r_1 ($\AA$)
Fe_{23}-Pd_{57}-P_{20}	2.82	2.87
Fe_{32}-Pd_{48}-P_{20}	2.85	2.84
Fe_{44}-Pd_{36}-P_{20}	2.88	2.80

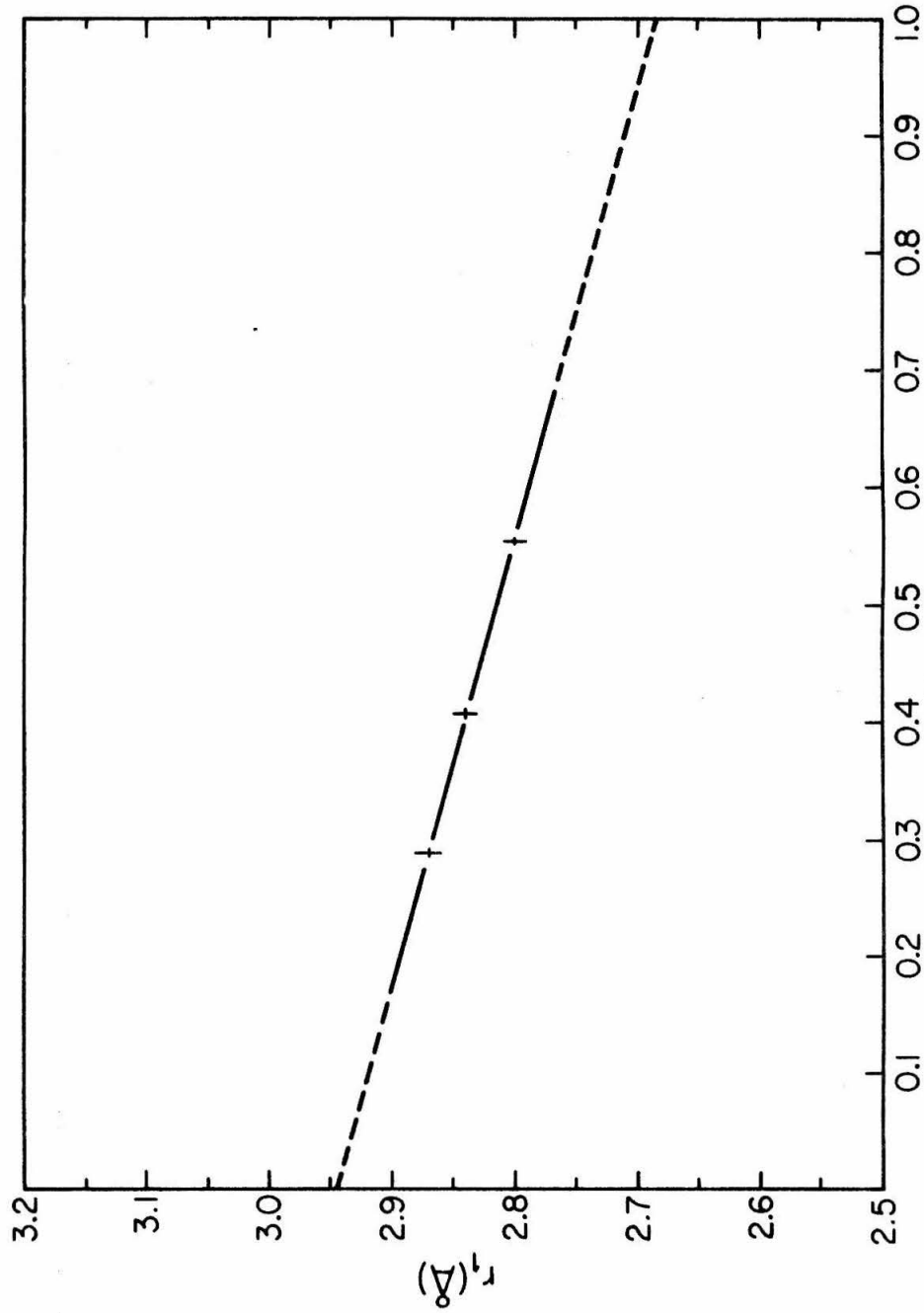

Fig. 15. Nearest neighbors interatomic distance in Fe-Pd-P amorphous alloys.

IV. ELECTRICAL RESISTIVITY

The amorphous alloys which are the object of this investigation exhibit rather characteristic transport properties. The study of electrical resistivity and specifically its variations with temperature and composition, is of particular interest. The presence of ferromagnetic elements (Fe and Ni) in these alloys suggested low temperature experiments in order to investigate whether or not a Kondo effect existed in these alloys. High temperature resistivity measurements yielded informations on the transformation from the amorphous to the crystalline state. Direct comparison of parameters such as temperature coefficient of resistivity and residual resistivity of amorphous and crystalline phases was also obtained.

A. Experimental procedure

Small rectangular samples of about 15 x 5 mm were prepared by electro-discharge machining of amorphous foils under oil. Current and potential leads made of 0.063 inch in diameter nickel or platinum wire were spot welded on the specimens. The currents and potentials were measured, by a null technique. Only potentials were measured, the currents being obtained from the potential drop across a standard resistor of 0.1Ω. Thermal gradient effect were minimized by current reversal. The resistivity measurements are presented on a relative scale and are given as a fraction of the resistivity of the amorphous phase at room temperature. Consequently, if $\rho(T)$ is the resistivity at a temperature T, the relative resitivity $r(T)$ is defined as

$\rho(T)/\rho(294^{\circ}K)$. A few absolute resistivity measurements were performed at room temperature on samples representative of each composition. The dimensions of these samples were carefully determined by use of a microscope equipped with a filar eyepiece. Precision was about $\pm$ 3% on thickness and $\pm$ 2 to 4% for the other dimensions, yielding about $\pm$ 10% error on the absolute value of the resistivity.

B. Results

The Ni-Pd-P and Fe-Pd-P amorphous alloys investigated showed metallic conduction. At room temperature their electrical resistivity was between two and three times the resistivity of the corresponding stable crystalline phases obtained by annealing at temperatures around 550°C, for periods of time ranging from one day to one month. The values obtained for the resistivity of the amorphous alloys ranged from 100 to 175 $\mu\Omega$-cm for the Ni-Pd-P alloys and from 160 to 180 $\mu\Omega$-cm for the Fe-Pd-P alloys. The dispersion of values was too large to show clearly the influence of composition. However, in the Ni-Pd-P system, which offered the largest range of compositions, the largest value (175 $\mu\Omega$-cm) was obtained for the alloy Ni_{53}-Pd_{27}-P_{20} and the resistivity seemed to decrease on both sides of this composition. The order of magnitude of these resistivity values is the same as that previously reported for amorphous Pd-Si[40] and Fe-P-C[17] alloys. They also compare favorably with the resistivity of both iron and nickel measured just above the melting point (110 $\mu\Omega$-cm and 85 $\mu\Omega$-cm respectively[41]).

1. Low temperature measurements

The most striking feature of the behavior of the resistivity of Fe-Pd-P and Ni-Pd-P alloys at low temperatures was the occurrence of a minimum in the resistivity curve. This minimum appeared at temperatures ranging from about $9^{o}K$ to $96^{o}K$, depending on the system. Moreover, for temperatures between the minimum temperature (T_m) and about $140^{o}K$ - $150^{o}K$, r(T) assumed a T^2 behavior. Typical low temperature behaviors are illustrated in Figs. 16 and 17 for Ni-Pd-P alloys and in Figs. 18 and 19 for Fe-Pd-P alloys. The existence of a resistivity minimum, and the presence of iron and nickel in the systems under investigation, led to consider a possible Kondo effect. Therefore r(T) was tentatively approximated by a function of the form:

$$r(T) = r_o + \beta T^2 + \Delta r_o - \alpha \text{ Log } T \qquad (1)$$

with r_o, Δr_o, α and β depending only on the composition and the structure of the amorphous alloy. The determination of these parameters was performed by plotting r(T) versus T^2 to obtain r_o and β, and then by plotting the difference $r(T)-r_o-\beta T^2 = r_2(T)$ versus Log T. Examples of such plots are given in Figs. 20 and 21 for Ni-Pd-P alloys and Figs. 22 and 23 for Fe-Pd-P alloys. Several samples of each composition were used for low temperature measurements, and the dispersion in experimental results was probably due to small differences in structure from one sample to the other. Tables XI and XII summarize the experimental results for Ni-Pd-P and Fe-Pd-P systems respectively.

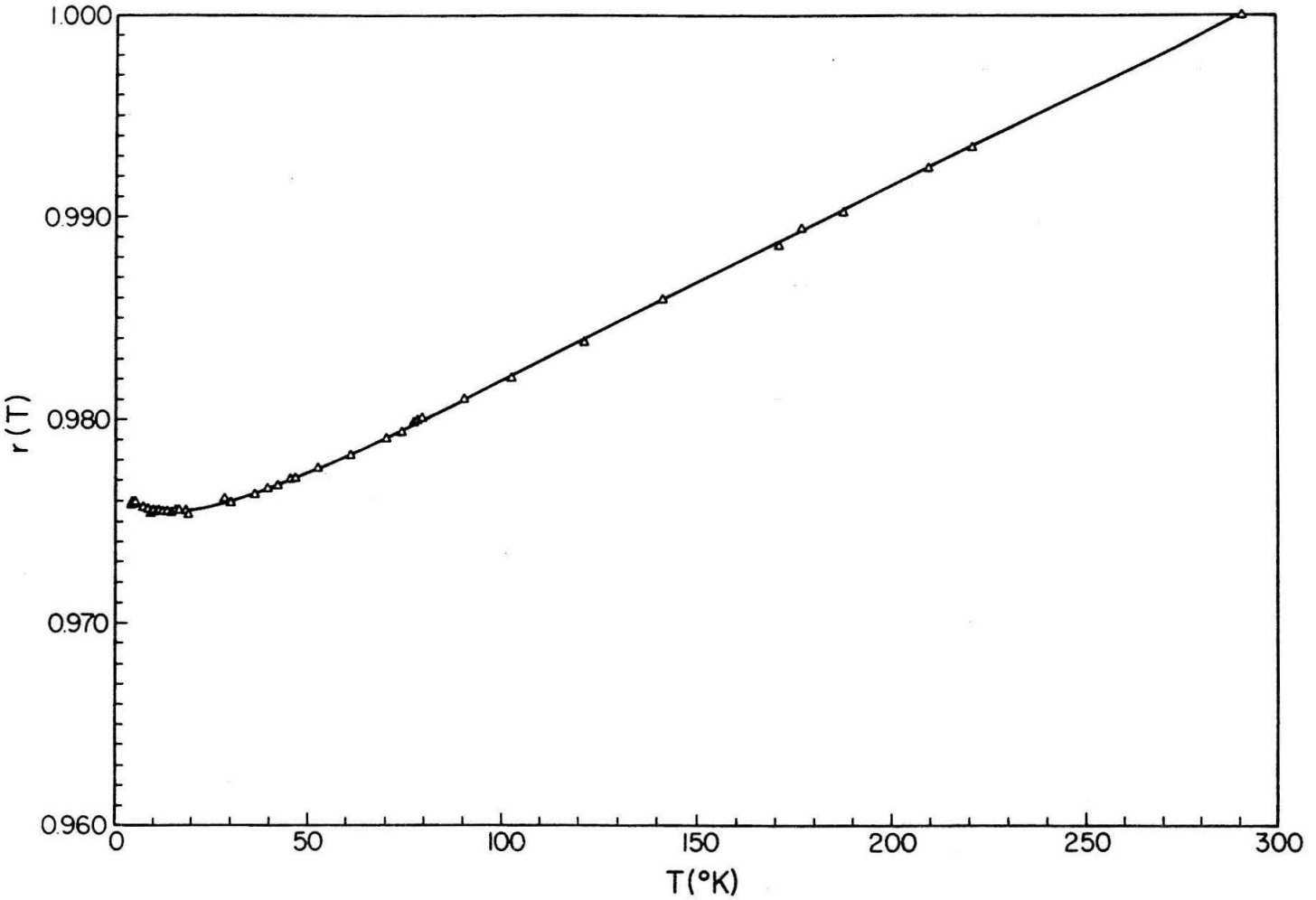

Fig. 16. Relative electrical resistivity of amorphous Ni_{63}-Pd_{17}-P_{20} alloy, from liquid helium temperature to room temperature.

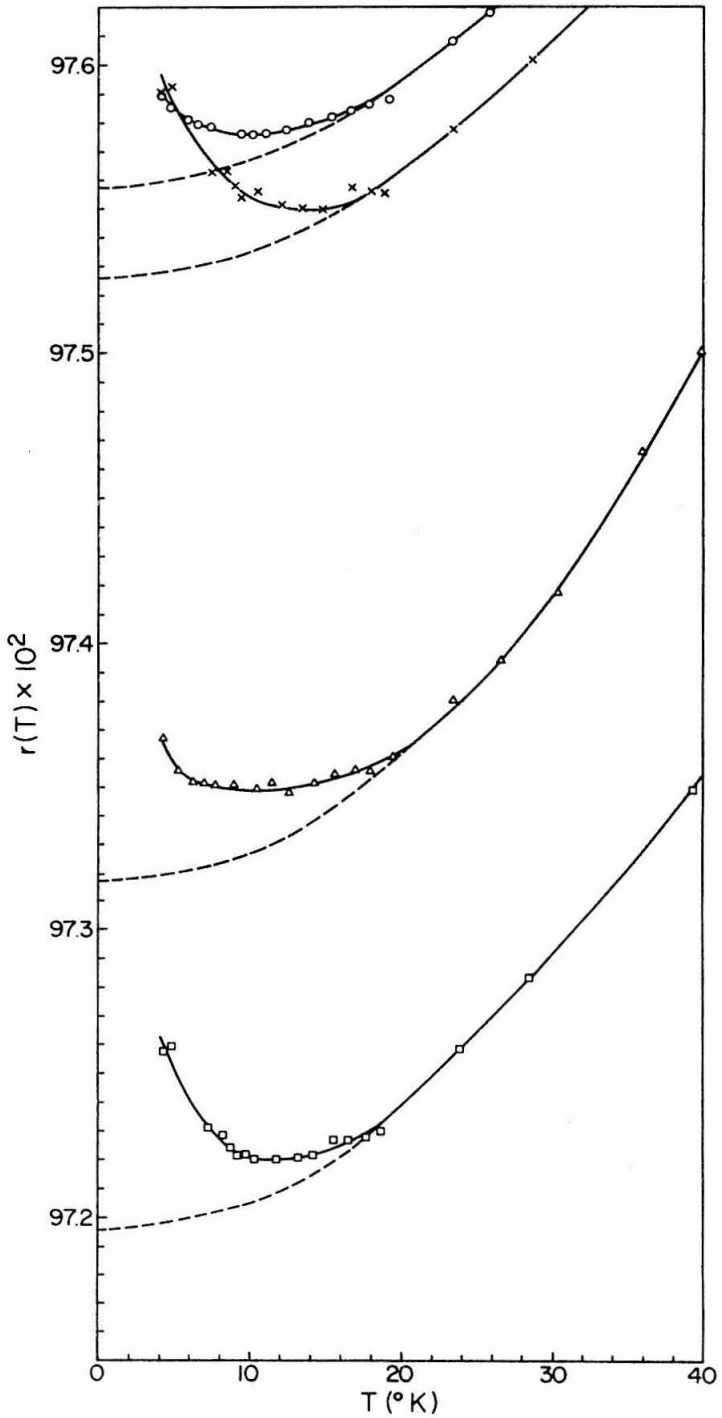

Fig. 17. Relative electrical resistivity at low temperature of four specimens of amorphous Ni_{63}-Pd_{17}-P_{20}.

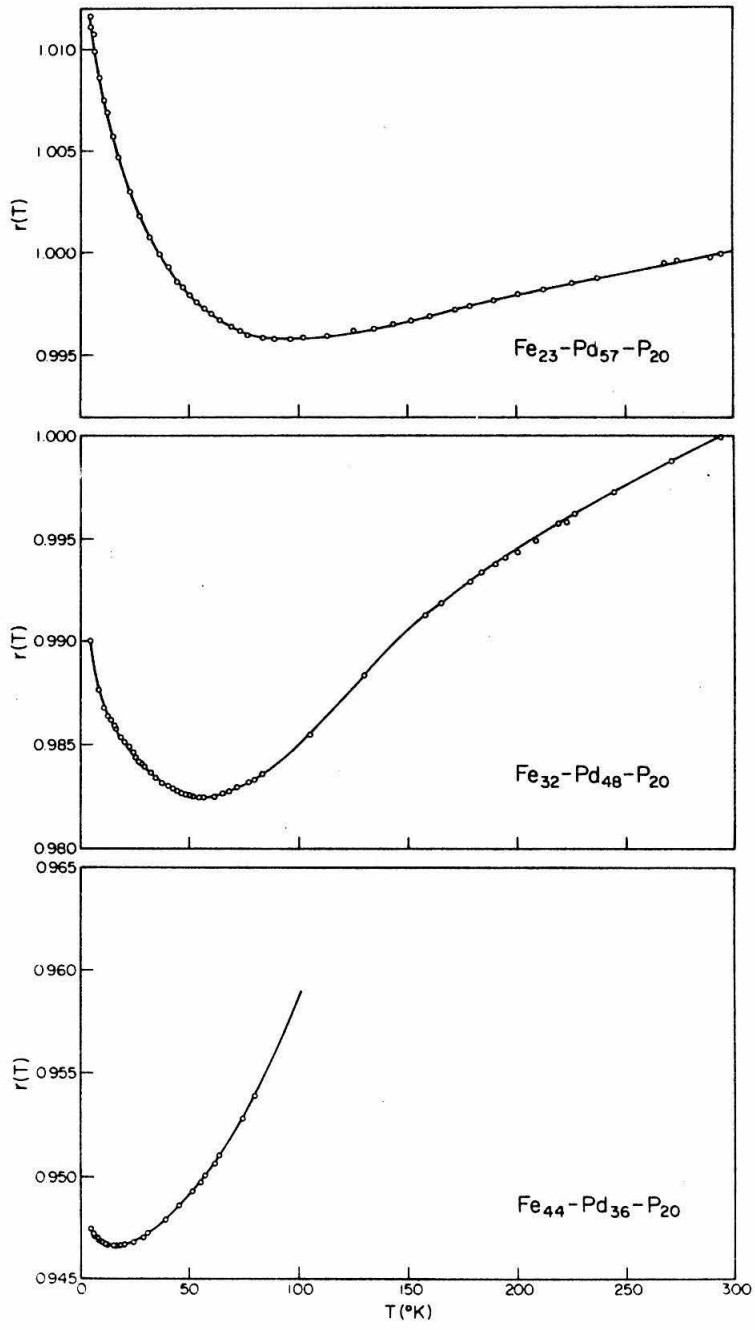

Fig. 18. Relative electrical resistivity of Fe-Pd-P amorphous alloys at low temperature.

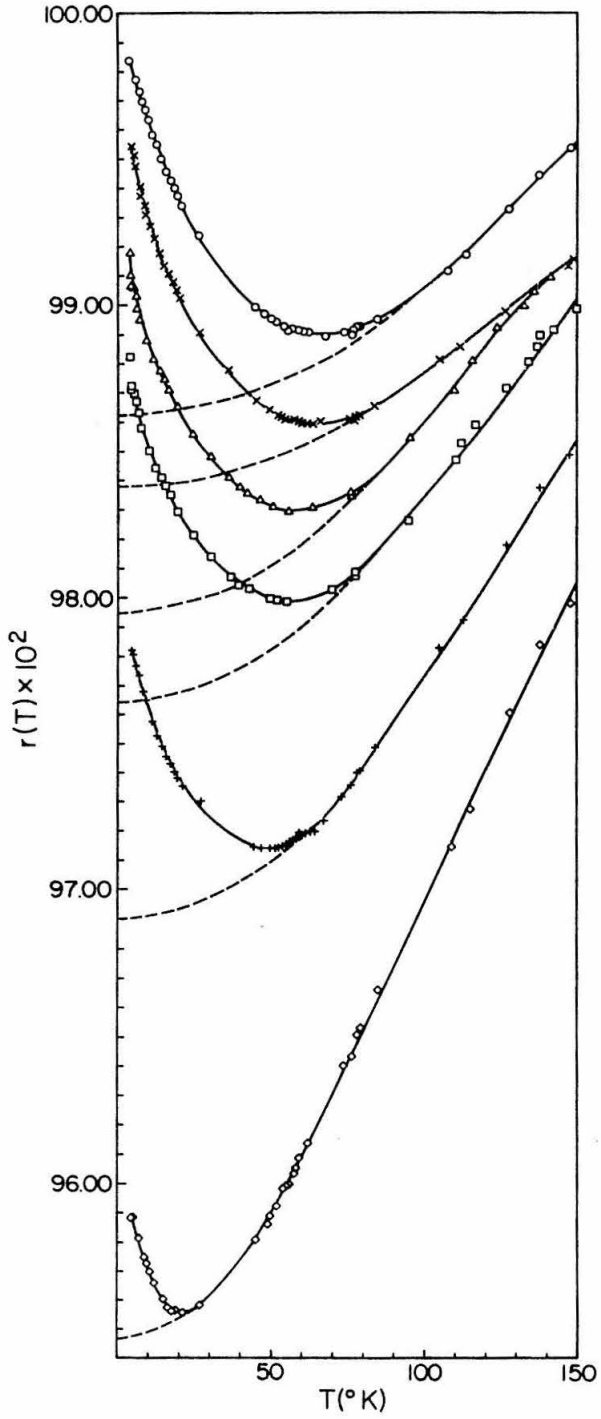

Fig. 19. Relative electrical resistivity at low temperature of six specimens of amorphous Fe_{32}-Pd_{48}-P_{20}.

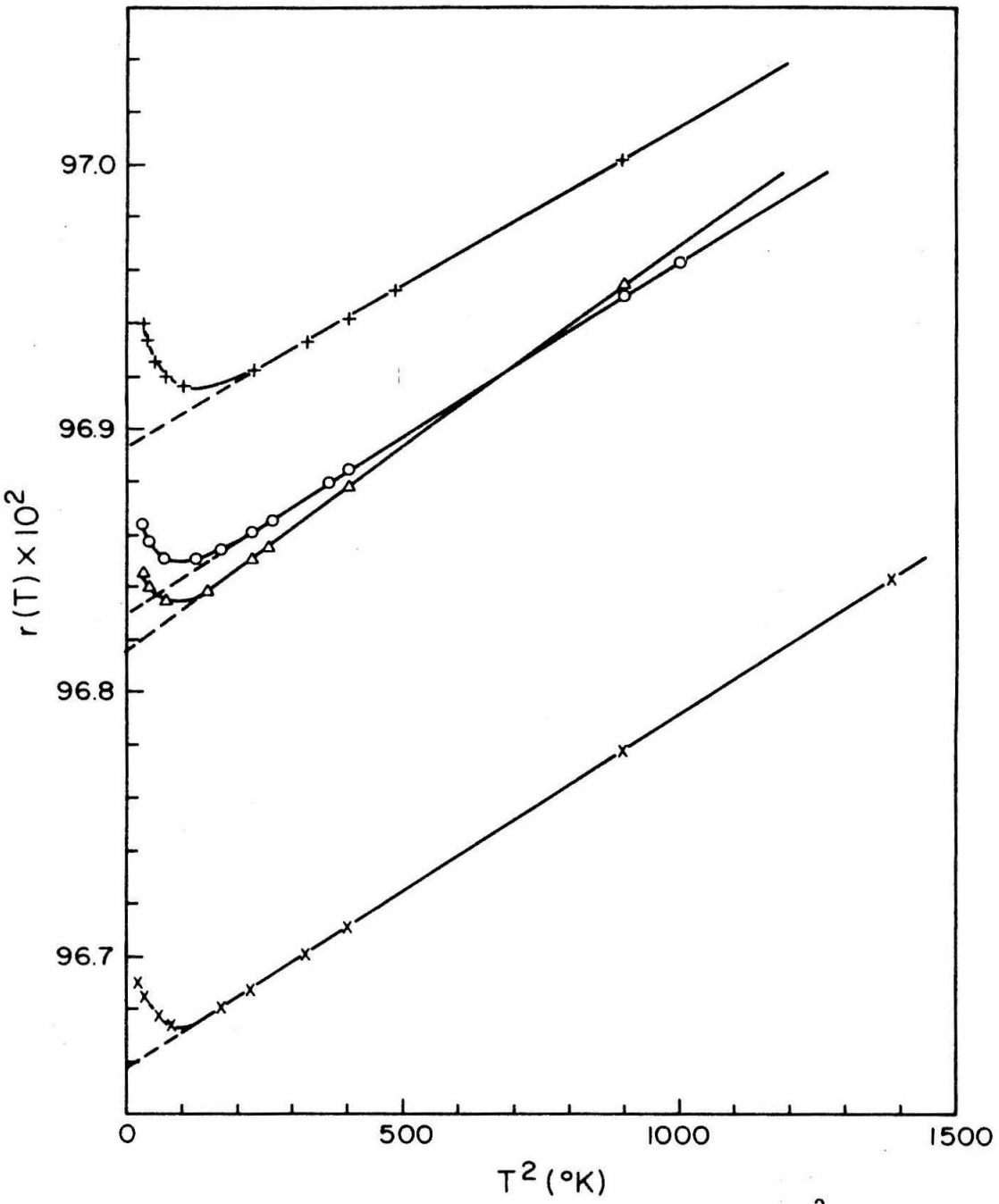

Fig. 20. Relative electrical resistivity versus T^2 of four specimens of amorphous Ni_{32}-Pd_{53}-P_{15}.

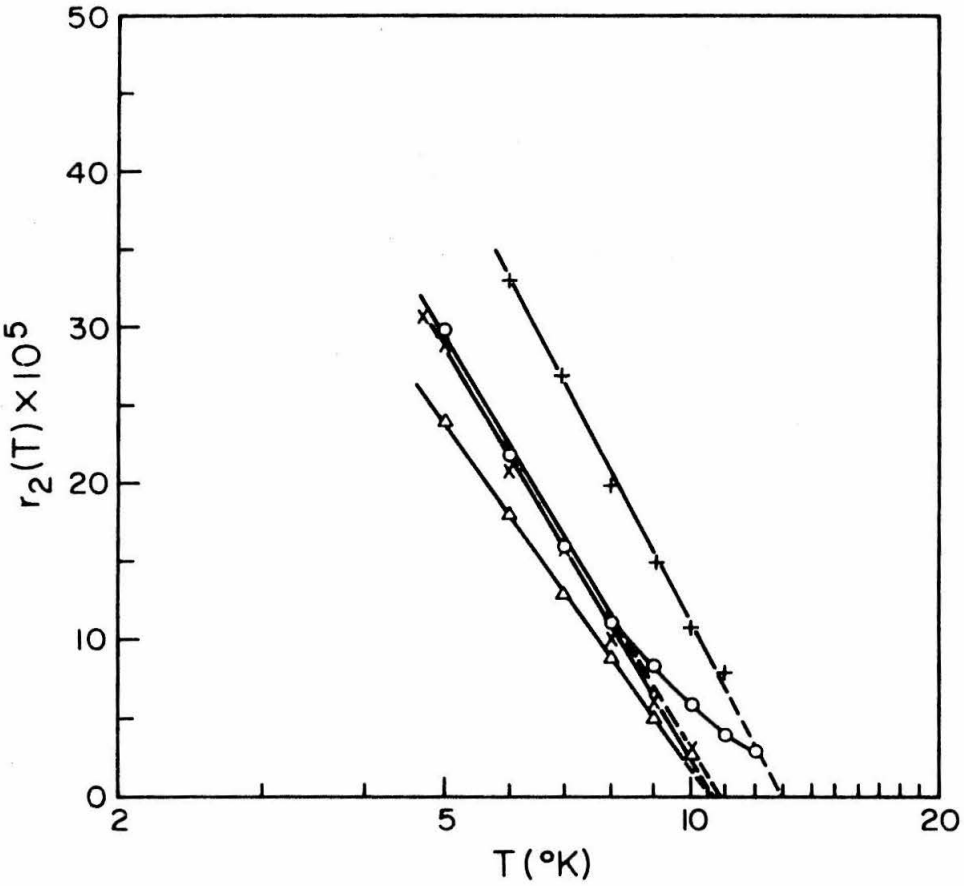

Fig. 21. Residual relative resistivity versus Log T for four specimens of amorphous Ni_{32}-Pd_{53}-P_{15}.

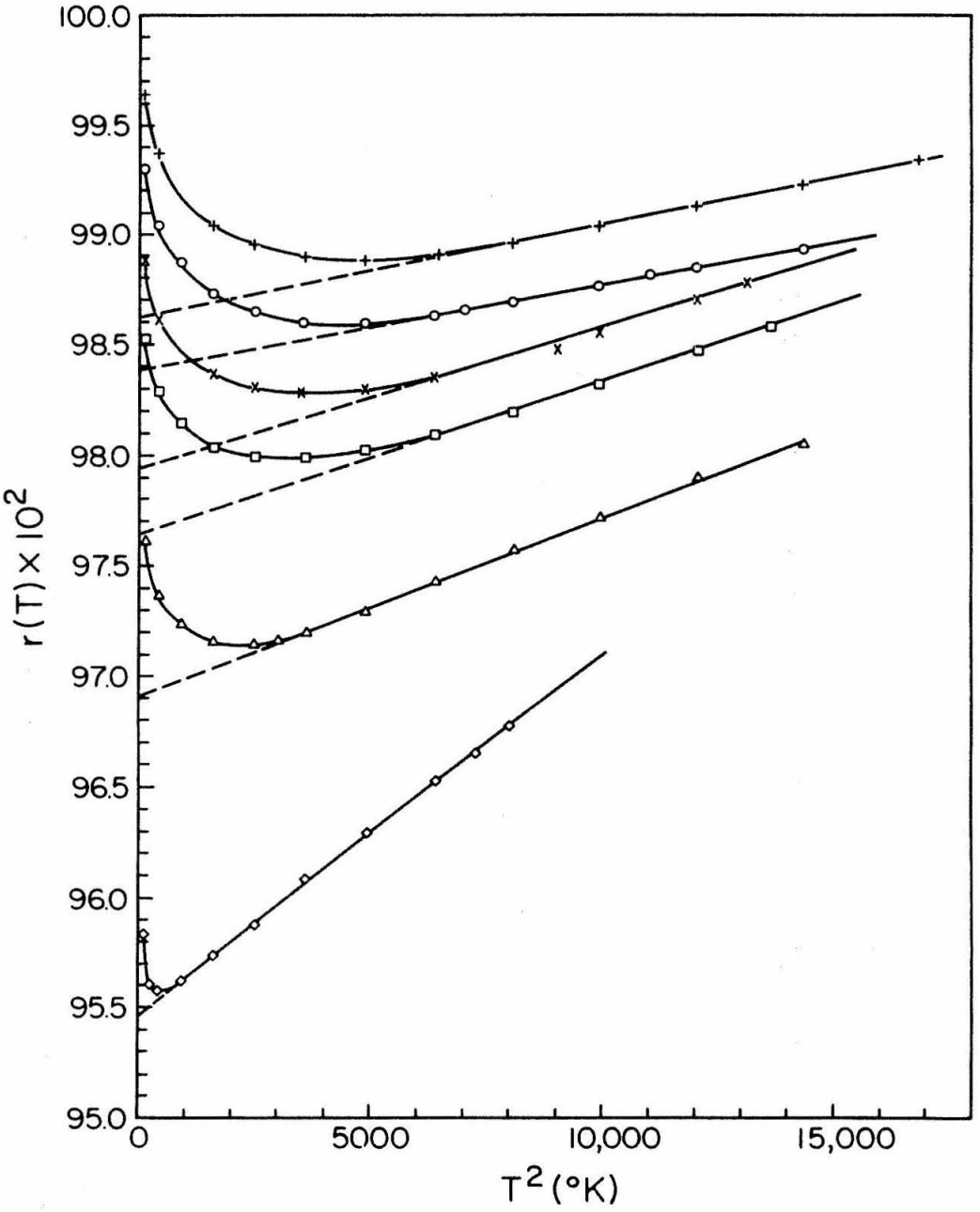

Fig. 22. Relative electrical resistivity versus T^2 of six specimens of amorphous Fe_{32}-Pd_{48}-P_{20}.

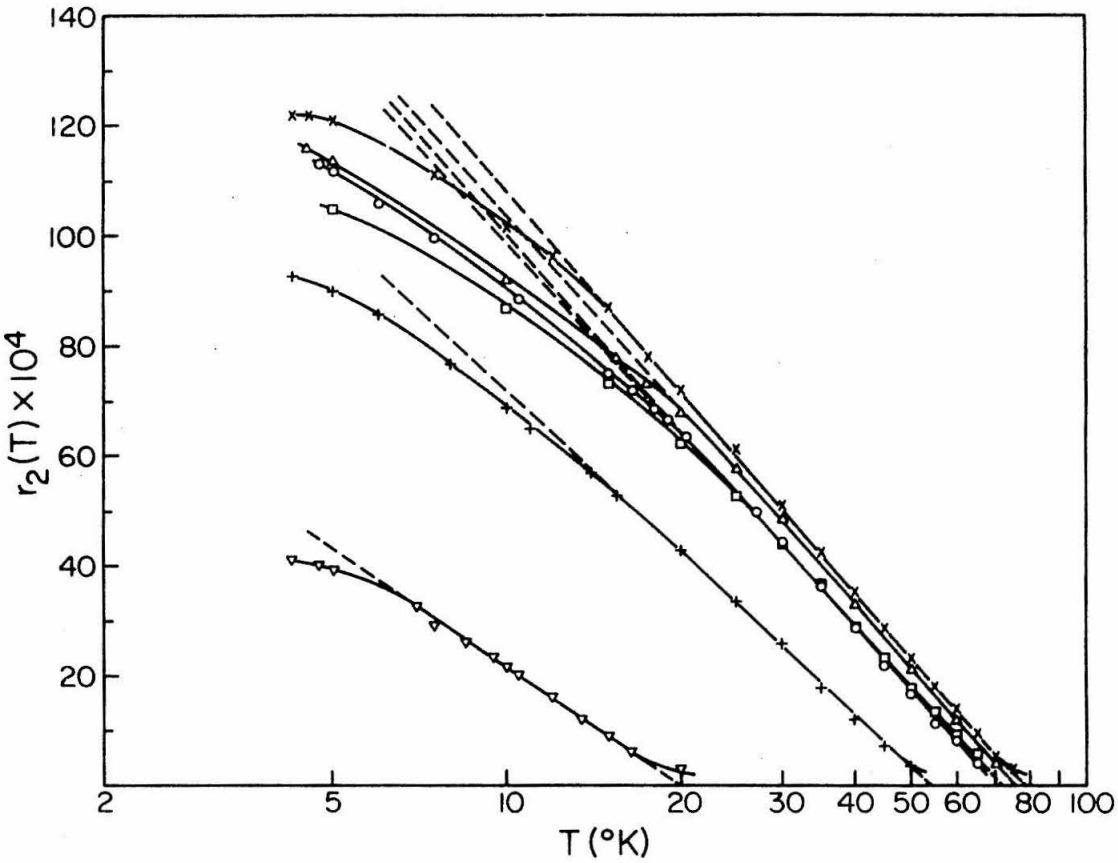

Fig. 23. Residual relative resistivity $r_2(T)$ versus Log T for six specimens of amorphous Fe_{32}-Pd_{48}-P_{20}.

TABLE XI

LOW TEMPERATURE RESISTIVITY DATA FOR NICKEL-PALLADIUM-PHOSPHORUS ALLOYS

Composition		$r_o(\times 10^2)$	$\alpha(\times 10^4)$	$\beta(\times 10^6)$	$T_m(^oK)$	$r_m(\times 10^2)$	$\Delta r(\times 10^4)$
Ni_{32}-Pd_{53}-P_{15}	1	96.657	3.820	1.34	9.5	96.674	1.6
	2	96.816	3.255	1.53	9.3	96.835	1.0
	3	96.830	3.890	1.33	9.8	96.849	1.4
	4	96.894	4.30	1.22	10.5	96.917	2.4
Ni_{43}-Pd_{37}-P_{20}	1	97.600	5.35	0.973	15.0	97.664	10.0
	2	96.580	6.35	1.5	13.5	96.632	8.2
Ni_{53}-Pd_{27}-P_{20}	1	98.198	4.18	0.63	12.5	98.213	4.1
	2	98.662	4.70	0.38	15.5	98.673	4.9
Ni_{63}-Pd_{17}-P_{20}	1	97.526	5.2	0.93	14.5	97.549	5.6
	2	97.196	5.05	0.89	13.5	97.220	5.0
	3	97.316	2.75	1.11	11.0	97.348	4.1
	4	97.558	2.31	0.89	10.5	97.576	2.6

TABLE XII

LOW TEMPERATURE RESISTIVITY DATA FOR IRON-PALLADIUM-PHOSPHORUS ALLOYS

Composition		$r_o(\times 10^2)$	$\alpha(\times 10^4)$	$\beta(\times 10^6)$	$T_m(^oK)$	$r_m(\times 10^2)$	$\Delta r(\times 10^4)$
Fe_{23}-Pd_{57}-P_{20}		99.480	65.0	0.16	96	99.580	150
Fe_{32}-Pd_{48}-P_{20}	1	97.640	49.8	0.69	56	97.990	92
	2	97.940	51.5	0.64	62	98.290	100
	3	98.620	53.4	0.43	71	98.890	116
	4	96.900	44.7	0.81	45	97.150	82.5
	5	98.380	52.0	0.39	66	98.600	110
	6	95.480	31.8	1.60	20	95.570	39.5
Fe_{44}-Pd_{36}-P_{20}	1	98.050	11.55	1.20	32	98.150	15.0
	2	94.512	8.35	1.23	17.5	94.665	8.9

These tables give α, β, r_o as well as T_m and $r(T_m) = r_m$. Also given is $\Delta r = r(5.0)-r_m$, which is a measure of the depth of the minimum.

Without anticipating the discussion, the following remarks can already be made. First, though all the amorphous alloys showed a minimum, the effect is strikingly more pronounced in Fe-Pd-P alloys. This can readily be seen by comparing the Δr which are about 10 to 100 times higher in the Fe-Pd-P alloys than in the Ni-Pd-P alloys. For all the alloys, r(T) showed a reasonably good fit to equation (1), but the dispersion was quite large as it appears in Fe_{32}-Pd_{48}-P_{20} for instance (cf. Figs. 22 and 23). No noticeable law of variation for α, T_m and r_m appeared in Ni-Pd-P alloys. For Fe-Pd-P alloys both α and T_m decreased from Fe_{23}-Pd_{57}-P_{20} to Fe_{44}-Pd_{36}-P_{20}, but the large dispersion of data for these compositions prevented from checking accurately the composition dependence.

2. <u>High temperature measurements</u>

The high temperature resistivity measurements were performed at constant rates of heating of approximately 1.2 to 2.0°C/min. Under these conditions the resistivity vs. temperature curve of all the amorphous alloys had the same general shape. The resistivity increased with temperature, with a small temperature coefficient of the order of $10^{-4}/^{o}C$, until a crystallization temperature t_{cr} was reached. At this temperature the resistivity dropped sharply at first, then reached a minimum before increasing again up to the melting point of the alloy. Typical behaviors of r(t) with t are given in Fig. 24 for

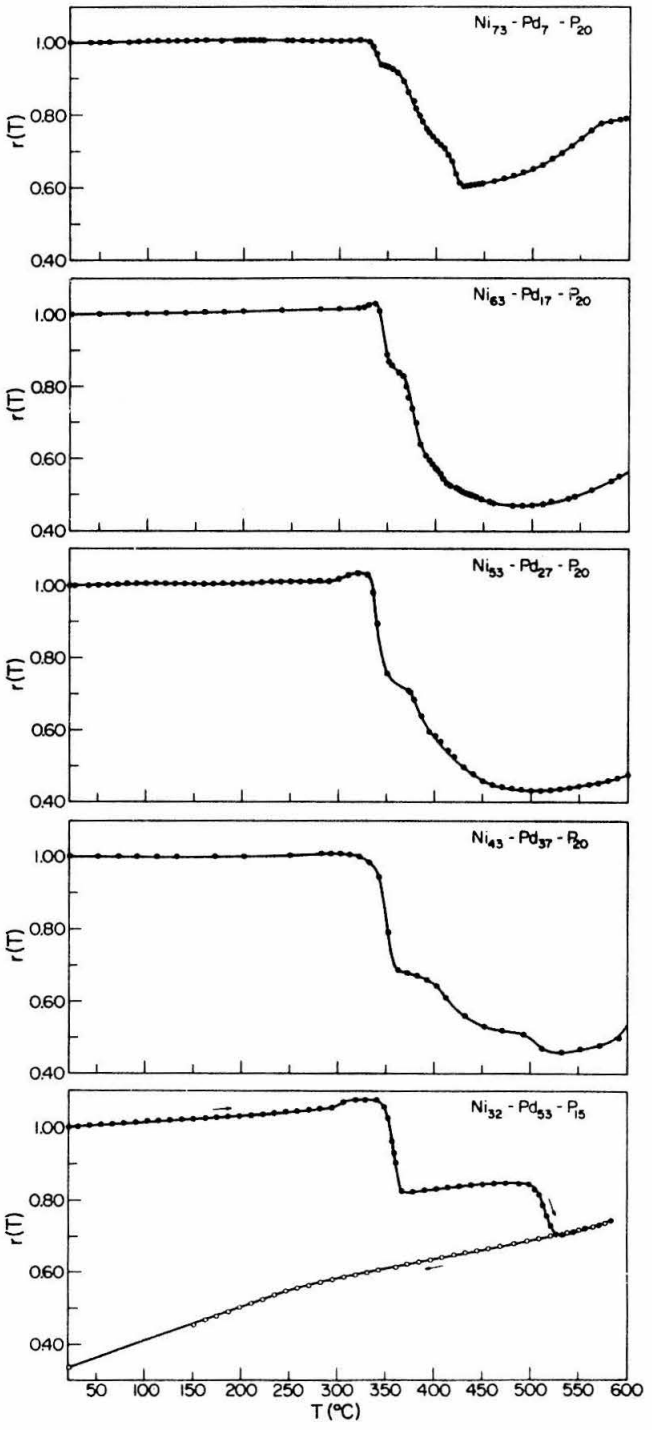

Fig. 24. Relative electrical resistivity of six Ni-Pd-P amorphous alloys measured with an average heating rate of 1.5°C/min.

Ni-Pd-P alloys. Only one composition (Fe_{33}-Pd_{47}-P_{20}) was investigated for the iron-palladium-phosphorus system (cf. Fig. 25), as attempts to investigate Fe_{44}-Pd_{36}-P_{20} alloy were deceived by the great brittleness of foils of this composition. Table XIII summarizes the important data for the alloys studied. For each composition, the following characteristic parameters are given: temperature coefficient μ, determined between 20°C and 220°C; crystallization temperature t_{cr}, with its dispersion Δt_{cr}, and temperature t_N, which is related to the small increase in resistivity which appears for most Ni-Pd-P alloys shortly before crystallization. More precisely t_N is the temperature characterizing the beginning of this anomalous deviation from a linear relationship of the type $r(t) = 1 + \mu t$, prior to the crystallization itself. From the data of Table XIII, it appears that t_{cr} is rather well defined, varying between 305°C, and 340°C for all the amorphous alloys. For slow rates of heating (1° to 5°/min), t_{cr} did not vary appreciably. The existence of a small increase in the resistivity prior to crystallization was found in Ni-Pd-P alloys only. This puzzling behavior has been noticed in other amorphous alloys[42] and a tentative explanation will be given in the discussion. The temperature t_N is characteristic of this pre-crystallization stage: usually t_{cr}-t_N is the order of 20°C to 40°C. The possible reversibility of the pre-crystallization stage was investigated, by stopping the heating at temperatures intermediate between t_N and t_{cr} for a Ni_{32}-Pd_{53}-P_{20} alloy. Whereas the truly amorphous range ($< t_N$) showed reversibility, cooling

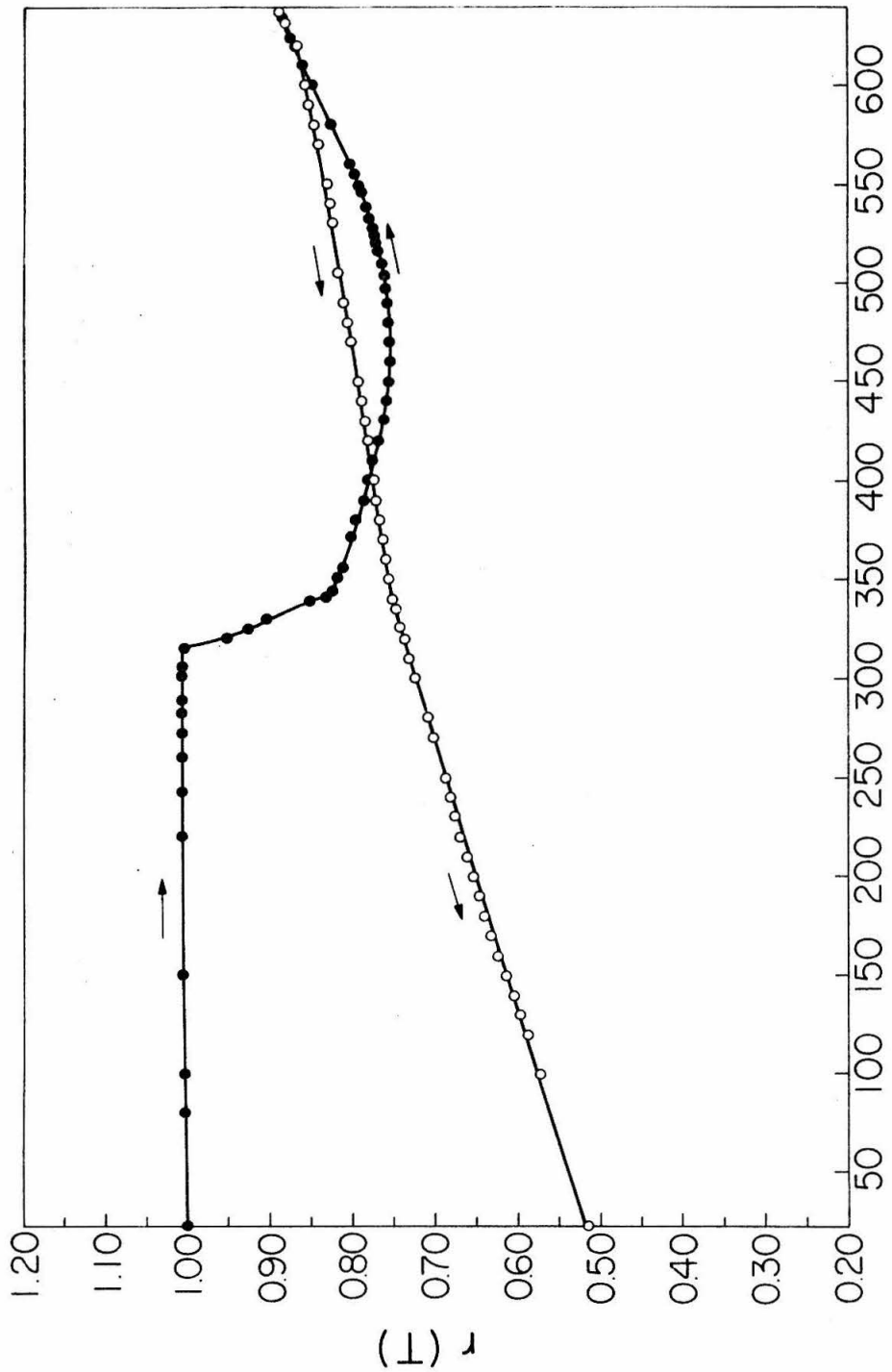

Fig. 25. Relative electrical resistivity of an amorphous Fe_{32}-Pd_{48}-P_{20} alloy measured with an average heating rate of 1.5°C/min.

TABLE XIII

ELECTRICAL RESISTIVITY OF AMORPHOUS Fe-Pd-P AND Ni-Pd-P ALLOYS ABOVE ROOM TEMPERATURE

Composition	$\mu(/^{o}C)x10^{4}$	$t_{cr}(^{o}C)$	t_N
Ni_{32}-Pd_{53}-P_{15}	1.5 - 3.0	335 ($\pm$10)	290($\pm$10)
Ni_{43}-Pd_{37}-P_{20}	1.4 - 0.4	305 ($\pm$5)	280
Ni_{53}-Pd_{27}-P_{20}	1.0 - 0.5	325	295
Ni_{63}-Pd_{17}-P_{20}	1.0 - 0.6	340	320
Ni_{73}-Pd_{7}- P_{20}	0.7	325	---
Fe_{33}-Pd_{47}-P_{20}	0.4 - 0.7	315 ($\pm$5)	---

from temperatures t such that $t_N < t < t_{cr}$ made obvious the irreversible character of this pre-crystallization transformation. The crystallization takes place in several steps, as it appears in Figs. 24 and 25. These steps are especially well defined in nickel-palladium-phosphorus alloys. The intermediate crystalline step which is very clear in Ni_{32}-Pd_{53}-P_{15} regresses in importance as the amount of nickel increases. It was found, by X-ray studies that this intermediate stage corresponded to metastable crystalline phases. Stable crystalline phases were attained, in all cases, before 550°C. The temperature behavior of r(t) for these stable crystalline phases was investigated for Ni_{32}-Pd_{57}-P_{20} and Fe_{33}-Pd_{47}-P_{20} alloys by measuring the resistivity during slow cooling from temperatures above 550°C. The crystalline alloys exhibited, as expected, larger temperature coefficient than the amorphous (10^{-3}/°C compared to 10^{-4}/°C). A change of slope, probably connected with a Curie point, appeared at 260°C for Ni_{32}-Pd_{53}-P_{15} and 345°C for Fe_{33}-Pd_{47}-P_{20}. The room temperature resistivities of the stable crystalline phases were respectively 32% and 52% of the values for the amorphous phases, in good agreement with previous observations[40,42].

V. CRYSTALLIZATION OF Fe-Pd-P AND Ni-Pd-P ALLOYS

A limited effort was devoted to the study of the rate of crystallization of the amorphous alloys and the structure of the corresponding crystalline phases. When these alloys are rapidly heated (at rates of about 400°C/min and above) crystallization occurs rapidly at a certain temperature, as previously reported for $Pd_{80}Si_{20}$[16] and Fe_{80}-P_{13}-C_7[17]. This temperature can be easily measured by spot welding thermocouple wires (0.005" in diameter) to a small alloy foil (about 5 x 5 mm) and immersing the specimen in a furnace. A typical temperature-time curve is shown in Fig. 26. From the height of the heat pulse, an approximate value for the heat of crystallization can be obtained. An average value for all the specimens investigated was about 700 cal/mole. The sudden crystallization temperature was $340^{\circ} \pm 5^{\circ}C$ for the Fe-Pd-P alloys and $375^{\circ} \pm 10^{\circ}C$ for the Ni-Pd-P alloys. Within the experimental uncertainties, this temperature did not vary with the ratios Fe/Pd and Ni/Pd.

Experiments were also performed in an effort to find what structural transformations might be responsible for the rather abrupt changes in the slope of the resistivity-temperature curves such as those shown in Figs. 24 and 25. Specimens suitable for X-ray diffraction analysis (1x2cm) were heated for a fixed time (20 min) at various temperatures with steps of 20°C. An X-ray diffraction pattern was taken after each step. This isochronal heat treatment corresponds to an average rate of heating of 1°C/min which is comparable with that

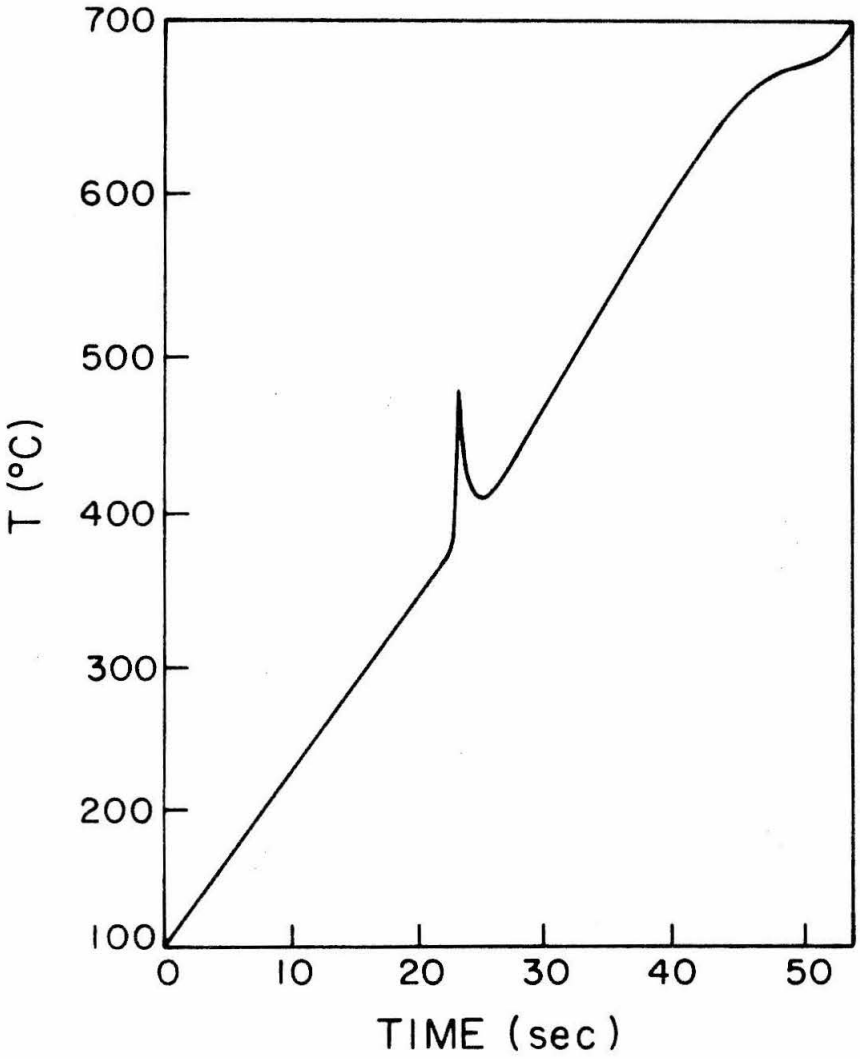

Fig. 26. Thermal analysis of an amorphous Ni_{53}-Pd_{27}-P_{20} alloy.

used for measuring electrical resistivity changes with temperature. Up to about 280°C, the diffraction pattern did not show any change (dotted line in Fig. 27). At 300°C, the width of the broad amorphous band of the pattern slightly decreased and the maximum of this band shifted to higher 2θ values (dash and dot curve in Fig. 27). At 320°C, additional sharpening occurred (dashed curve in Fig. 27). At 340°C, rather sharp diffraction peaks were present although the amorphous band can still be recognized. At this state of transformation, the alloys consists of an amorphous matrix, in which crystals are embedded. The crystal structure of the crystalline phase (or phases) is not known, but it is most probably that these are metastable intermediate phases. This statement is based on the fact that, as the temperature was increased, the intensity of most of the reflections shown in Fig. 27 decreased and disappeared at about 500°C. At the same time, new reflections corresponding to the equilibrium phases became visible and increased in intensity. At 550°C, equilibrium was achieved and further annealing of the specimen for more than one month at this temperature did not bring any change in the diffraction pattern.

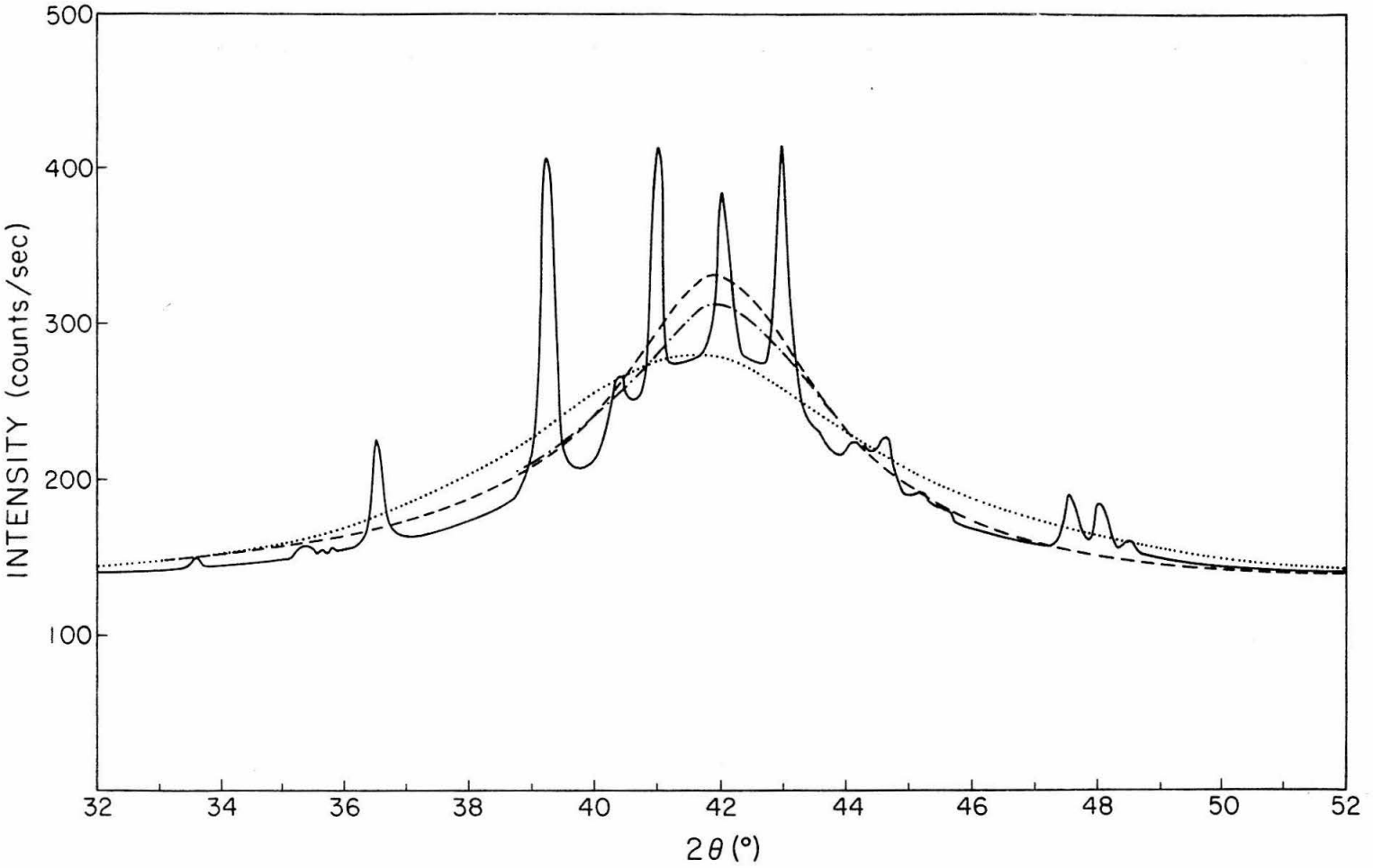

Fig. 27. Diffraction pattern (CuK_α radiation) of a Ni_{32}-Pd_{53}-P_{15} amorphous alloy after different stages of isochronal heat treatment, 20 min every 20°C: . . . . . room temperature; —·—·— 300°C;- - - - - - - - 320°C;——— 340°C.

VI. MAGNETIC MOMENTS

A. Experimental Procedure

The magnetic moments of Fe_{23}-Pd_{57}-P_{20}, Fe_{33}-Pd_{47}-P_{20}, Fe_{44}-Pd_{36}-P_{20} and Ni_{32}-Pd_{53}-P_{15} were measured with a low temperature magnetometer, which is described in reference 43. This magnetometer is of the null-coil pendulum type. The pendulum is made of a fused silica rod bearing a small coil located at its bottom and the sample is placed close to the coil. The upper part of the rigid pendulum is connected to a bronze beam with silicon strain gages bonded to its surface. The output voltage of the strain gages is entered in an a.c. bridge circuit utilizing a lock-in amplifier as detector. Uniform magnetic fields up to 8.4 kOe can be obtained at the sample location. Direct currents ranging from 0 to 100 mA can be sent through the pendulum coil, which is adequate to attain an equilibrium under the highest field. Coil currents were calibrated with a pure nickel sample as reference. Additional checks were made by measuring the susceptibilities of diamagnetic Bi and paramagnetic Hg $Co(SCN)_4$.

Small samples were cut out of quenched foils and carefully weighed with a microbalance. Weights of 2 to 5 mg were sufficient for ferromagnetic samples, whereas about 50 mg were used in the case of paramagnetic samples. The magnetic moments of the alloys were measured from liquid helium temperature up to room temperature. This range was, when necessary, extended towards lower temperatures by pumping the helium and temperatures down to 1.6^{o}K were obtained by

this procedure. Temperatures were measured with a germanium resistor up to 50°K and a copper-constantan thermocouple up to room temperature. Between 1.6°K and 4.2°K the vapor pressure of helium was used for temperature determination. An automatic temperature control helped to attain good thermal stability.

B. Results

Two alloy compositions, Fe_{32}-Pd_{48}-P_{20} and Fe_{44}-Pd_{36}-P_{20}, showed a clear ferromagnetic behavior at low temperatures, though they gave evidence of substantial magnetic "hardness" since, even in the highest magnetic field (8.4 kOe), saturation was not completely reached. The alloy Fe_{23}-Pd_{57}-P_{20} had a rather complex behavior which, at first, could be mistaken for normal ferromagnetism. For reasons explained later in this paragraph this alloy was assumed to exhibit superparamagnetism.

For each measurement in the ferromagnetic range of temperatures the saturation was evaluated by assuming a law of approach of the type:

$$\sigma_{H,T} = \sigma_{\infty,T}(1 - a/H^2)$$

where $\sigma_{H,T}$ is the magnetization per unit mass under the field H and at a temperature T and $\sigma_{\infty,T}$ is the saturation magnetization, for all magnetic domains oriented in the same direction[44,45]. At least three values of the field were used and a least square fitting yielded $\sigma_{\infty,T}$ in each case. In order to obtain the saturation magnetization at 0°K($\sigma_{\infty,0}$), values of $\sigma_{\infty,T}$ were fitted along a law in $T^{3/2}$ through a least square procedure (a T^2 fitting was less satisfactory):

$$\sigma_{\infty,T} = \sigma_{\infty,0}(1 - bT^{3/2})$$

The saturation moment was then evaluated in units of Bohr magnetons. The variations of magnetic moments (per unit mass of iron) with temperature are given in Fig. 28. Whereas a clear ferromagnetic region can be recognized at low temperatures, a pronounced tail effect occurs for the transition from ferromagnetism to paramagnetism. It was consequently rather difficult to determine a Curie point with precision. The Curie points were determined using the following method. First the inflexion point of the curve $\sigma_{H,T} = f(T)$ (for H = 8.35 kOe) was considered to give a good approximation of the ferromagnetic Curie temperature. A more elaborate analysis was subsequently used to check these values. In the vicinity of the Curie point, on the ferromagnetic side, $\sigma_{H,T}$ behaves like $(T-T_c)^{\frac{1}{2}}$; on the paramagnetic side, assuming a Curie-Weiss behavior, $\sigma_{H,T}/H$ behaves like $1/(T-T_c)$. Consequently a plot of $\sigma^2_{H,T}$ versus $H/\sigma_{H,T}$ should yield a straight line through the origin for $T = T_c$[46]. The intercepts of these straight lines with one of the axis of coordinates are then used for a more precise determination of T_c, by interpolation or extrapolation. This procedure confirmed that Fe_{32}-Pd_{48}-P_{20} and Fe_{44}-Pd_{36}-P_{20} were normal ferromagnetic alloys, in spite of the important tail effect apparent in Fig. 28. The alloy Fe_{44}-Pd_{36}-P_{20} had a Curie point which was extrapolated to about 380°K, whereas a Curie point of approximately 165°K was obtained for the alloy Fe_{32}-Pd_{48}-P_{20}. The intercepts of the straight lines $\sigma^2_{H,T} = \gamma\, H/\sigma_{H,T}$ with the axis $H/\sigma_{H,T} = 0$ were always

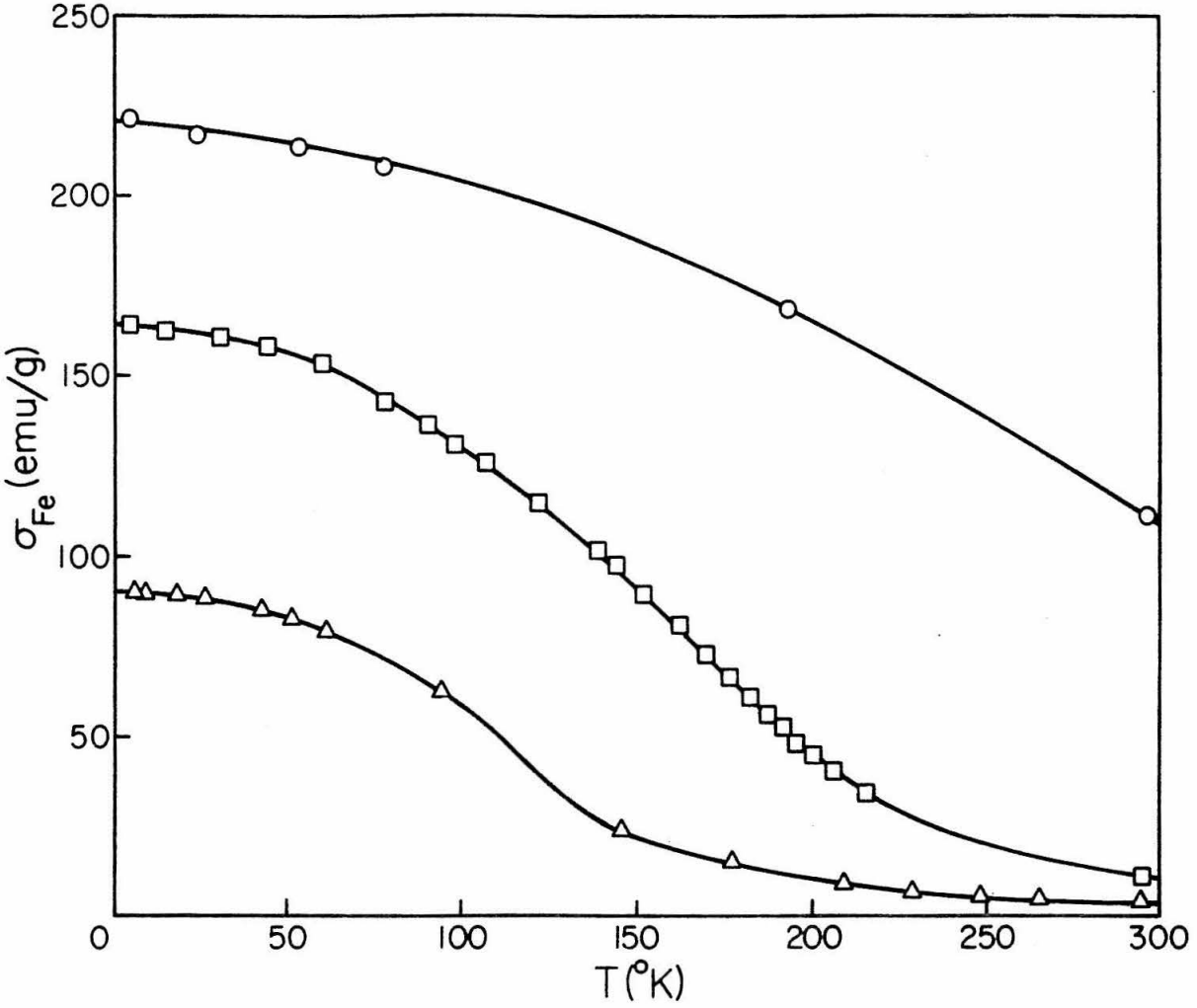

Fig. 28. Magnetization (per unit mass of iron) in a field of 8.35 kOe versus temperature for Fe_{44}-Pd_{36}-P_{20} (circles), Fe_{32}-Pd_{48}-P_{20} (squares) and Fe_{23}-Pd_{57}-P_{20} (triangles).

negative for Fe_{23}-Pd_{57}-P_{20}, down to 6.5°K, and linear extrapolation confirmed that no Curie temperature existed for this alloy, thus implying a lack of long range ferromagnetism for this composition. This fact was confirmed by the magnetization curves obtained for Fe_{23}-Pd_{57}-P_{20} (cf. Fig. 29), which revealed a magnetization still far from saturation, even at the lowest temperature (6.5°K). The magnetic behavior of Fe_{23}-Pd_{57}-P_{20} appears to be similar to the "superparamagnetism" recognized in AuFe alloys by Crangle et al.[47]. A paramagnetic behavior following a Curie-Weiss law was recognized above 135°K (cf. Fig. 30). The constant C in the Curie-Weiss relation $\chi = C/(T-135)$ yielded a moment of 5.98 μ_B per atom of iron, giving therefore some backing to the assumption of superparamagnetic behavior for this alloy. The saturation magnetization was obtained for this alloy by extrapolation to $1/H=0$[48]. All three values of $\sigma_{\infty,0}$ and T_c (Curie temperature) are given in Table XIV.

Preliminary experiments show that all the amorphous Ni-Pd-P alloys are paramagnetic at room temperature. Only Ni_{32}-Pd_{53}-P_{15} was investigated down to 1.6°K. Paramagnetism, with a very approximate 1/T dependence, was observed down to 1.6°K though a small permanent moment, probably due to some iron impurities in palladium, was observed. The gram susceptibility (χ_g) was 1.45×10^{-6} e.m.u. at room temperature for Ni_{32}-Pd_{53}-P_{15}, increasing to 10.0×10^{-6} e.m.u. at 1.6°K.

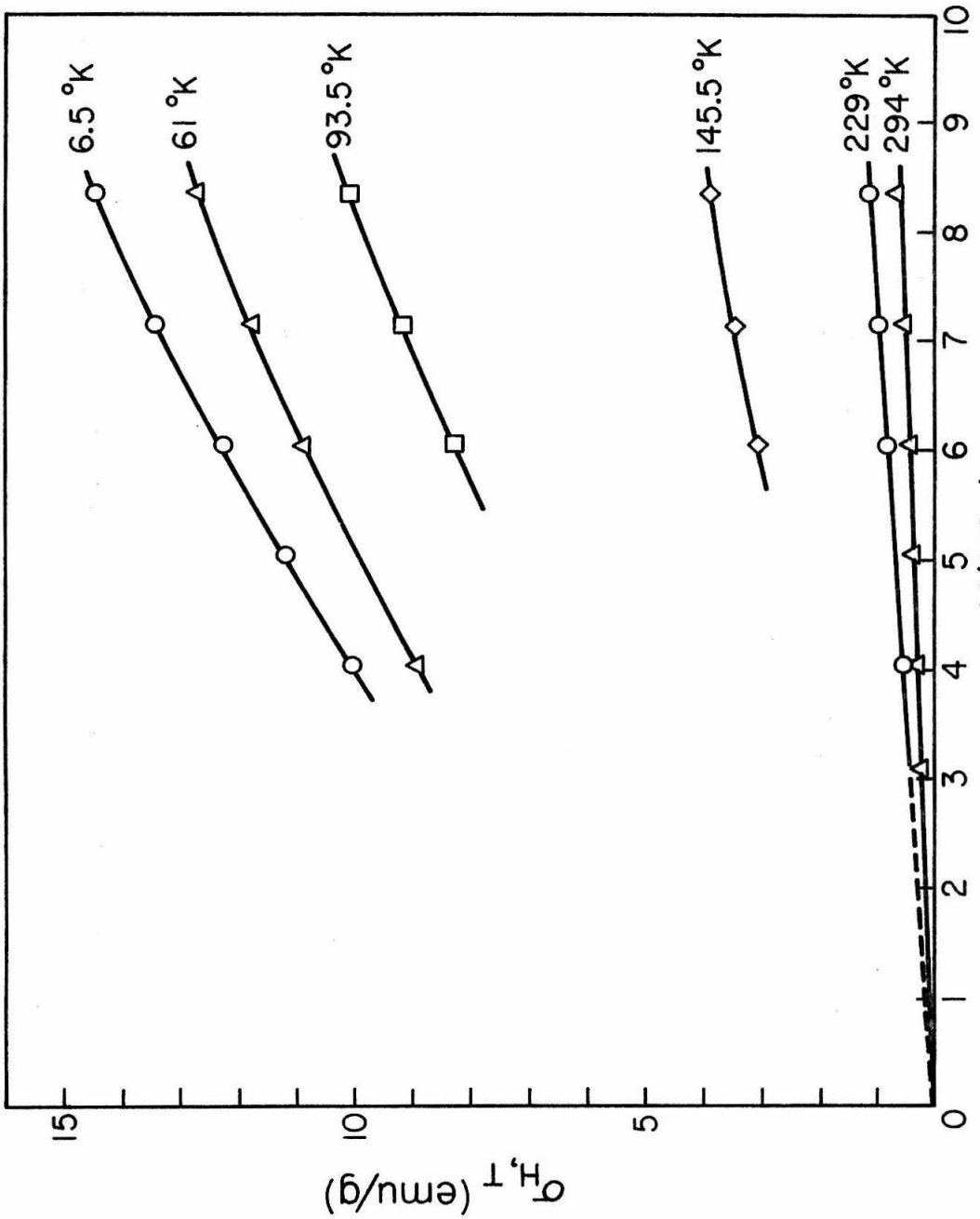

Fig. 29. Magnetization of an amorphous Fe_{23}-Pd_{57}-P_{20} alloy versus magnetic field at different temperatures.

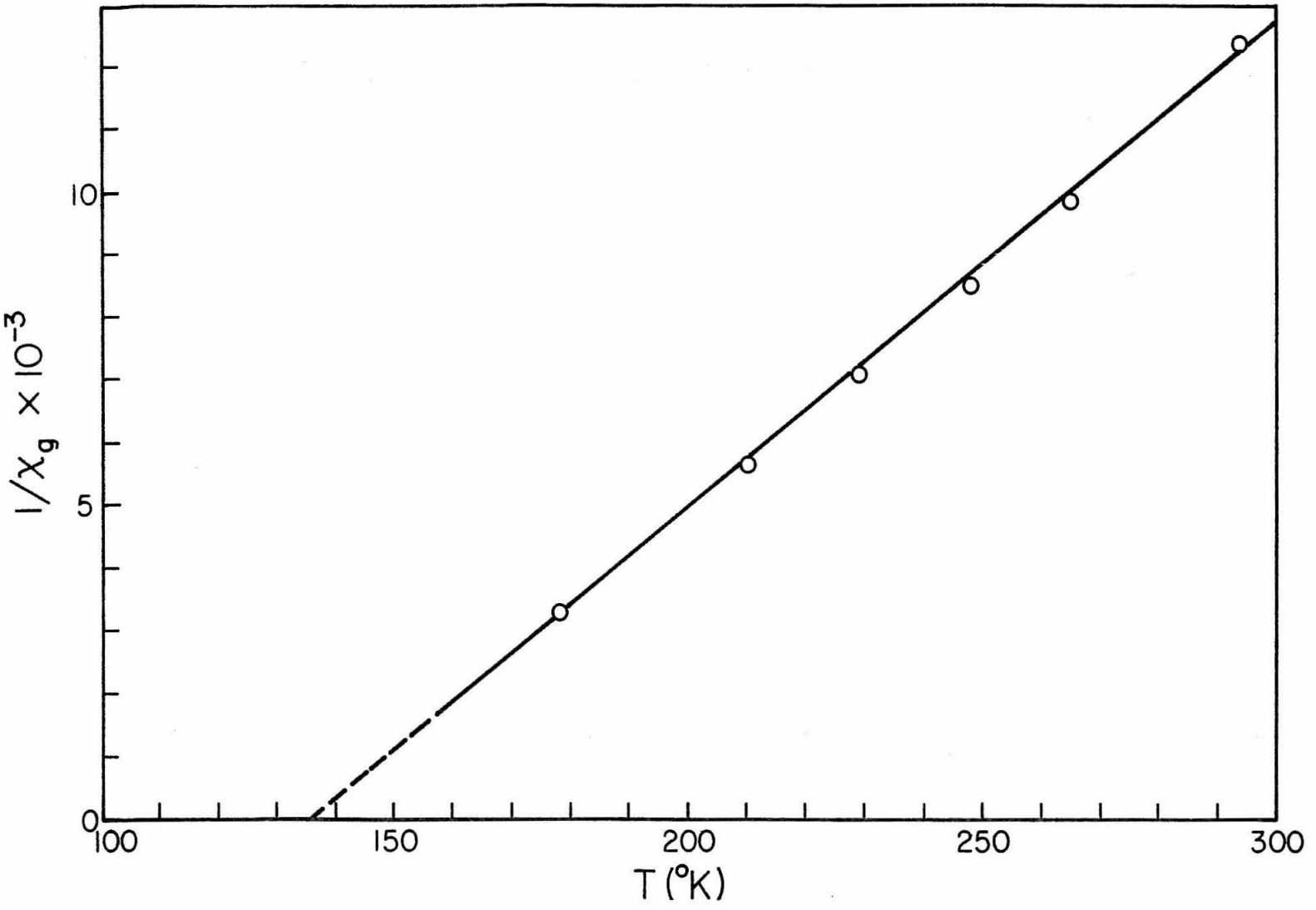

Fig. 30. Inverse gram susceptibility of Fe_{23}-Pd_{57}-P_{20} versus temperature, showing the Curie-Weiss temperature dependence.

TABLE XIV

SATURATION MOMENTS AND CURIE POINTS

OF AMORPHOUS Fe-Pd-P ALLOYS

Composition	$\sigma_{\infty},0(\mu_B)$	T_c (^oK)
Fe_{23}-Pd_{57}-P_{20}	1.07	135 (paramagnetic)
Fe_{32}-Pd_{48}-P_{20}	1.70	165($\pm$5)
Fe_{44}-Pd_{36}-P_{20}	2.16	380($\pm$10)

VII. DISCUSSION

During the last decade, a considerable amount of research has been devoted to the study of amorphous solids, resulting in a better understanding of the amorphous state. Amorphous or glass-like structure does not imply randomness of the atomic arrangement. Some degree of local order may prevail, though the true characteristic of crystallinity - namely the invariance of the atomic structure under translation in three directions defining a space lattice - is absent. The number of translations of a unit cell required to define a solid as crystalline is a controversial subject. Consequently, amorphous and crystalline solids have a common boundary which is the smallest microcrystalline state in which the size of the microcrystals is of the order of magnitude of the unit cell size.

A. Structure of the quenched Fe-Pd-P and Ni-Pd-P alloy phases

Most of the experimental information on the structure of the Fe-Pd-P and Ni-Pd-P alloys resulted from the X-ray investigations leading to the radial distribution functions reported in section III-E. The X-ray diffraction patterns of the quenched foils showed broad maxima and no sign of crystalline Bragg reflections. It can, of course, be argued that small grain size and stresses can broaden the Bragg peaks of crystalline solids. By applying the Scherrer formula to the observed width of the diffraction peaks. the crystal size for the Fe-Pd-P and Ni-Pd-P alloys would be about 13 to 15 Å. Since in the rapidly quenched foils internal stresses are undoubtedly present,

they also contribute to the broadening of the peak and consequently the crystal sizes given above might be slightly less than the actual values. Additional evidence for the lack of crystallinity was obtained by electron microscopy. Whereas previous investigators[40] utilized the "lace like" edges of the quenched foils for transmission electron microscopy, this investigation was performed by using the center of quenched foils thinned by electropolishing until they reached a suitable thickness. No evidence of microcrystals was found at a magnification of 80,000. The remarkable lack of contrast of bright as well as dark field images and the broad diffraction patterns (cf. Fig. 31) are strong indications of lack of well-defined crystallinity.

The X-ray diffraction patterns (cf. Fig. 4) exhibit a first relatively sharp peak and subsequent oscillations around the coherent homogeneous scattering curve $\sum_i x_i f_i^2$. The linear relationship obtained between the values of r_1 and alloy compositions (cf. Figs. 11 and 15) suggests that a continuity of structure exists through the whole range of metallic concentrations and that Ni or Fe atoms can be substituted for Pd atoms without drastic changes in the structure, just like in a crystalline solid solution. The point corresponding to Ni_{32}-Pd_{53}-P_{15} in Fig. 11 does not fall on the straight line, and this can be explained by the fact that this particular alloy contained only 15 at.% P instead of 20 at.%. The linear relationship between r_1 and concentration can be considered as an extension of Vegard's law to amorphous alloys. It is unfortunate that the amorphous range does not

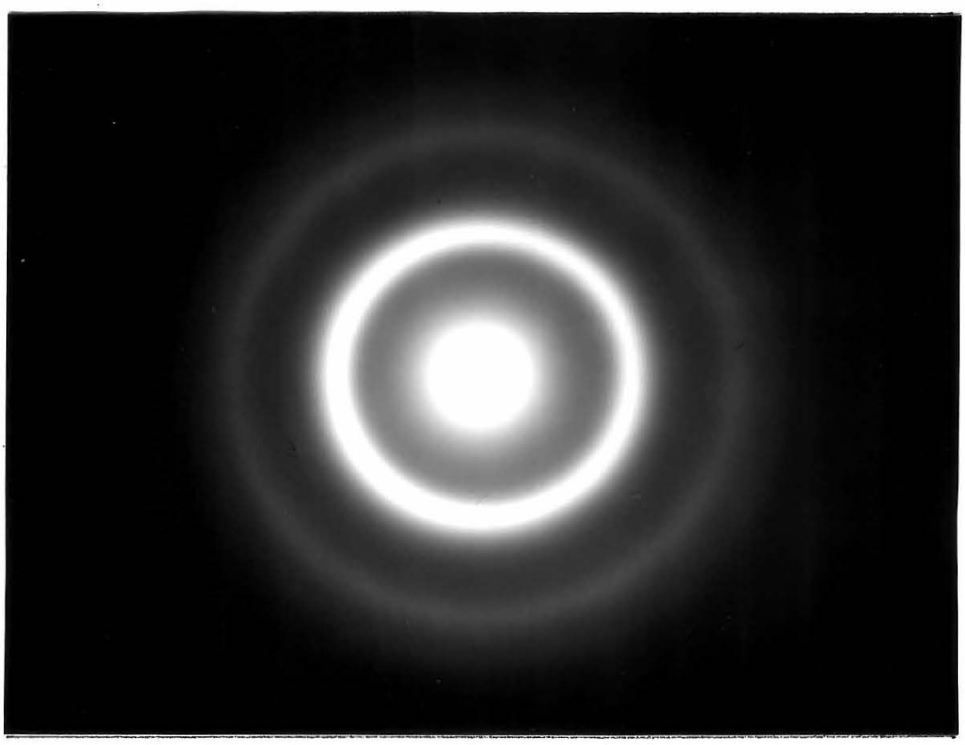

Fig. 31. Electron diffraction pattern of an amorphous Ni_{32}-Pd_{53}-P_{15} alloy.

include the binary alloys Pd-P, Fe-P and Ni-P. The approximate values of r_1 for these compositions, however, can be obtained by extrapolating the straight lines of Figs. 11 and 15. This leads to $r_1 = 2.97$ Å for Pd-P and $r_1 = 2.61$ Å for Ni-P, based on the Ni-Pd-P results and $r_1 = 2.95$ Å for Pd-P and $r_1 = 2.68$ Å for Fe-P, based on the Fe-Pd-P results. The usefulness of the extrapolated values on the choice of possible models for the amorphous state will be considered later. The radial distribution functions established for the Fe-Pd-P and Ni-Pd-P alloys yield additional indications of continuity of structure all through the amorphous range. The invariance of the ratios r_i/r_1 (for $i = 2,3,4$) throughout Fe-Pd-P and Ni-Pd-P alloys also implies similarity of structural arrangement. As explained before, only the first peak of the radial distribution functions can yield meaningful information on coordination numbers. Though some errors, partly due to an imperfect knowledge of the density of the amorphous alloys, were involved, the coordination numbers were found to be around 13 for the overall coordination and 10 to 11 for the metallic coordination (cf. Tables V and IX).

The diffraction patterns and radial distribution functions of Fe-Pd-P and Ni-Pd-P alloys show some resemblance with those obtained for liquids[49,50,51]. The successive "shells" corresponding to increasing interatomic distances around an arbitrary atom become less and less marked after the "nearest neighbors" shell. The smoothness of the oscillations of the radial distribution function around the homogeneous

parabola $4\pi r^2 \rho_o (\Sigma_i x_i K_i)^2$, shows a dispersion of interatomic distances obviously more "liquid like" than "crystal like", making appropriate the qualification of "frozen liquids" sometimes applied to the quenched amorphous alloys. Palladium, nickel and γ-iron are fcc metals but, unfortunately, only iron has been studied in the liquid state. Ruppersberg[52] found a coordination close to 8 which seems to indicate an arrangement comparable with a bcc structure in the crystalline state. More truly fcc types in the liquid state, are copper[51] and gold[53] (cf. Fig. 32). When compared with the radial distribution of these metals, the amorphous Fe-Pd-P and Ni-Pd-P alloys show a sharper "nearest neighbors" peak and a clear splitting of the RDF in two shells between 4 Å and 6 Å (cf. Fig. 8 in particular). This splitting is an interesting and real feature of the radial distribution function of this category of quenched amorphous alloys[17,40,54] and has also been observed in Ni-P amorphous alloys obtained by electrodeposition[55] or chemical deposition[11]. The shape of the first peak in the amorphous Fe-Pd-P and Ni-Pd-P alloys is also rather different from the shape exhibited in the RDF of liquid metals. To a good approximation the first peak of the RDF of the amorphous alloys is gaussian, which suggests atomic displacements centered around an average interatomic distance more sharply defined than in a liquid metal. The deviations of atomic distances around an ideal interatomc distance corresponding to the first peak in the RDF are given in Tables V and IX and correspond to mean square displacements of the order of 0.06 $Å^2$. This value is larger for the second shell though overlapping of the second

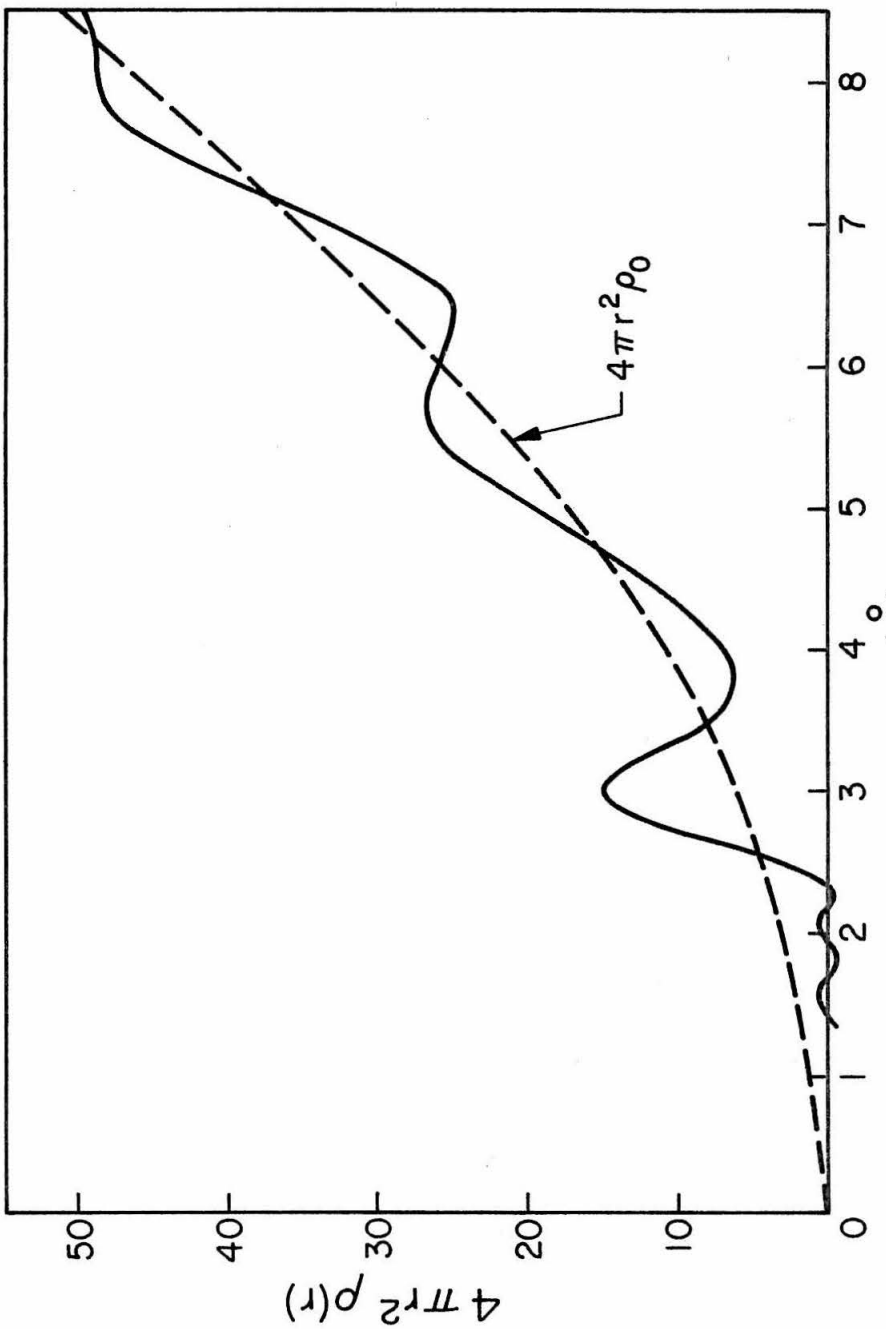

Fig. 32. Atomic radial distribution of liquid gold (Ref. 53).

and third shells prevents an accurate determination. Thermal displacements obviously cannot account for more than a small fraction of the mean square displacement which is, consequently, essentially a static displacement. The large value of this mean square displacement for the first atomic shell is an argument against the hypothesis of microcrystallinity with microcrystals of the order of 15 Å, since such crystals would yield a sharper "nearest neighbors" peak. Independent experiments by Lesueur[56] on a rapidly quenched $Pd_{80}Si_{20}$ alloy (believed to have a structure close to Ni-Pd-P and Fe-Pd-P alloys) confirm the existence of important displacement disorder. Lesueur observed that under irradiation by fission products, the amorphous structure of the quenched $Pd_{80}Si_{20}$ was unaltered whereas irradiation would produce a progressive amorphization of the stable crystalline phases in the equilibrium crystalline $Pd_{80}Si_{20}$ alloy.

A suitable model for the amorphous state of Fe-Pd-P and Ni-Pd-P alloys must, obviously, take into account the role played by phosphorus since, without phosphorus, the quenched binary alloys Fe-Pd and Ni-Pd are always crystalline. In their study of an electrodeposited amorphous Ni_{83}-P_{17} alloy Dixmier et al.[11] suggested a model consisting of regularly spaced but randomly oriented layers of atoms arranged as in the (111) plane of an fcc structure. Their model, unfortunately, does not show the role of phosphorus. In a separate investigation, however, Legras[57] showed that the chemical bonding between Ni and P in the electrodeposited Ni_{83}-P_{17} was identical to the bonding existing in Ni_3P. Informations on the bonding between

phosphorus and metallic atoms can be obtained from the study of transition metal phosphides. The transition metal phosphides have been studied thoroughly by Rundqvist[38] who pointed out some interesting facts concerning their structure. In the crystalline state, transition metal phosphides with less than 40% atomic phosphorus exhibit tetradecahedral arrangements with phosphorus atoms at the center and metallic atoms at the corners of the polyedron. A tetradecahedron is a polyedron with fourteen triangular faces, which can be better described as made of a square triangular prism with three half octahedron sharing its rectangular sides. The number of metal neighbors varies from 8 to 10 (usually 9) around one phosphorus atom. The tetradecahedral unit for Fe_3P, as an example, is shown in Fig. 33. Whereas the average phosphorus-metal ligancy revolves around 9, the metal-metal ligancy varies between 10 and 12 indicating a rather good packing, not too remote from fcc close packing. On the other hand, the chemical bonding between phosphorus and metal atoms seems rather strong[58], at least stronger than the metal-metal bonds. Besides their importance in the structure of transition metal phosphides, the tetradecahedra have been mentioned as possible structural units in liquids, from a geometrical standpoint (Bernal polyedra[59,60]).

An attempt will now be made to describe the amorphous structure of the Fe-Pd-P and Ni-Pd-P alloys in terms of the structural units which exist in crystalline phosphides of corresponding phosphorus content. In binary alloys of Fe, Ni, Pd with P, the stable metal rich phosphides are Fe_3P, Ni_3P, $Ni_{12}P_5$ and Pd_3P[39]. These compounds are either orthorhombic (Pd_3P) or tetragonal (Fe_3P, Ni_3P, $Ni_{12}P_5$) but all exhibit

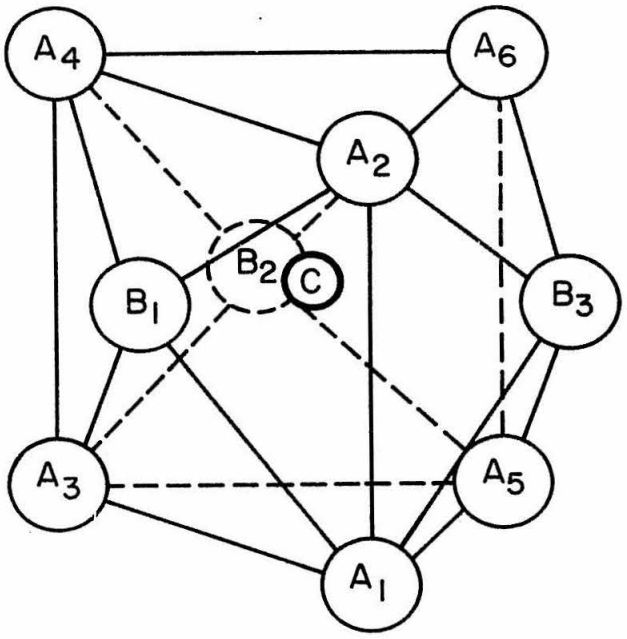

Fig. 33. Tetradecahedral environment of phosphorus in the Fe_3P structure: C is a phosphorus atom; A_i and B_i are iron atoms.

tetradecahedral structural units more or less deformed[38]. The Pd_3P phase shows a range of homogeneity from the stochiometric Pd_3P to "Pd_4P". The decrease in phosphorus is accompanied by a decrease in the volume of the unit cell, and has been accounted for by phosphorus vacancies[61]. On the other hand the eventuality of continuous solid solution $(Fe,Pd)_3P$ and $(Ni,Pd)_3P$ must be considered as such continuous solid solutions have been reported in the Fe-Ni-P ternary system[62]. Let us consider the "nearest neighbors" shell in the crystalline Fe_3P, Ni_3P, $Ni_{12}P_5$ and Pd_3P compounds. The mean interatomic distances for "nearest neighbors" (both around a metal atom and a phosphorus atom) and the average ligancy for the type of pairs considered (which is not necessarily an even number since we consider the average ligancy around non-equivalent atomic positions) are given in Table XV. As previously mentioned, the extrapolated value of r_1 for the binary alloy Pd_{80}-P_{20} would be about 2.96 Å, which is quite close to the nearest neighbors distance in "Pd_4P" (Pd rich Pd_3P phase), though slightly larger. This is to be expected since the amorphous alloys are more disordered than the corresponding crystalline phases. Another experimental fact corroborates the usefulness of the extrapolation of r_1 to the palladium side of the diagram. Quenched Pd_{80}-P_{20} binary alloy consisted almost exclusively of the crystalline phase "Pd_4P" (Palladium rich Pd_3P). In the light of these facts a model based on the atomic arrangement in "Pd_4P" was considered.

The model was considered from the quasi-crystalline approach starting with the atomic shell distances and occupation numbers of an

TABLE XV

NEAREST NEIGHBORS INTERATOMIC DISTANCES r_1 AND COORDINATION NUMBERS N IN METAL RICH PHOSPHIDES

Compound	Metal-Metal		Phosphorus-Metal	
	r_1 (Å)	N	r_1 (Å)	N
Fe_3P	2.72	10.66	2.34	9
Ni_3P	2.68	10.66	2.29	9
$Ni_{12}P_5$	2.60 (2.67)	7.66 (9.00)	2.39	9
Pd_3P (P-rich)	2.965	11.33	2.49	9
Pd_3P (Pd-rich)	2.905	11.33	2.44	9

assumed lattice[30,50]. A gaussian broadening function was then applied to each shell to account for mean-square displacements around the center of the shell (thermal or disorder displacements). Finally a correlation function provided an increasing damping of the oscillations due to the different shells with increasing radial distance. Each atomic shell is represented by the function

$$B(r-r_i) = \left[C_i/(2\pi\sigma_i^2)^{\frac{1}{2}}\right]\exp(-(r-r_i)^2/2\sigma_i^2)$$

and the quasi-crystalline atomic radial distribution function is:

$$4\pi r^2\rho(r) = D(r,d)\left[\sum_i\left[C_i/(2\pi\ \sigma_i^2)^{\frac{1}{2}}\right]\exp(-(r-r_i)^2/2\sigma_i^2) - 4\pi r^2\rho_o\right] + 4\pi r^2\rho_o$$

where:

r_i = radial distance to the i^{th} shell

C_i = number of atoms in i^{th} shell

σ_i^2 = mean square displacement around r_i

d = critical correlation distance

$D(r,d)$= damping function depending on the critical correlation distance

ρ_o = homogeneous density (atoms/$\mathring{A}^3$)

The quasi-crystalline approach was first applied to a simple fcc model in which metal-metal interatomic distances only were considered and complete substitutional disorder between iron or nickel and palladium atoms was assumed. When multiplied by the appropriate average number of electrons per metal atom, the electronic radial distribution

function based on the fcc model was unable to give even an approximate fitting of the 2nd and 3rd shells of the amorphous alloys. Even an average of the 2nd and 3rd shell, as suggested by some authors[63] yielded a poor fitting since the 2nd and 3rd shells in the amorphous alloys revealed shorter interatomic distances. The quasi-crystalline model based on Pd_3P (Pd-rich) yielded a much better approximation. Metal-metal shells only were considered since their contributions are preponderant in the outcome of the radial distribution function. The analytical form of the damping function D(r,d) was evaluated as a function of r/d according to the method outlined by Kaplow et al.[30]. A critical correlation distance of about 18 Å was deduced from the experimental radial distribution functions of Ni-Pd-P and Fe-Pd-P alloys, corresponding to the distance beyond which no appreciable oscillations around the homogeneous parabola $4\pi r^2 (\sum_i x_i K_i)^2 \rho_o$ can be observed. The σ_i were also approximated from the experimentally determined radial distribution functions.

The radial distribution function $4\pi r^2 \rho(r)$ and the function $4\pi r(\rho(r)-\rho_o)$ for such a quasi-crystalline model are shown in Fig. 34. Both the radial distribution function and the distribution function W(r) compare well with the results obtained for the four different amorphous alloys shown in Figs. 7, 8, 9, 12 and 13. The qualitative features of the model show a rather sharp first shell, quite well isolated from the second and third shells which are hard to separate, especially on the atomic radial distribution curve. The coordination for the third shell appears slightly larger in the model than actually

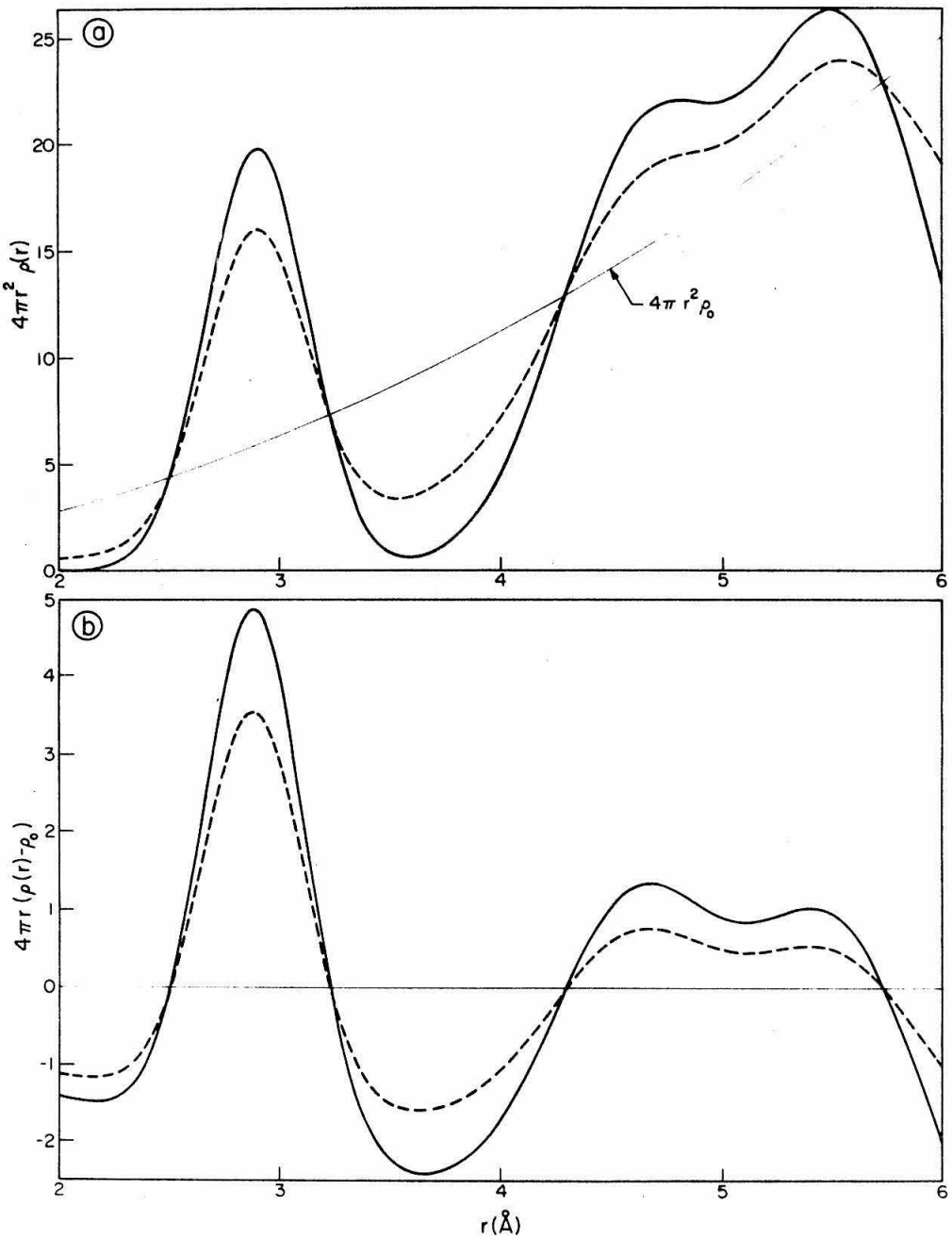

Fig. 34. Atomic RDF (a) and function W(r) (b) for quasi-crystalline models with d = ∞ (solid lines) and d = 18 Å (dotted lines).

observed in the amorphous alloys, but this can be attributed to having chosen too small a value for σ_3^2 (that is, underestimating the amount of displacement disorder for the third atomic shell). Quantitatively the metal-metal coordination number for the first shell was about 10.5 which compares quite well with 10.6, the average value obtained for the amorphous alloys. More striking were the similarities of the ratios r_2/r_1 and r_3/r_1. The model gave $r_2/r_1 = 1.68$ and $r_3/r_1 = 1.91$, while the average values for the amorphous alloys were 1.66 and 1.89 respectively. The structure of the amorphous Fe-Pd-P and Ni-Pd-P alloys can, therefore, be described quite satisfactorily by a quasi-crystalline model based on the Pd_3P (Pd-rich) structure. As an example, Fig. 35 shows the comparison between the distribution functions W(r) obtained for Ni_{32}-Pd_{53}-P_{15} and for a quasi-crystalline model. The model was computed by assuming a linear dependence of r_1 which was the same as the one observed for the amorphous alloys. The progressive substitution of iron or nickel for palladium does not change the structural disordered network based on the Pd_3P structure. The extrapolation on the nickel side of the diagram indicates a nearest neighbors distance of 2.61 Å which can be considered as the nickel-nickel distance in a nickel-rich Ni_3P ("Ni_4P"), though such a compound is not ordinarily stable. The extrapolation on the iron side is more dubious because of the lack of data for alloys containing more than about 44 at.% Fe, which is the end of the amorphous range. The existence of a small range in phosphorus content without change in the amorphous structure can be accounted for by phosphorus vacancies in the tehadecahedral

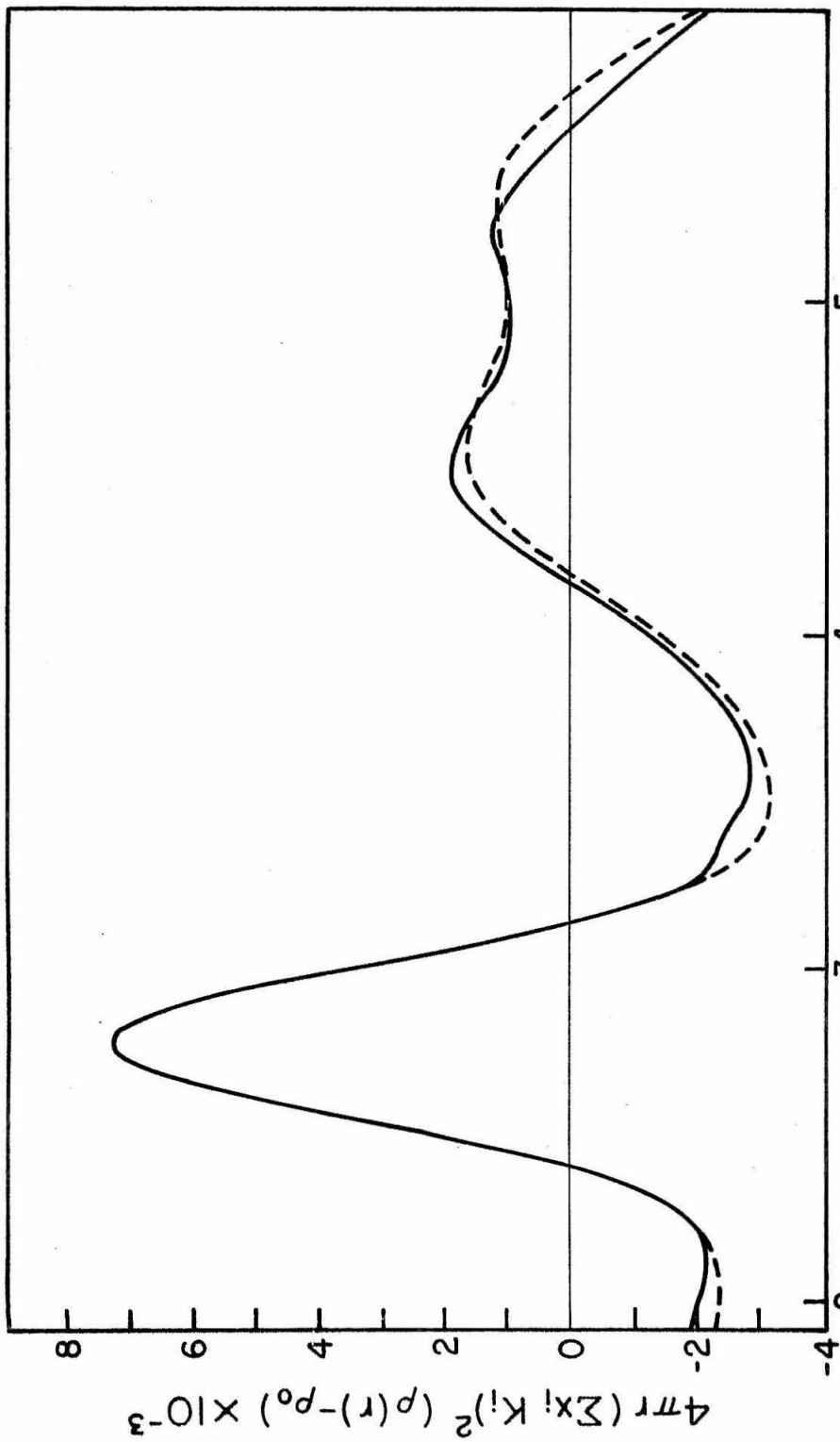

Fig. 35. Distribution function W(r) for Ni_{32}-Pd_{53}-P_{15} (solid line) compared with quasi-crystalline model (dotted line).

arrangements[61] leading to shorter metal-metal interatomic distances. This would explain the value of r_1 obtained for Ni_{32}-Pd_{53}-P_{15}, which is about 1.5% shorter than expected for 20 atomic % phosphorus. The lack of evidence of short phosphorus-metal interatomic distances in the amorphous alloys can be accounted for by the small scattering factor of phosphorus compared with those of Pd, Ni and Fe, as well as by probably slightly larger phosphorus-metal distances than in the crystalline phases. The combination of these two effects leads to the inseparable mixing of all types of interatomic pairs in the first shell. This fact however, was accounted for when coordination numbers were calculated from the radial distribution functions.

The structure of the amorphous Fe-Pd-P and Ni-Pd-P alloys, quenched from the liquid state, can be satisfactorily described by a quasi-crystalline model based on the structure of transition metal phosphides. The glass-forming elements are believed to be tetradecahedral units which are probably already present in the melt. The existence of a linear dependence of interatomic distances on composition is in agreement with the proposed structure.

B. Magnetic moments in amorphous Fe-Pd-P alloys

In the Fe-Pd-P amorphous alloys, two compositions, namely Fe_{44}-Pd_{36}-P_{20} and Fe_{32}-Pd_{48}-P_{20} were found to be ferromagnetic, while the third one, Fe_{23}-Pd_{57}-P_{20} is probably superparamagnetic. Amorphous ferromagnetic alloys have been previously reported in Au-Co alloys obtained by vapor deposition[64] and in Fe-P-C alloys quenched from the

liquid state[65]. The existence of ferromagnetism in amorphous solids was theoretically predicted by Gubanov[66] who showed that only short range interactions are required for ferromagnetism, and that there is no need to assumed long range crystalline order. Since, as explained in section VII, the structure of amorphous Fe-Pd-P alloys is based on the existence of local order similar to that found in crystalline ferromagnetic phosphides, it is not too surprising to find that the amorphous alloys are also ferromagnetic.

The crystalline phosphides Fe_3P, Fe_2P and FeP are ferromagnetic, with saturation moments of 1.84, 1.32 and 0.36 Bohr magnetons per iron atom respectively, whereas FeP_2 is antiferromagnetic[45]. The moments in the iron phosphides are lower than in pure iron mainly because of the filling of the 3d orbitals of iron by electron transfer from phosphorus[67]. Similar filling of the d orbitals of iron group metals have been reported in other phosphides[68], as well as in borides and carbides, which also have a tetradecahedral atomic arrangement for metal rich compounds around the composition Me_3X. A plot of saturation ferromagnetic moments in the crystalline iron phosphides as a function of the ratio of the atomic concentrations of Fe to Fe+P is shown in Fig. 36. The variation of the moment per iron atom with the concentration ratio is almost linear and extrapolates to a zero moment at a concentration ratio of about 0.44. The saturation moments measured for the three amorphous Fe-Pd-P alloys also shown in Fig. 36 fall approximately on a straight line which is above that of the crystalline phosphides and seems to have a slightly larger slope.

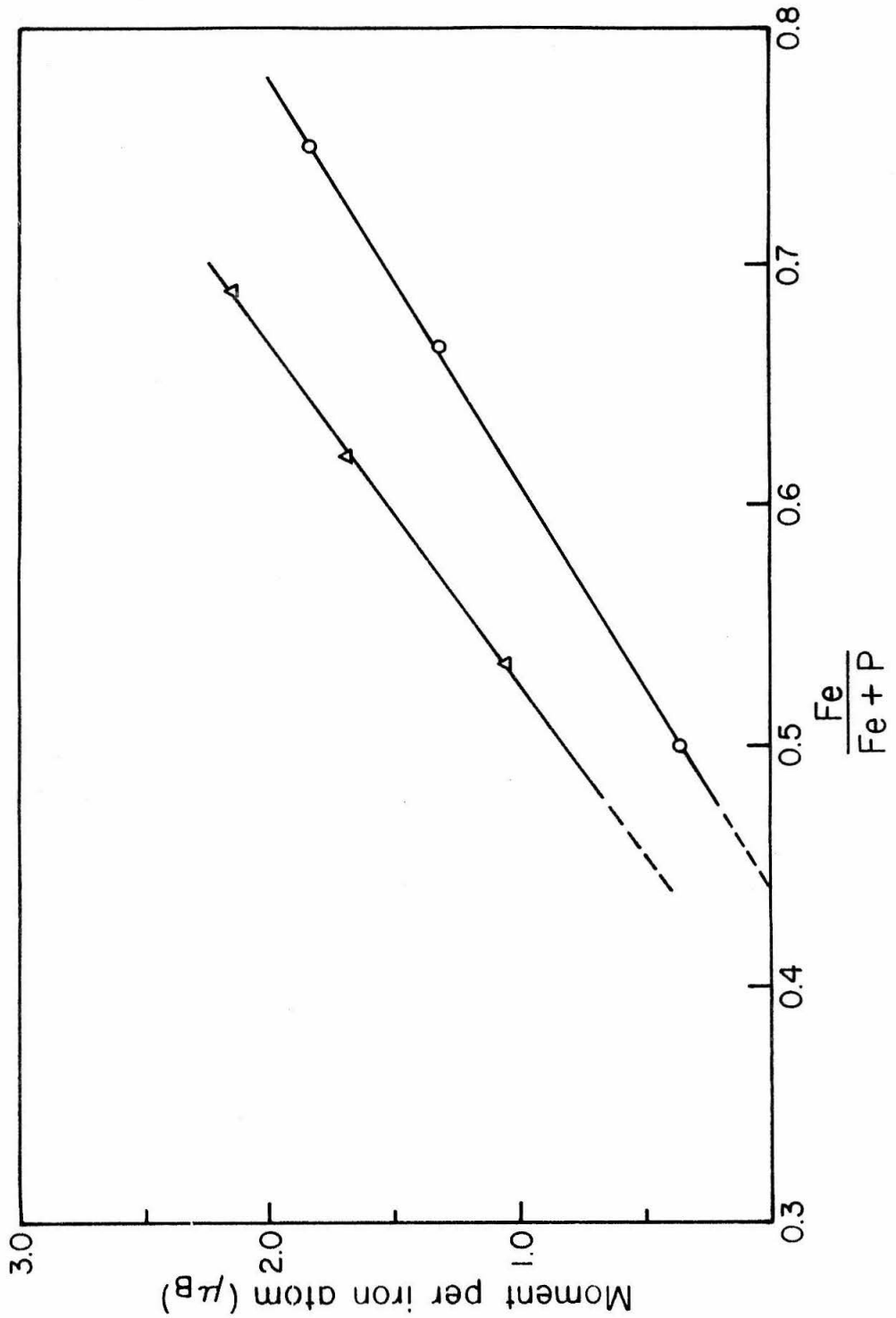

Fig. 36. Saturation moments in amorphous Fe-Pd-P alloys (triangles) and in iron phosphides (circles)

The fact that for a given concentration ratio Fe/(Fe+P) the moments for the amorphous alloys are larger than those in the crystalline phosphides can be interpreted in different ways. The most probable explanation, however, is the existence of simultaneous electron transfer from phosphorus to iron and palladium: the linear decrease of the saturation moment of the amorphous Fe-Pd-P alloys with decreasing Fe/Fe+P ratio can be attributed to the progressive filling of the holes in the 4d band of Pd and the 3d band of Fe by electron transfer. In the amorphous alloys, however, the number of holes in the d bands is probably different from the values in the pure elements, due to a different overlap of s and d bands. The presence of larger moments in Fe-Pd-P amorphous alloys suggests also a possible contribution of palladium to the overall ferromagnetism. Additional evidence of the ferromagnetic coupling between iron and palladium is given by the superparamagnetic behavior of the alloy Fe_{23}-Pd_{57}-P_{20}. The fact that palladium may contribute to the ferromagnetism of alloys containing iron-group metals has been recognized by a number of investigators (cf. Ref. 69 for instance). This contribution to the bulk ferromagnetism has been diversely interpreted and the actual moment carried by individual palladium atoms has been estimated anywhere from 0.1 μ_B to 0.7 μ_B. However, it seems rather well established that palladium contributes to the building of ferromagnetic complexes (or "atmospheres")[47] around iron (or cobalt) atoms in ordinary fcc alloys. This has the effect of favoring clusters of iron and palladium atoms which bear,

as a whole, rather large moments. The large value of 5.98 μ_B/iron atom obtained from the Curie constant in the paramagnetic range of Fe_{23}-Pd_{57}-P_{20} could hardly be explained by assuming that iron is in a triply ionized state (Fe^{3+}) with a spin moment of 5.92 μ_B/atom. As pointed out by Wollan[70], such highly ionized state are very unlikely for conducting metallic systems. The only other alternative consists of clustering via polarization of palladium atoms. Actually such an explanation has been proposed to explain the experimentally observed magnetic moments in Pd-Co-Si amorphous alloys[40]. In view of the superparamagnetic behavior of the approach to saturation at low temperatures and of the large moment per iron atom, it seems, therefore, probable that some clustering occurs in Fe_{23}-Pd_{57}-P_{20}, in spite of the neutralizing effect of phosphorus. Such a clustering is all the more likely in amorphous systems where only the closest atomic shells (and mainly the nearest neighbors shell) contribute to the short range order. Determination of the cluster size is not possible in the absence of data for lower iron concentrations. The large tail effect present in the magnetization versus T behavior of the alloys Fe_{32}-Pd_{48}-P_{20} and Fe_{44}-Pd_{36}-P_{20} before a clear bulk ferromagnetism is attained, can probably be accounted for by the high degree of disorder of the amorphous alloys and some degree of clustering accompanied by palladium polarization. Some of the clusters might still act paramagnetically while the rest of the solid already shows ferromagnetism, as it was suggested for the Pd-Co-Si amorphous alloys[40]. Such an interpretation might also account for the peculiar behavior of the low temperature

resistivity of the amorphous Fe-Pd-P alloys.

The model proposed for the structure of amorphous Fe-Pd-P and Ni-Pd-P alloys implies a short range order quite similar to that existing in the metal rich phosphides. The magnetic moments of the Fe-Pd-P amorphous alloys are in agreement with such a model, in which electron transfer from phosphorus to the metals reduces the saturation moments. A small moment can be attributed to the palladium atoms which contribute to ferromagnetic ordering.

C. Electrical resistivity of amorphous Ni-Pd-P and Fe-Pd-P alloys

The amorphous Fe-Pd-P and Ni-Pd-P alloys investigated are metallic conductors. Their resistivity at room temperature is approximately 100 to 150 $\mu\Omega$-cm, which is about two to three times that of the crystalline alloys of the same composition. The larger resistivity of the amorphous alloys is the result of the rather high degree of disorder which characterizes the amorphous state. Between $480^{o}K$ and about $160^{o}K$, the resistivity of all alloys decreases almost linearly with temperature. The slope of the linear part of this curve is only about 10^{-8} Ω-cm/^{o}K which is of the order of magnitude of one-tenth that of the same alloys in the equilibrium crystalline state. This small temperature coefficient of resistivity can also be attributed to the large disorder in the amorphous structure and to the absence of long range periodicity, since the contribution of the phonon scattering is expected to be very small in amorphous structures[16]. According to Ziman's theory, extended by Gubanov to amorphous metallic conductors[66],

the main temperature dependent term in the mean free path of conduction electrons is the correlation function, which is a slowly varying function of temperature.

The most striking feature of the low temperature resistivity of the amorphous Fe-Pd-P and Ni-Pd-P alloys is the existence of a minimum at temperatures varying from 9 to 96°K, according to the alloys. As it was shown in section IV, the low temperature resistivity can be reasonably well described by a relation of the type:

$$r(T) = r_o + \beta T^2 + \Delta r_o - \alpha \text{ Log } T \qquad (1)$$

where $r(T) = \rho(T)/\rho(294^oK)$. This relation is best valid below the temperature T_m of the minimum. At temperatures above T_m, the T^2 term is dominant until the linear variation is reached. The variation in T^2 can be explained in terms of the band structure of the Fe-Pd-P and Ni-Pd-P alloys which contain 80 at.% transition elements. It has been shown that electron-electron interactions in the transition metals contribute substantially to the resistivity at low temperature through collisions between s electrons (conduction electrons) and d electrons which are mainly bound electrons. Such s-d electron-electron interactions contribute a T^2 term in addition to the normal lattice resistivity[71]. In the amorphous alloys where the main characteristics of the s and d bands are expected to prevail, such a T^2 contribution appears clearly at low temperature since the electron-phonon contribution to resistivity is small. The resistivity minimum is related to

the existence of a -Log T term in equation (1). This logarithmic contribution is indicative of a Kondo effect. According to Kondo's analysis[72], s-d interactions in dilute magnetic alloys result in a -Log T contribution to the resistivity, provided the exchange integral J of the s-d interaction is negative (antiferromagnetic coupling). This s-d interaction is actually the coupling between localized and conduction electrons spins.

The occurrence of a Kondo effect in Fe-Pd-P amorphous alloys constitutes a puzzling fact in several respects. The hypothesis of Kondo implies the existence of localized moments and requires the non-correlation of the localized spins. Such a picture is rather hard to conceive for ferromagnetic alloys where strong d-d interactions take place. Moreover, iron could hardly be considered an impurity in alloys containing 23 at.%, 32.4 at.% and 44 at.% iron. However, it can be noticed that the importance of the Kondo effect, as characterized by the depth of the minimum, decreases drastically with increasing iron content. Though the dispersion of data is quite large, this fact appears quite clearly in Table XII. In addition, the largest effect occurs in the Fe_{23}-Pd_{57}-P_{20} alloy, which is assumed to be superparamagnetic. It appears therefore, that the strong d-d interactions existing in the ferromagnetic alloys are quite detrimental to the occurrence of the resistivity minimum, but cannot suppress it completely. The magnetization of the amorphous Fe-Pd-P alloys was shown to exhibit large tail effects at the onset of ferromagnetic ordering. It is, therefore,

likely that the bulk ferromagnetism cannot prevent the existence of localized moments on a small fraction of the iron atom, provided, for instance, they have a sufficient palladium environment. Such an hypothesis is consistent with the fact that the Kondo effect is increased for higher palladium concentrations. The existence of localized moments in otherwise ferromagnetic alloys has been recognized by some investigators and theoreticians[73,74]. In the amorphous Fe_{23}-Pd_{57}-P_{20} alloy, the postulated clusters of iron atoms and associated polarized palladium atoms are only partly coupled and one can therefore expect a more pronounced Kondo effect. Investigations on alloys with lower iron content would be very helpful in providing more clues on the Kondo effect in the amorphous Fe-Pd-P alloys. Unfortunately, the amorphous range does not appear to extend to very low iron contents.

The Kondo effect observed for the amorphous Ni-Pd-P alloys seems to be easier to explain in terms of localized moments due to magnetic impurities. The magnetization measurements performed on the amorphous alloy Ni_{32}-Pd_{53}-P_{15} showed an intermediate behavior between weak paramagnetism and Pauli paramagnetism, with a very small residual moment even at room temperature. Such a behavior could be explained by the presence of a very small concentration of iron in palladium (and possibly nickel). Evidence that the palladium utilized for the preparation of these amorphous alloys contains a very small concentration of iron has been confirmed by magnetic[75] and resistivity[76] measurements. A Kondo effect due to very small concentrations of iron has been observed in

copper and gold[77] for instance. The fact that no significant trend of variations of T_m or α with nickel content (cf. Table XI) was observed confirms that iron impurities present in both palladium and nickel are probably responsible for the Kondo effect. If this effect were due to localized moments on nickel atoms, one might expect a linear variation of α with nickel concentration and a variation of T_m proportional to the square root of concentration.

The high temperature resistivity measurements performed on Fe-Pd-P and Ni-Pd-P amorphous alloys were particularly helpful in following the crystallization process, and were correlated with X-ray diffraction experiments. The increase in resistivity shown by most of the amorphous alloys in the range of 280 to 320°C seems to be related to the formation of very small crystallites embedded in the amorphous matrix. Evidence of very small microcrystals in an amorphous matrix appears in the X-ray diffraction patterns of this pre-crystallization stage, as characterized by very broad Bragg peaks superimposed on the amorphous band. Such microcrystals probably act as additional scattering centers during the earliest stages of their development, when they are still rather far apart. In the Fe-Pd-P and Ni-Pd-P alloys, the crystallization temperature t_{cr} is always about 40°C higher than the temperature of onset of the increase in resistivity t_N. The sharp drop in resistivity observed at t_{cr} corresponds to the rapid growth of crystalline phases. In the Ni-Pd-P alloys, these phases are metastable and revert to the stable phase mixture at higher temperatures. The

behavior of the resistivity of the stable crystalline phases did not exhibit any singularities except changes of slope probably related to a Curie point (cf. Figs. 24 and 25).

VIII. SUMMARY AND CONCLUSIONS

The structure and properties of iron-palladium-phosphorus and nickel-palladium-phosphorus alloys quenched from the liquid state have been investigated. Since these alloys can be obtained in the amorphous state within a relatively large range of concentrations for the metallic atoms, both structure and properties could be studied as a function of composition. In both ternary systems, a linear relationship was found between the nearest neighbor interatomic distances r_1 and concentration. The ratios between the second and third neighbor distances (r_2 and r_3) and r_1 also varied linearly with concentration. These relationships constitute an extension to amorphous alloys of the well known Vegard's law generally applicable to crystalline solid solutions.

The structure of the amorphous alloys was tentatively explained by a quasi-crystalline model based on the crystal structure of metal rich phosphides. The structural unit used for the model is that found in Pd_3P, except that it has a distorted atomic packing. The radial distribution functions computed for the model were in satisfactory agreement with those experimentally determined.

The iron rich amorphous alloys Fe_{44}-Pd_{36}-P_{20} and Fe_{32}-Pd_{48}-P_{20} were found to be ferromagnetic, whereas the Fe_{23}-Pd_{54}-P_{20} alloy is probably superparamagnetic. The saturation magnetic moments observed for these three alloys were 2.16, 1.70 and 1.07 Bohr magnetons per iron atom respectively. The progressive reduction in the magnetic

moments with decreasing iron content was attributed mostly to electron transfer from phosphorus to the d band of the transition metals. Palladium atoms appeared to contribute to the overall ferromagnetism through the formation of "atmospheres" around iron atoms which could account for clustering in the alloy Fe_{23}-Pd_{57}-P_{20}. The Ni-Pd-P amorphous alloys investigated were weakly paramagnetic.

All the amorphous alloys were electrical conductors. Their temperature coefficients of resistivity were about ten times smaller than those of the corresponding crystalline alloys. These results gave additional evidence for the non-crystalline nature of the quenched alloys. A minimum in the resistivity temperature curves was observed for the amorphous Fe-Pd-P alloys. This minimum was in the range from 17.5 to 96^{o}K depending on the composition of the alloys, and its importance increased with decreasing iron content. The resistivity minimum was tentatively attributed to a Kondo effect due to localized moments on a small fraction of the iron atoms. The amorphous Ni-Pd-P alloys also showed a resistivity minimum in a range of temperatures from about 9 to 14^{o}K depending on composition. This Kondo effect was attributed to the presence of small amounts of iron impurities in the palladium, nickel and perhaps also phosphorus used for alloys preparation.

The validity of the model proposed for the structure of the amorphous Fe-Pd-P and Ni-Pd-P could be further tested by several types of experiments. The analysis leading to the radial distribution function was complicated by the presence of three kinds of atoms. It

the non-metallic atom had a very low scattering factor (which was not the case of phosphorus) its contribution to the diffracted intensity compared to those of the metals, could be neglected. Recent experiments indicate that ternary Ni-Pd-B alloys might be quenched into an amorphous phase, and if so, this system should be considered for further investigations. Diffraction experiments with X-rays only may not be sufficient to establish the fine details of the structure of ternary amorphous alloys. Neutron diffraction experiments would certainly help in solving the problem. but the small size of the quenched specimens, especially their thickness, may create experimental difficulties.

A more detailed study of the ferromagnetic transition could be done by Mössbauer spectroscopy. This technique would also be useful in verifying the assumption of clustering in the amorphous Fe_{23}-Pd_{57}-P_{20} alloy. Furthermore, some information on the postulated localized moments responsible for the Kondo effects observed could be expected from these experiments. In this respect, magneto-resistance experiments might also be of interest, since a negative magnetoresistance would be a strong indication of localized moments.

REFERENCES

1. J. Prins., in Physics of Non-crystalline Solids, edited by J. Prins., p. 1, North Holland publishing Co. - Amsterdam (1965).
2. J. Stevels, in Physics of Non-crystalline Solids, edited by J. Prins., p. 497, North Holland publishing Co. - Amsterdam (1965).
3. K. Evstropyev, in The Structure of Glass: Proceedings of a Conference on the Structure of Glass-Leningrad (1953), Consultants Bureau - New York (1958).
4. A. Levedev, Bull. Acad. Sci. USSR, Phys. Ser. 4, No.4 (1940).
5. Tamman, Der Glaszustand - Leipzig (1932).
6. S. Fujime, Japan J. Appl. Phys., 5, 764 (1966).
7. S. Mader, J. Vacuum Science and Techn., 2, 35 (1965).
8. S. Fujime, Japan J. Appl. Phys., 5, 643 (1966).
9. C. Wagner, T. Light, N. Holder and W. Lukens, J. Appl. Phys., 39, 3690 (1968).
10. B. Bagley and D. Turnbull, Technical Report No. 17-Division of Engineering and Applied Physics - Harvard University - April 1968.
11. J. Dixmier, K. Doi and A. Guinier, in Physics of Non-crystalline Solids, ed. by J. Prins., p. 67, North Holland publishing Co. - Amsterdam (1965).
12. P. Pietrokowsky, Rev. Sci. Instr., 34, 445 (1962).
13. Pol Duwez, Trans. A.S.M., 60, 607 (1967).
14. Pol Duwez and R. Willens, Trans. A.I.M.E., 227, 362 (1963).

15. W. Klement Jr., R. Willens and Pol Duwez, Nature, 187, 869 (1960).

16. Pol Duwez, R. Willens and R. Crewdson, J. Appl. Phys., 36, 2267 (1965).

17. S. Lin, Ph.D. Thesis, California Institute of Technology (1968).

18. H. Luo and Pol Duwez, Appl. Phys. Letters, 2, 21 (1963).

19. D. Harbur, J. Anderson and W. Maraman, Rapid Quenching Drop Smasher, Los Alamos Scientific Laboratory of the University of California, Report No. La - 3584 (1966).

20. P. Debye, Ann. Physik., 46, 809 (1915).

21. B. Warren, H. Krutter and O. Morningstar, J. Am. Ceram. Soc., 19, 202 (1936).

22. R. W. James, The Optical Principles of the Diffraction of X-rays, Vol. II in the Crystalline State, published by G. Bell and Sons, Ltd. - London (1948).

23. J. Waser and V. Schomaker, Revs, Modern Phys., 25, 671 (1953).

24. C. Pings and J. Waser, J. Chem. Physics, 48, 3016 (1968).

25. R. F. Kruh, Chem. Revs., 62, 319 (1962).

26. P. Mikolaj and C. Pings, J. Phys. and Chem. of Liq., 1, 93 (1968).

27. A. Guinier, X-Ray Diffraction, W. H. Freeman and Co. - San Francisco and London (1963).

28. G. Fournet, Trans. Faraday Soc., Discussion 10-11, 121 (1951).

29. R. Ruhl, B. Giessen, M. Cohen and N. Grant, Acta Met., 15, 1693 (1967).

30. R. Kaplow, S. Strong and A. Averbach, Phys. Rev., 138, A1336 (1965).

31. S. Strong and R. Kaplow, Rev. Sci. Instr., 37, 1495 (1966).

32. W. Ruland, Brit. J. Appl. Phys., 15, 1301 (1964).

33. D. Cromer and J. Waber, Acta Cryst., 18, 104 (1965).

34. International Tables for X-ray Crystallography, Vol. III, Kynoch Press - Birmingham (1962).

35. K. Furukawa, Rep. Prog. in Phys., 25, 395 (1962).

36. T. Ino, J. Phys. Soc. Japan, 12, 495 (1957).

37. Finbak, Acta Chem. Scand., 3, 1293 (1949).

38. S. Rundqvist, Arkiv Kemi, Bd 20/7, 98 (1963).

39. W. Pearson, Hand book of Lattice Spacings and Structure of Metals, Vol. 2, Pergamon Press (1967).

40. R. Crewdson, Ph.D. Thesis, California Institute of Technology (1966).

41. N. Mokrovskii and A. Regel, Zh. Tekhn. Fiz., 23, 2121, (1953).

42. H. Chen and D. Turnbull, J. Chem. Phys., 48, 2560 (1968).

43. M. Weiner, Ph.D. Thesis, California Institute of Technology (1968).

44. R. Bozorth, Ferromagnetism, Van Nostrand - New York (1951).

45. A. Meyer and M. Cadeville, J. Phys. Soc. Japan, 17 Suppl. B-I, 223 (1961).

46. D. Williams, The Magnetic Properties of Matter, Elsevier Publishing Co. - New York (1966).

47. J. Crangle and W. Scott, J. Appl. Phys. 36, 921 (1965).

48. J. Crangle and W. Scott, Phy. Rev. Letters, 12, 126 (1964).

49. S. Steeb, Fortschr. Chem. Forsch., Bd. 10/4, 473 (1968).

50. R. Kaplow, S. Strong and B. Averbach, in Local Atomic Arrangements Studied by X-ray Diffraction, Metallurgical Society of the A.I.M.E., Vol. 36, p. 159 (1965).

51. H. Ruppersberg, Mém. Sc. Rev. Mét., LXI/10, 709 (1964).

52. H. Ruppersberg and H. Seemann, Z. Natursforsch, 21a, 820 (1966).

53. O. Pfannenschmid, Z. Naturforsch., 15a, 603 (1960).

54. J. Dixmier and A. Guinier, Mém. Sc. Rev. Mét., LXIV/1, 53 (1967).

55. B. Bagley and D. Turnbull, J. Appl. Phys., 39, 5681 (1968).

56. D. Lesueur, C. R. Acad. Sc. Paris, 226, 1038 (1968).

57. C. Legras, Mémoire pour l'obtention du diplôme d´ ingénieur du Conservatoire des Arts et Métiers, Paris (1964).

58. Schönberg, Acta Chem. Scand., 8, 226 (1954).

59. J. Bernal, in Liquids: Structure, Properties, Solid Interactions, edited by T. Hugel, p. 25, Elsevier publishing Co. - (1965).

60. J. Bernal, Nature, 185, 68 (1960).

61. Fruchart and Triquet, C. R. Acad. Sci. Paris, 252, 1323 (1961).

62. Nowotny and Henglein, Monatsh. Chem., 79, 385 (1948).

63. S. Fujime, Japan J. Appl. Phys., 5, 1029 (1966).

64. S. Mader and A. Nowick, Appl. Phys. Letters, 7, 57 (1965).

65. Pol Duwez and S. Lin, J. Appl. Phys., 38, 4096 (1967).

66. A. Gubanov, Quantum Electron Theory of Amorphous Conductors, Consultants Bureau - New York (1965).

67. R. Gambino et al., J. Appl. Phys., 38, 1253 (1967).

68. P. Albert et al., J. Appl. Phys., 38, 1258 (1967).

69. J. Crangle, Phil. Mag., 5, 335 (1960).

70. E. Wollan, Phys. Rev., 112, 1710 (1962).

71. J. Ziman, Electrons and Phonons, Clarendon Press - Oxford (1963).

72. J. Kondo, Prog. Theor. Phys., 32, 37 (1964).

73. T. Moriya, in Rendiconti della Scuola Internazionale di Fisica "Enrico Fermi", XXXVII Corso, Academic Press - New York (1967).

74. V. Jaccarino, J. Appl. Phys., 39, 1166 (1968).

75. M. Weiner, private communication.

76. R. Hasegawa, private communication.

77. G. Van den Berg, in Proceedings of the 7th International Conference on Low Temperature Physics, edited by G. M. Graham and A. Hollis-Hawlett, University of Toronto Press (1961).

APPENDIX I

Phase diagrams in binary Fe-P, Ni-P and Pd-P systems

(cf. M. Hansen, Constitution of binary alloys, Mac Graw-Hill - New York (1958)).

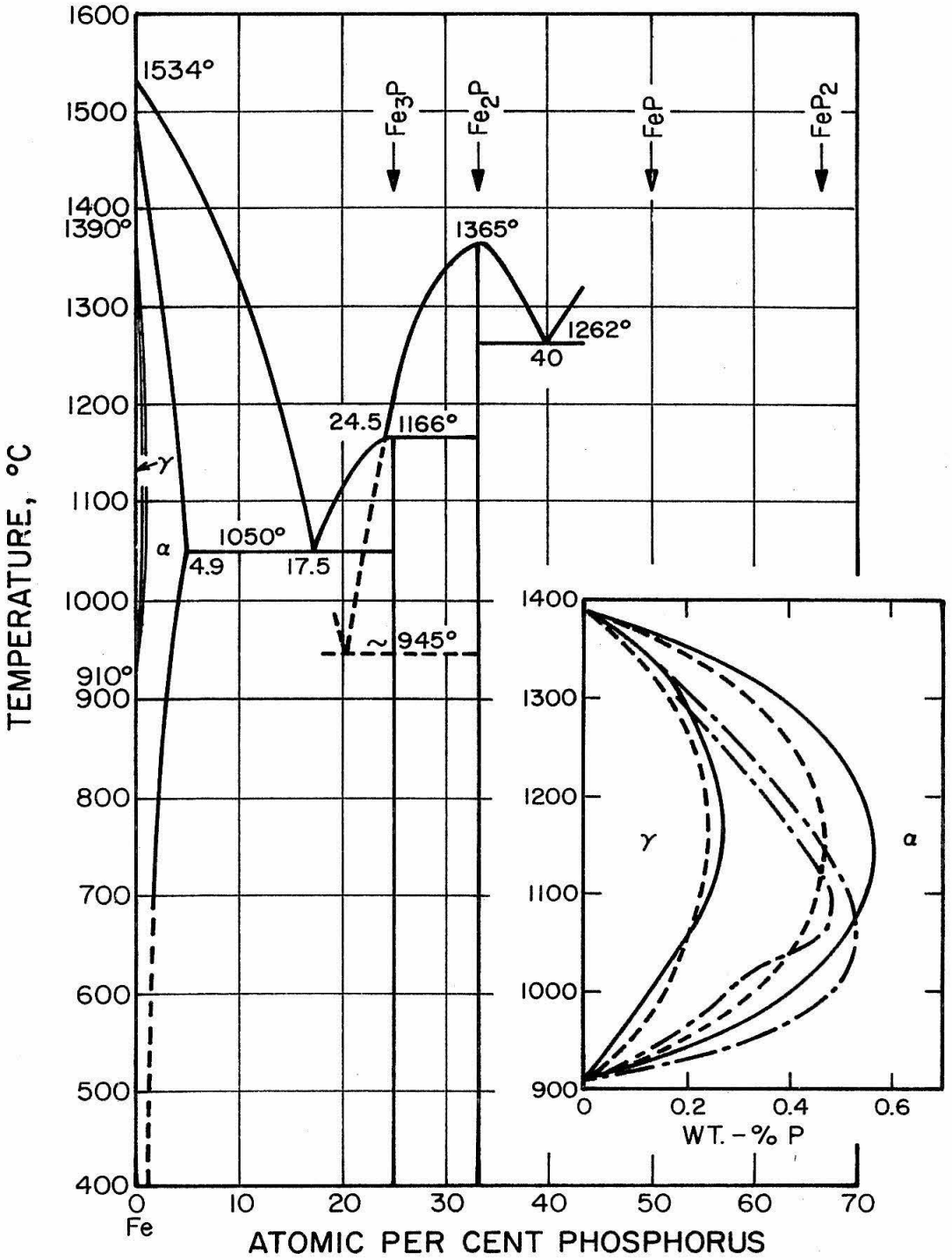

Fig. 37. Fe-P binary phase diagram

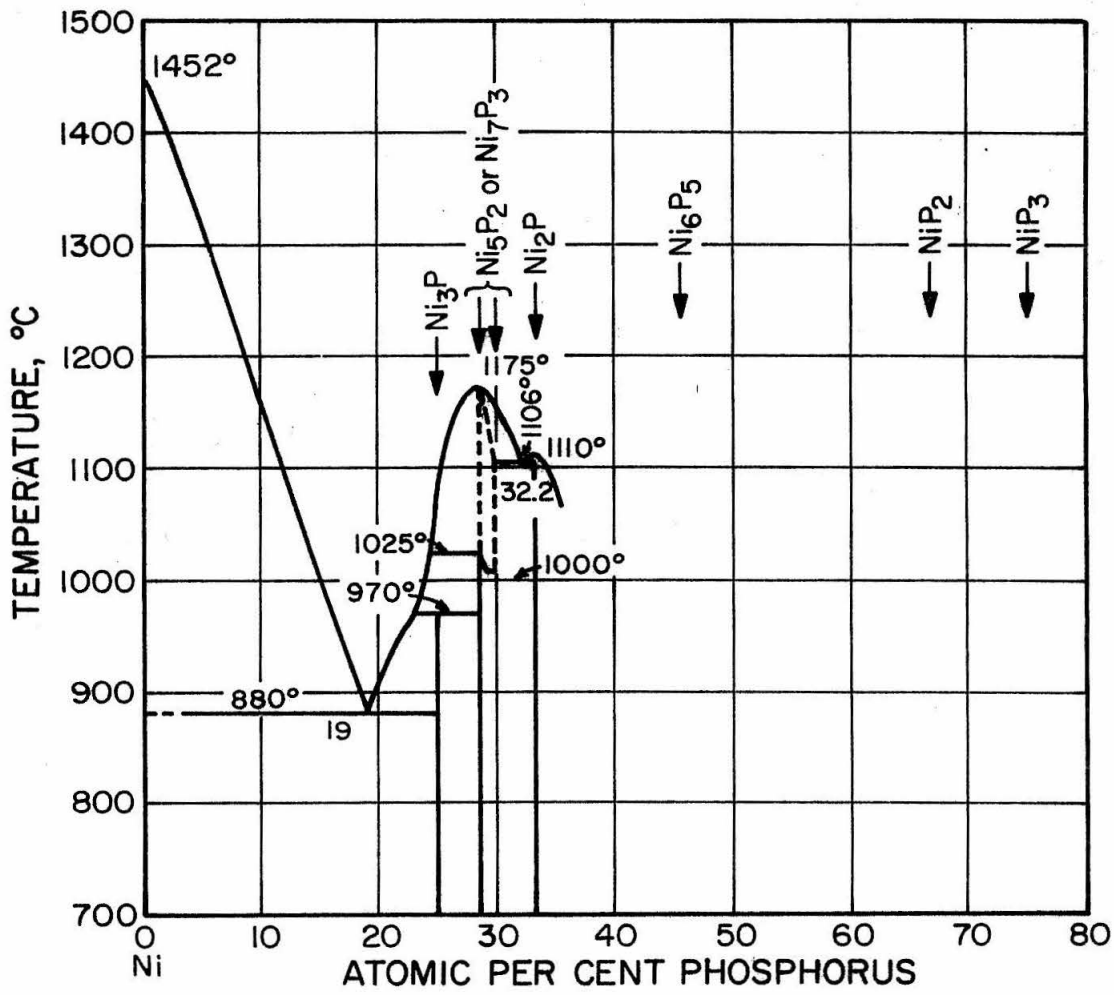

Fig. 38. Ni-P binary phase diagram

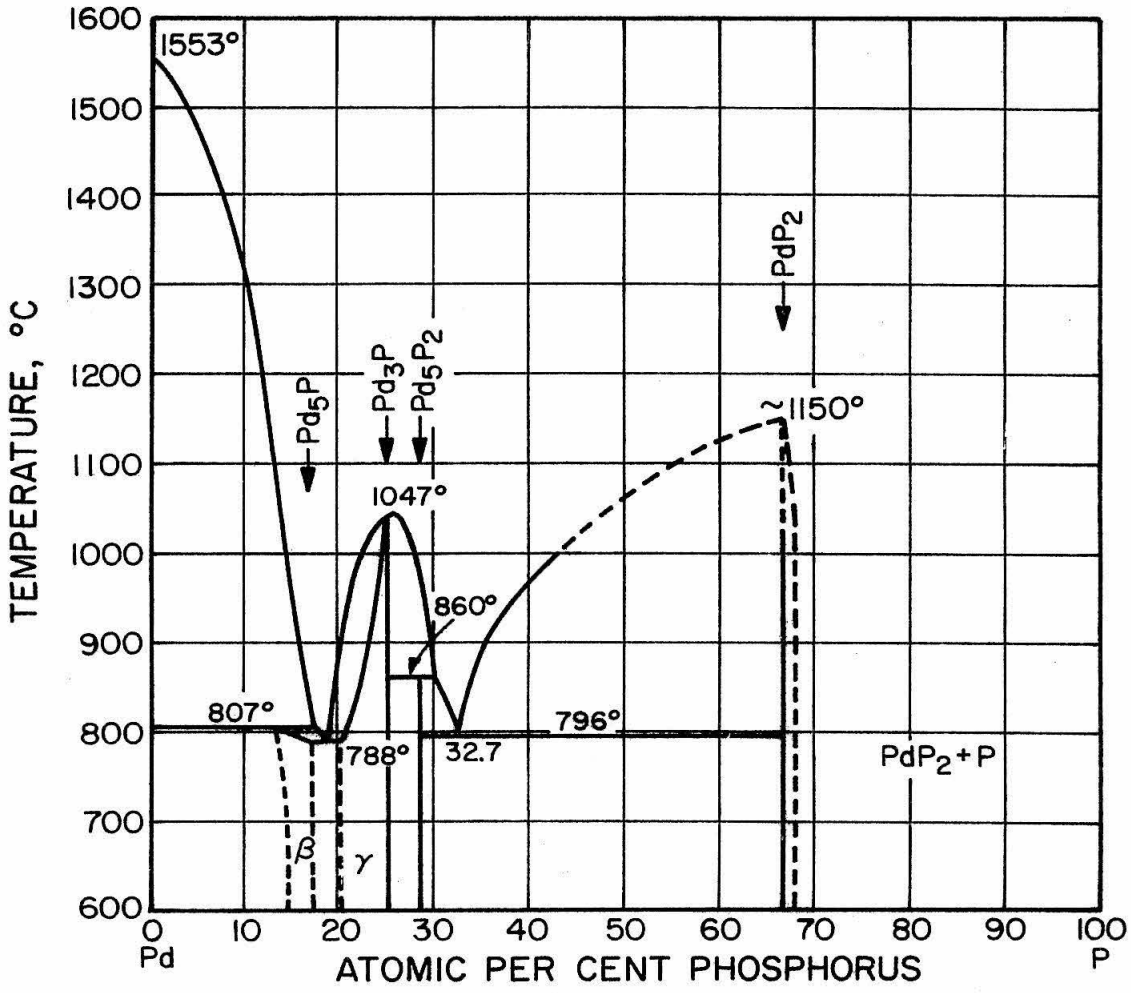

Fig. 39. Pd-P binary phase diagram

APPENDIX II

Program used for the determination of Electronic Radial Distribution Functions

This program is written in FORTRAN IV language for processing through an IBM 360/75 or an IBM 7094 system.

1) Input data

- Composition in atomic %
- Density (in atoms/$\mathring{A}^3$)
- Experimental intensity, in counts per second: 601 readings, corresponding to one datum every 0.2° up to $2\theta=80^\circ$, and one datum every 0.4° up to $2\theta=160^\circ$.
- Background intensity, in counts/sec.
- Tables of scattering factors for the appropriate radiation.

2) Sequence of Operations

Part 1 Input of diffraction data; correction for background; Polarization correction.

Part 2 Computation of $\langle f^2 \rangle = \sum_i x_i f_i^2$ for each of the 601 values of $s = 4\pi \frac{\sin\theta}{\lambda}$; correction for anomalous dispersion; computation of $\langle f_e^2 \rangle = (\sum_i x_i f_i)^2 / (\sum_i x_i Z_i)^2$

Part 3 High angle fitting, yielding the coherent intensity scaled in electron units. Computation of the interference function sI(s) for all 601 values of s.

Part 4 Fourier inversion yielding W(r) and the actual radial distribution function r W(r). The Fourier integration is performed by the trapezoidal method which is accurate enough for such a large number of points. W(r) and r W(r) are evaluated usually for values of r increasing from 0 to 10 Å, by steps of 0.05 Å.

3) Plots

The program provides plots of the scaled coherent intensity, the interference function sI(s) and the functions W(r) and r W(r).